

# **Stream temperature modeling in mountainous environments**

THÈSE N° 7160 (2016)

PRÉSENTÉE LE 26 AOÛT 2016

À LA FACULTÉ DE L'ENVIRONNEMENT NATUREL, ARCHITECTURAL ET CONSTRUIT  
LABORATOIRE DES SCIENCES CRYOSPHERIQUES  
PROGRAMME DOCTORAL EN GÉNIE CIVIL ET ENVIRONNEMENT

ÉCOLE POLYTECHNIQUE FÉDÉRALE DE LAUSANNE

POUR L'OBTENTION DU GRADE DE DOCTEUR ÈS SCIENCES

PAR

**Aurélien GALLICE**

acceptée sur proposition du jury:

Prof. A. Rinaldo, président du jury  
Prof. M. Lehning, Dr H. Huwald, directeurs de thèse  
Dr R. Moussa, rapporteur  
Prof. D. Moore, rapporteur  
Prof. B. Schaefli, rapporteuse



ÉCOLE POLYTECHNIQUE  
FÉDÉRALE DE LAUSANNE

Suisse  
2016





*À mon grand-père,  
en souvenir de nos parties de pêche pendant les grandes vacances,  
même si je n'ai jamais rien attrapé de mieux qu'une perche-soleil...*

The image on the previous page is extracted from “Lagaffe mérite des baffes” by Franquin, edited by Dupuis (2009).



# Acknowledgements

Albeit generally considered as a personal work, a thesis necessarily leaves you indebted to a long list of people. I hope not to have forgotten anyone of importance here.

First of all I would like to thank Hendrik Huwald and the Swiss Federal Office for the Environment (FOEN) for having made this adventure possible. Hendrik supervised me during those three years and a half, supporting me in the decisions I had to make and cheering me up when I was down. Thank you Hendrik for your good mood and for always being ready to give a hand. FOEN participated to the financing of the thesis and provided me with some guidance regarding the strategical choices to be made along the way. I wish to particularly thank Thilo Herold from FOEN for his enthusiasm and general faith in the predictions of numerical models. I also wish to acknowledge Adrian Jakob for following my work from its very start and taking care of the administrative side of it at FOEN.

I would like to deeply thank Michael Lehning, who accepted me as a PhD student in his group and always lent me an attentive ear when I was expressing some difficulties. Thank you very much also for agreeing to my unusual requests of remote working, it was very much appreciated.

Particular thanks go to Bettina Schaepli, who has frequently devoted some of her time to help me—although she was not officially involved in my work. Thank you very much Bettina for the interesting discussions and your very precious inputs. Thank you also for always keeping an eye on my work, even from your far-off new office at UNIL.

I wish to also thank all my colleagues in Lausanne, with whom I could share my frustration and joy on a daily basis. Particular thanks go to Tristan and Francesco, who have been much more than office mates: thank you very much for the shared laughs, wraths and despairs. Some memories will stay for long, such as the one of a particular field day in the snow-covered Dischma with kilos of equipment on our backs. Thank you also to my other office mates Annelen and Varun for their constant cheerfulness and for giving an international touch to the office. I really appreciated Annelen's repeated attempts at constraining Varun's tendency to slowly increase the size of his working place at the expense of his co-workers. Bien sûr, tout ce petit monde ne pourrait pas tourner sans une sympathique secrétaire toujours prête à rendre service: merci beaucoup Jessica. Merci aussi à Béatrice, qui a remplacé Jessica pendant son congé maternité et n'était jamais à court de petits ragots à propos des membres de l'institut.

Je tiens également à remercier tous les membres du laboratoire LISAH de l'INRA de Montpellier, où j'ai effectué un très agréable séjour de deux mois. Un merci tout particulier à Roger

## Acknowledgements

---

Moussa, sans qui mon expérience montpelliéraine n'aurait tout simplement pas été possible. Merci beaucoup pour ta gentillesse et l'intérêt que tu as porté à mon travail, j'ai vraiment apprécié nos discussions ensemble. Merci aussi à tous les autres membres du laboratoire, et en particulier Nissaf, ma collègue de bureau durant ces deux mois, avec qui j'ai partagé mes joies et mes peines. J'espère que ta nouvelle vie de maman te comble pleinement et que l'on aura l'occasion de se recroiser prochainement, en Tunisie ou ici. Merci aussi à Sébastien, Mahmoud, Jeanne, Guillaume, Marthe, Anne-Sophie et les autres pour les parties de Mölkky après le repas... j'ai tellement accroché que j'en ai commandé un pour Noël !

Enfin, un grand merci à mes parents, mes frères, ma famille et mes amis, qui m'ont soutenu pendant ces quelques années de dur labeur. Je tiens à faire une dédicace toute particulière aux membres du club astro (dans sa version étendue) pour nos rencontres toujours très ludiques et que j'apprécie toujours autant. Je mesure toute ma chance d'avoir pu conserver un tel groupe d'amis depuis le lycée... à part quand il s'agit de trouver des gens motivés pour jouer à *Small World*. Merci aussi à Christine, avec qui nous avons pu comparer nos expériences académiques respectives—très similaires au demeurant. Je te souhaite le meilleur pour la suite de ta carrière, en espérant que tu parviendras à trouver une voie qui te convienne.

Et bien sûr, un immense merci à toi, Emilie, pour ta patience et ton amour. Les trois années passées n'ont pas toujours été faciles à gérer avec la distance, mais sache que je ne t'en aime que d'autant plus fort (sans compter que l'on a pu découvrir plein de coins de France que l'on ne connaissait pas). Aux soixante prochaines années ensemble...

*Lausanne, le 26 août 2016*

A. G.

# Abstract

Stream temperature is one of the key variables affecting the habitat suitability of numerous aquatic species. Over the past decades, research efforts on this topic have concentrated on low-land rivers of North-America, whereas mountainous environments have received much less attention—above all in Europe. The present thesis introduces two new models for stream temperature prediction in Alpine watersheds. Both are tested over selected catchments in Switzerland, a mountainous country which presents the advantage of possessing a dense network of automatic stream temperature measurement stations.

The first model is specifically designed to provide stream temperature estimates in ungauged catchments, so as to compensate for the scarcity of temperature measurement sites in mountainous environments. As opposed to standard statistical models, which are common to many disciplines, the present one aims at incorporating some of the physics controlling stream temperature in its own structure. Its formulation is derived from an analytical solution to the equation describing the energy balance of an entire stream network. Some terms of this solution cannot be readily determined based on data available at the regional scale; they are approximated using standard statistical techniques. The resulting model is statistical in nature, but includes elements of thermodynamic principles. Its accuracy is shown to be similar to the one of a standard statistical model, with a root mean square error of  $1.3^{\circ}\text{C}$  at the monthly time scale. In virtue of its physical basis, the model can be used to investigate into more detail the factors controlling stream temperature at the regional scale, as shown through a simple example.

The second model is intended to provide deterministic stream temperature predictions, to be used for example in climate change studies. It builds upon an existing physically-based model, which has been entirely written anew in order to clarify its structure and ease future developments. Conceived as an add-on to the spatially distributed snow model *Alpine3D*, it simulates the flows of both water and energy within the catchment based on a semi-distributed approach. Some components of the model can be represented using various alternatives; for example, three different techniques are available to simulate the temperature of subsurface runoff. This flexibility allows the model to be tuned to the specific needs of each user, but also permits a more thorough assessment of the simulation uncertainty by comparing the predictions of the various alternatives. Evaluation of the model in a high alpine watershed indicates that hourly mean discharge is reproduced with a Nash-Sutcliffe efficiency (NSE) of 0.82, and hourly mean stream temperature with a NSE of 0.78.

Both models are shown to contribute to a better understanding of stream temperature dynam-

## Abstract

---

ics in Alpine environments. In particular, it is found that the temperature of subsurface runoff has a marked impact on stream temperature—a fact which has usually been neglected or underestimated in previous studies. Future work involves further research on the structure of the statistical model, as well as the application of the deterministic model within the framework of climate change studies.

**Key words:** stream temperature, alpine hydrology, deterministic modeling, statistical modeling, prediction in ungauged basins (PUB)



## Résumé

La température des cours d'eaux influe sur de nombreux aspects de l'écosystème rivulaire, et notamment sur la distribution géographique de multiples espèces aquatiques. Jusqu'à ce jour, les travaux de recherche dans ce domaine ont principalement été menés sur des rivières de plaine nord-américaines. En comparaison, les cours d'eau d'altitude ont été bien moins étudiés—et ce d'autant moins en Europe. La présente thèse introduit deux nouveaux modèles visant à prédire la température dans des cours d'eau alpins. Ces modèles sont évalués sur des rivières de Suisse, un pays qui présente l'avantage—outre son caractère montagneux—de posséder un vaste réseau de mesure de température des cours d'eau.

Le premier modèle permet l'estimation de la température dans des bassins-versants non jaugés, dans le but de palier au faible nombre de sites de mesure en milieu montagneux. Il fournit des prédictions de la température moyenne mensuelle sur la base d'une approche statistique originale. Contrairement aux modèles statistiques standards, tels que la régression multilinéaire ou les réseaux de neurones, le présent modèle incorpore des éléments de la thermodynamique des cours d'eau au sein même de sa structure. Il se base pour cela sur une solution analytique de l'équation régissant la conservation de l'énergie d'un réseau hydrographique. Certains termes de cette solution ne peuvent être calculés à partir des données disponibles à l'échelle régionale ; ils sont approximés à l'aide de techniques statistiques standards. Il en résulte un modèle dont la nature est statistique, mais qui se base sur des principes physiques. Son évaluation sur une sélection de bassins-versants suisses indique que la racine de l'erreur quadratique moyenne de ses prédictions s'élève à  $1.3^{\circ}\text{C}$ , ce qui se trouve être du même ordre de grandeur que les modèles statistiques standards. Le fait que le présent modèle incorpore des éléments de thermodynamique peut être mis à profit pour explorer les principaux facteurs influant sur la température des cours d'eau à l'échelle régionale. La démonstration en est faite au travers d'un exemple simple.

Le second modèle vise à fournir des prédictions déterministes de la température des cours d'eau à l'échelle de temps horaire. Il a été conçu à des fins de prévision à long terme pour des études de changement climatique en milieu alpin. Il se base sur un modèle déterministe préexistant qui a été entièrement réécrit afin de clarifier sa structure et de faciliter son développement futur par de tierces personnes. Conçu comme une extension du modèle de neige *Alpine3D*, il simule le transport d'eau et d'énergie dans le bassin-versant à l'aide d'une approche semi-distribuée à base physique. Certains composants du modèle peuvent être simulés de multiples manières, comme par exemple le calcul de la température de l'écoulement de sous-surface qui pénètre dans la rivière. Cette flexibilité permet d'adapter le modèle aux

## Résumé

---

besoins particuliers de chaque utilisateur, mais aussi d'estimer les erreurs de prédiction du modèle en comparant les résultats obtenus à partir des diverses méthodes mises à disposition. En guise d'exemple d'application, le modèle est testé sur un bassin-versant de haute altitude en Suisse orientale. La comparaison avec les données mesurées indique qu'il parvient à reproduire le débit et la température horaires du cours d'eau avec des indices de Nash-Sutcliffe respectifs de 0,82 et 0,78.

Au-delà de la conception des deux modèles, c'est une contribution à la recherche sur la température des cours d'eau en milieu montagneux qui a été visée. L'application des deux modèles a notamment permis d'observer que la température de l'écoulement de sous-surface a un impact significatif sur la température des cours d'eau, un fait qui a généralement été négligé ou sous-estimé par les études antérieures. La poursuite des travaux engagés dans cet ouvrage devra se concentrer sur une étude plus approfondie de l'approche adoptée pour développer le modèle statistique, ainsi que sur une utilisation du modèle déterministe dans le cadre d'études de changement climatique.

**Mots-clefs :** température des cours d'eau, hydrologie alpine, modèle déterministe, modèle statistique, prédiction dans des bassins-versants non-jaugés

# Contents

<b>Acknowledgements</b>	<b>i</b>
<b>Abstract (English/Français)</b>	<b>iii</b>
<b>List of figures</b>	<b>ix</b>
<b>List of tables</b>	<b>xi</b>
<b>1 Introduction</b>	<b>1</b>
<b>2 Stream temperature prediction in ungauged basins</b>	<b>9</b>
2.1 Introduction . . . . .	9
2.1.1 Predictions with limited precision . . . . .	10
2.1.2 Few models can predict the stream temperature annual cycle . . . . .	12
2.1.3 Space-averaging of the predictor variables . . . . .	14
2.1.4 State-of-the-art in the European Alps . . . . .	15
2.1.5 Investigation of a new modelling approach . . . . .	15
2.2 Data description . . . . .	17
2.2.1 Selected catchments for model evaluation . . . . .	17
2.2.2 Stream temperature data . . . . .	19
2.2.3 Meteorological data . . . . .	20
2.2.4 Thermal regime classification . . . . .	21
2.3 Formulations of the stream temperature models . . . . .	23
2.3.1 Physics-inspired statistical model . . . . .	23
2.3.2 Standard regression model . . . . .	31
2.4 Model evaluation . . . . .	33
2.4.1 Model formulations . . . . .	34
2.4.2 Model performance . . . . .	35
2.4.3 Influence of the stream network resolution . . . . .	37
2.4.4 Comparison with the standard regression model . . . . .	39
2.5 Discussion . . . . .	41
2.6 Conclusions . . . . .	46

## Contents

---

<b>3</b>	<b>Deterministic stream temperature modeling in high alpine watersheds</b>	<b>49</b>
3.1	Introduction . . . . .	49
3.2	Model description . . . . .	53
3.2.1	Subwatershed modeling . . . . .	55
3.2.2	Stream network modeling . . . . .	56
3.3	Model implementation . . . . .	62
3.3.1	Program main architecture . . . . .	63
3.3.2	Input reading . . . . .	65
3.3.3	Output writing . . . . .	66
3.3.4	Calibration module . . . . .	66
3.4	Case study . . . . .	67
3.4.1	Study site and measurement data . . . . .	67
3.4.2	Model setup . . . . .	69
3.4.3	Model evaluation . . . . .	72
3.5	Conclusions . . . . .	82
<b>4</b>	<b>Discussion</b>	<b>85</b>
4.1	Complementarity of the modeling approaches . . . . .	85
4.2	Extent of the spatial domain of application . . . . .	86
4.3	Temporal resolution . . . . .	87
4.4	Utility of the models for biologists and stakeholders . . . . .	88
4.5	Role of subsurface runoff temperature . . . . .	91
<b>5</b>	<b>Conclusions</b>	<b>93</b>
<b>A</b>	<b>Analytical solution to the energy-balance equation</b>	<b>95</b>
<b>B</b>	<b>Original formulation of <i>StreamFlow</i>'s subwatershed bucket model</b>	<b>99</b>
B.1	Subwatershed outflow discharge computation . . . . .	99
B.2	Subwatershed outflow temperature computation . . . . .	100
<b>C</b>	<b>Validation of the scheme used to solve the heat balance equation</b>	<b>103</b>
C.1	Analytical solutions to the heat balance equation . . . . .	103
C.1.1	Analytical solution of test case 1 . . . . .	105
C.1.2	Analytical solution of test case 2 . . . . .	106
C.2	Validation of the numerical splitting scheme . . . . .	107
	<b>Bibliography</b>	<b>127</b>
	<b>Curriculum Vitae</b>	<b>129</b>

# List of Figures

1.1	Examples of species whose habitat suitability depends on stream temperature	2
1.2	Locations of the automatic gauging stations measuring stream temperature in Switzerland . . . . .	4
1.3	Main types of stream temperature models and their respective applications . .	5
2.1	Locations of the gauging stations selected for the evaluation of the stream temperature models . . . . .	17
2.2	Classification of the thermal regimes of the selected catchments . . . . .	22
2.3	Prediction error of the physics-inspired statistical model for different resolutions of the stream network . . . . .	38
2.4	Non-linear relationship between the $z$ scored stream and air temperatures averaged over 14 reference meteorological stations . . . . .	39
2.5	Comparison of modelled against measured slopes of the regression line between stream and air temperatures . . . . .	43
2.6	Seasonal values of the weighting factors appearing in Eq. (2.8) . . . . .	44
3.1	Schematic representation of the work flow in <i>StreamFlow</i> . . . . .	54
3.2	Available methods for spatially discretizing the stream reaches in <i>StreamFlow</i> .	56
3.3	Structure of <i>StreamFlow</i> 's source code . . . . .	64
3.4	Map of the Dischma catchment . . . . .	68
3.5	Comparison between the measured and simulated snow depth at the Stillberg meteorological station . . . . .	71
3.6	Comparison between the measured and simulated hourly mean discharge at the catchment outlet . . . . .	73
3.7	Distributions of the 300 best sets of parameters associated with water transport	75
3.8	Water depth simulated by the model in hydrological year 2014 using various channel water routing techniques . . . . .	76
3.9	Comparison between the simulated and measured stream temperature at the catchment outlet . . . . .	78
3.10	Comparison between predictions of stream temperature at the catchment outlet based on various methods for estimating the temperature of subsurface runoff	81
A.1	Schemas illustrating the notation introduced while deriving the analytical solution to the stream energy balance equation . . . . .	96

## List of Figures

---

B.1	Illustration of the original approaches used in <i>StreamFlow</i> for the computation of subsurface runoff discharge and temperature . . . . .	100
C.1	Root mean square error of the splitting scheme used to solve the heat balance equation in two test cases . . . . .	107
C.2	Stream temperature profile at the end of the simulation in two test cases . . . .	108

## List of Tables

2.1	Publications on statistical stream temperature prediction in ungauged basins .	11
2.2	List of the selected Swiss catchments used to evaluate the model . . . . .	18
2.3	Calibration parameters of the physics-inspired statistical model . . . . .	31
2.4	Formulations of the physics-inspired statistical model selected in each season based on their corresponding AICc value . . . . .	36
2.5	Performance of the best physics-inspired statistical model in each season . . .	37
2.6	Best multi-linear regression models for the prediction of annual mean and standard deviation of the monthly mean stream temperature . . . . .	40
2.7	Performance of the standard regression model . . . . .	40
3.1	List of reviewed semi-distributed hydrological models simulating both stream discharge and stream temperature . . . . .	52
3.2	Parameters used by <i>StreamFlow</i> to simulated water depth, discharge and tem- perature using various approaches . . . . .	70
3.3	Comparison of the total volumes of water flowing in and out of the catchment each year . . . . .	72
3.4	Accuracy of the hourly mean discharge simulations performed by <i>StreamFlow</i> using the instantaneous water routing technique . . . . .	74
3.5	Accuracy of the hourly mean stream temperature predictions, based on various approaches for advecting water in the stream channels and computing the temperature of subsurface runoff . . . . .	80
C.1	Values chosen for the parameters of two test cases used to validate the numerical splitting scheme . . . . .	106





# 1 Introduction

Stream temperature is often referred to as one of the key variables for stream ecosystems. Its predominant role on many aspects of riverine biology has been known for long and continues to be the subject of intense scientific research. Among the current studies, some focus on the impacts of climate or land use change on various aquatic species, while others—like the present thesis—concentrate more on the better understanding and modeling of stream temperature dynamics.

From an ecological perspective, stream temperature determines the habitat suitability of many aquatic species. The most emblematic among them are the salmonids—regrouping trouts, salmon and chars—as they support a substantial economic sector in some regions of the world such as Canada, Scotland or some states of the US (e.g. Nelitz et al., 2007; Loinaz et al., 2014). Being ectothermic, salmonids are particularly sensitive to the temperature of their environment, which controls various aspects of their physiology and behavior. For example, the dates of spawning and fry emergence have been observed to strongly depend on stream temperature (e.g. Armstrong et al., 2003; Elliott and Elliott, 2010). The latter is also known to become lethal above a certain threshold; for instance, the eggs of arctic char (*Salvelinus alpinus*; see Fig. 1.1a) do usually not survive if temperature exceeds 8°C (Elliott and Elliott, 2010). In addition, stream temperature plays an important role in the feeding, growth rate and metabolic rate of salmonids. As such, fishes tend to eat more and grow faster within a preferred temperature range, which varies among the species (Armstrong et al., 2003; Elliott and Elliott, 2010). Some recent studies have shown that not only the value, but also the temporal dynamics of stream temperature are relevant for fish (e.g. Wehrly et al., 2007). For example, the upper lethal temperature limit experienced by the salmonids depends on the duration of the exposition period: the longer the period, the lower the limit. Fish sensitivity to warm temperatures is exacerbated by the proliferation of diseases such as the Proliferative Kidney Disease (PKD) at higher stream temperatures, which tend to drastically reduce the populations of salmonids (e.g. Hari et al., 2006).

Apart from salmonids, many other aquatic species are directly or indirectly impacted by stream temperature. As examples drawn from the general public literature, one can cite the



Figure 1.1: Examples of species whose habitat suitability is impacted by stream temperature: **(a)** Arctic char (already grilled and stuffed with onions, mushrooms and carrots—for the recipe, see <http://thierrygrandnord.com>; picture credits: T. Chevillard), **(b)** freshwater pearl mussel (picture credits: L. Jurek) and **(c)** Eurasian water shrew (picture credits: T. Whittaker).

freshwater pearl mussel (*Margaritifera margaritifera*; see Fig. 1.1b), portrayed two years ago in issue 101 of the French naturalist journal *La Hulotte* (Déom, 2014), and the Eurasian water shrew (*Neomys fodiens*; see Fig. 1.1c), depicted in this year's special issue of the magazine edited by the Swiss association *Pro Natura* for the protection of Nature (Strässle et al., 2016). The freshwater pearl mussel was commonly found on the gravel bed of many clear water rivers of the northern hemisphere until the middle of the 19<sup>th</sup> century, but is now considered as an endangered species by the International Union for Conservation of Nature (IUCN; Mollusc Specialist Group, 1996). Over-exploitation for jewelry purposes, water pollution and river regulation are among the main factors responsible for its drastic decline over the past century (Déom, 2014). In addition to these factors, stream temperature also impacts the populations of freshwater pearl mussel through its effect on the mussel reproduction cycle. As a matter of fact, the mussel larvae, after being ejected from their parent into the water, attach to the

---

gills of a salmon or a trout. They grow there for almost one year, before leaving their host and burying themselves into the river bed. The rising stream temperatures tend to decrease the populations of salmonids, hereby impacting the mussel populations as well. In a similar way, the water shrew is indirectly affected by stream temperature through the sensitivity of its preys to temperature. Indeed, it mainly feeds on insect larvae, crustaceans and even small fishes (Strässle et al., 2016), whose habitat suitability is known to be strongly dependent on temperature (see e.g. Hawkins et al., 1997; Mouthon and Daufresne, 2006).

The ecological relevance of stream temperature extends beyond its impact on the above-cited aquatic species. It also affects water quality by controlling the concentration of various chemical species, such as dissolved oxygen. The toxicity of some dissolved substances has also been shown to increase with stream temperature (Langford, 1990). In general, stream temperature rise is associated with relatively negative consequences from an ecological point of view. This is all the more worrying in the actual context of climate change, since stream temperature is observed to follow the air temperature trend in many regions of the globe. This phenomenon is even expected to worsen in the near future, especially in summer due to the predicted lower flows.

From an economic perspective, stream temperature is particularly important for the production of electricity, since many thermal power plants have been built along rivers in order to use water as a cooling means. This cooling is less efficient at high water temperatures, hereby decreasing the amount of generated electricity (Durmayaz and Sogut, 2006). As such, some studies have pointed out that thermal power plants may produce between 0.5 and 1 % less electricity per degree increase in river temperature, depending on the type of power plant and cooling technology (e.g. Durmayaz and Sogut, 2006; Linnerud et al., 2011; Hoffmann et al., 2013). Some power plants might actually see a decrease of up to 60 % of their production at the end of the century as a result of legal regulations (Hoffmann et al., 2013). Indeed, water pumped by thermal power plants in rivers is usually rejected in the same rivers. In order to protect downstream ecology, regulations have been put into place which limit water temperature downstream of the plant after complete mixing between the river water and the rejection water. Compliance with these regulations might oblige power plants to reduce their production or even be temporarily shut down so as to avoid over-heating of downstream water. The International Atomic Energy Agency (IAEA) reports that more than 400 of these “outages” are already taking place each year worldwide and are expected to increase in the future as a result of climate change (IAEA, 2015). By 2060, this might result in power production decreasing by 6.3 to 19 % in Europe (van Vliet et al., 2012b).

As opposed to most of the studies conducted to date, the present thesis focuses on stream temperature in mountainous environments—and more particularly in Switzerland. Mountain streams are particularly valuable from an ecological point of view, since they host many populations of macroinvertebrates and provide a suitable spawning habitat for various salmonid species. Their thermal regime is relatively similar to the one of low-land rivers; in particular, most of their energy exchanges with the surrounding environment occur at the air–water

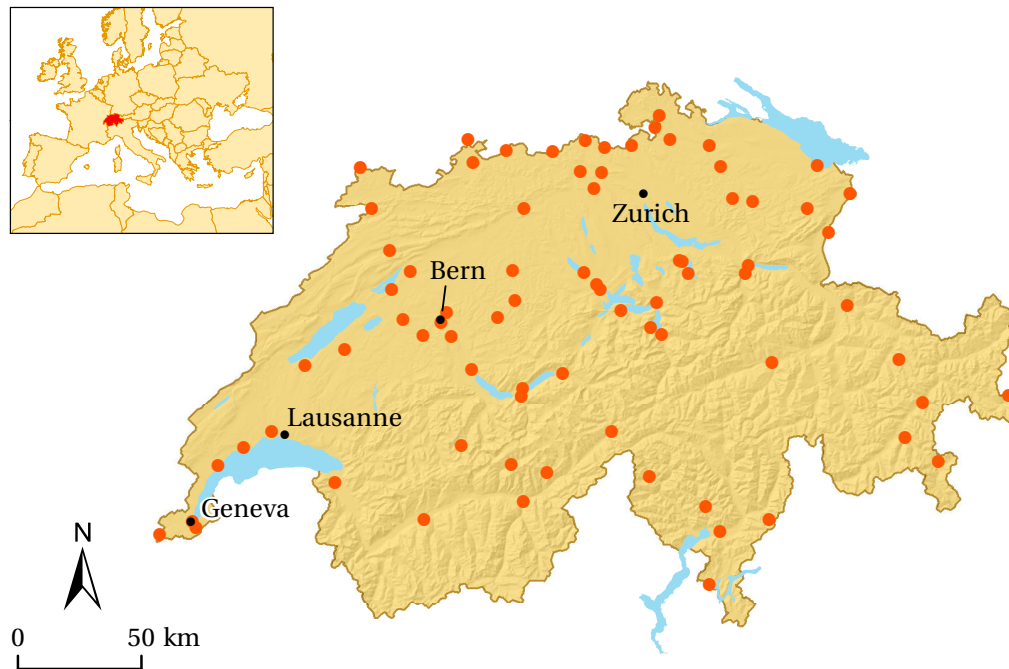


Figure 1.2: Locations of the automatic gauging stations measuring stream temperature in Switzerland. Only the stations operated by the Swiss Federal Institute for the Environment (FOEN) are shown; some cantons additionally operate their own measurement sub-network.

interface (Webb et al., 2008). Incoming radiation represents their main heat source during daytime, which explains the typical sinusoidal shape of their temperature curve on daily and annual time scales (Caissie, 2006). The largest fraction of their heat losses is generally attributable to emitted long-wave radiation. Heat conduction with the stream bed and the latent and sensible heat fluxes act as secondary heat sources or sinks depending on the time of the day/year or geographical environment. Interestingly, some studies have pointed out that friction with the stream bed might represent a significant source of heat in steep mountainous streams, above all in winter (Webb et al., 2008). High-altitude streams are also strongly impacted by snow and/or glacier melt in spring and summer, which translates into mitigated stream temperatures during these periods of the year. In addition, as opposed to low-land rivers, proximity with the mountains implies a marked effect of topographical shading on solar radiation. Many processes involved in the energy budget of mountainous streams are still not fully understood, though. For example, the role of the lateral inflows on stream temperature has generally received little attention. It is also not clear to which extent the latent and sensible heat fluxes are enhanced by the strong turbulence typical of alpine streams. Similarly, some authors have noticed that turbulence had a significant impact on the water albedo due to the formation of small air bubbles (Richards and Moore, 2011), but more research is needed on this subject to fully understand the relative importance of this phenomenon.

Following the gradual awareness of the relevance of stream temperature and in order to

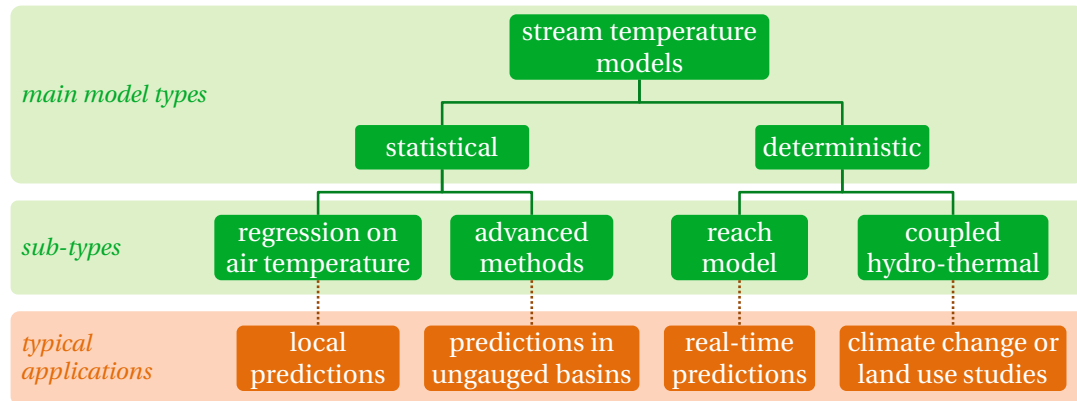


Figure 1.3: Main types of stream temperature models and their respective domains of application (adapted from Caissie, 2006).

help answering the above-mentioned open questions, some states have decided to invest in country-wide automatic measurement networks. As an example, Switzerland has opted around 2002 to significantly increase the number of its gauging stations measuring stream temperature, resulting in a network of more than 70 stations (see Fig. 1.2). It should be mentioned that this network is particularly dense with regards to international standards, especially for such a mountainous country. However, even in the case of Switzerland, gauging stations cannot be installed in each and every river, and the measurement network necessarily suffers from gaps. This represents a major constraint to the public environmental services regulating water intakes or rejections in streams, since their decisions must often be based on incomplete information about the actual state of the streams. In addition, the identification of sensitive streams to be protected from e.g. land use or climate change is often hampered by the low spatial representativeness of the measurement network.

As an additional challenge, public authorities are confronted with the anticipation and mitigation of the effects of climate change on stream temperature. Some of these effects have been already identified, as will be discussed into more detail in Chap. 3. The stream temperature increase resulting from the rise in air temperature might be exacerbated in summer due to an increase in the frequency of drought events. In addition, the magnitude of the spring freshet is expected to decrease in many regions, therefore reducing its mitigating impact on stream temperature during spring. In general, it is nevertheless admitted that our understanding of the future dynamics of stream temperature is rather incomplete and needs further investigation.

As a means to address the above challenges, some numerical models have been developed over the last decades with the objective to provide estimates of stream temperature in ungauged rivers (e.g. Chang and Psaris, 2013; Moore et al., 2013; Segura et al., 2014) or deliver detailed real-time and long-term forecasts of stream temperature (e.g. Ferrari et al., 2007; Haag and Luce, 2008; Isaak et al., 2010; van Vliet et al., 2012b). Depending on their structure, these models can be classified into one of the following two categories (adapted from Caissie, 2006, see Fig. 1.3):

**The statistical models** As their name suggests, these models are based on standard regression techniques—of which the most popular is certainly (multi)linear regression, although more intricate machine learning algorithms such as artificial neural networks or random forests tend to gain in popularity. These models can be sub-divided into two types, depending on whether they need to be calibrated over each stream separately or not. In the models requiring a separate calibration for each river, stream temperature is usually approximated as a function of air temperature alone (see Fig. 1.3). A good example is the model devised by Mohseni et al. (1998), obtained by regressing a logistic function to the stream–air temperature measurements in the catchment of interest. Some authors include discharge as an additional predictor to improve the model accuracy (e.g. Caissie et al., 2001), but this practice is somewhat less common. In the case of models applicable over multiple watersheds, physiographic properties of the catchments are often used as extra predictors in complement to air temperature. For example, Moore et al. (2013) could successfully express stream temperature as a linear combination of catchment area, glacier cover fraction, mean catchment area and air temperature on top of a few other predictors. The choice of physiographic properties used as predictors is typically very eclectic and depends on the geographic area of interest and the data at hand. As a result of their rather simple structure, most statistical models require a time step larger than a day. The vast majority of them actually provide stream temperature estimates at weekly or monthly time scales. Moreover, their lack of physical basis questions the validity of their long-term predictions, which in turn prevents their use in climate change studies. On the other hand, their simplicity often allows them to be used over large areas, hereby making them particularly useful when it comes to prediction in ungauged basins. A current research challenge consists in developing such a model to provide reliable long-term predictions while at the same time keeping the model simple and applicable over large areas.

**The deterministic models** Based on the numerical solution to the energy conservation equation (also known as the heat balance equation), these models compute the different heat fluxes entering or leaving the stream using more or less physical expressions. Most of them simulate only a portion of a stream, i.e. a reach with usually no affluent draining into it (e.g. Sinokrot and Stefan, 1993; Westhoff et al., 2007; Roth et al., 2010). They expect the user to specify all the external water fluxes and some of the external heat fluxes—such as the incoming water discharge at the upstream reach inlet—consequently restricting their use to highly instrumented river reaches. As a response to this limitation, some deterministic stream temperature models have been recently coupled to hydrological models (e.g. Haag and Luce, 2008), hereby offering the possibility to simulate entire catchments. These models offer new perspectives, since they simulate the interactions between flow and temperature and therefore allow for the investigation of current open questions such as the impact of land use on stream temperature. Be they coupled or not, deterministic models typically require a high amount of input data and large computational resources, which constraints their use to limited areas. However, their physical basis gives more credit to their long-term predictions as compared to those



---

of the regression models, making them specifically suited for climate change studies. In addition, they can usually run with time steps of one hour or less, hereby offering the possibility to simulate small time scales. Current research efforts with this kind of model concentrate on the assessment of the validity of the long-term simulations, as well as the coupling with climate or vegetation growth models in order to better assess the effects of climate and land-use change.

The present work aims, to some extent, at contributing to the research on stream temperature modeling. More specifically, it focuses on the development of two new models:

- (a) A statistical model to be used for stream temperature predictions in ungauged basins. This model is ultimately intended to help in the spatial identification of thermally sensitive zones where protection or restoration measures should be put into place in order to mitigate stream temperature rise.
- (b) A coupled hydro-thermal model aimed at providing detailed stream temperature forecasts in high-altitude watersheds. This model is expected to help in the detailed prediction of the climate-change impacts on the thermal regime of Alpine streams.

These two models are tested over selected catchments in Switzerland, a country being mostly covered with mountains and which presents the advantage of having a dense network of stream temperature sensors (see Fig. 1.2). The choice of Switzerland as a test ground also conforms to the wish of the Swiss Federal Office for the Environment (FOEN), which is financially involved in the present thesis.

Chapter 2 is entirely devoted to the description of the statistical model. Rather than using an existing model, it was decided to create one in an attempt at testing a new idea. Indeed, the vast majority of the models used for prediction in ungauged basins are currently based on *standard* statistical approaches. From the simplest to the most intricate, all of these approaches are generic in some sense. In other words, most of them are not specific to stream temperature modeling, but can be used in many other disciplines. As a drawback to this versatility, their structure cannot integrate any prior knowledge on the dynamics of the modeled system. As an example, artificial neural networks use a set of hyperbolic tangents to relate the predicted variable to the list of predictors. Of course, calibration will automatically transfer some of the system dynamics into the coefficients weighting the respective contributions of the hyperbolic tangents. However, the relationship between the predictand and the predictors will always be modeled as a combination of tanh functions, whatever the values of the weighting coefficients are. In the present work, it was tested whether it is possible to devise a statistical model whose very internal structure could incorporate some of the known dynamics controlling stream temperature. It should be noted that the same idea was tested in parallel by Toffolon and Piccolroaz (2015), with whom I collaborated on the redaction of a scientific article (Piccolroaz et al., 2016).

## Chapter 1. Introduction

---

Chapter 3 details the structure and performance of a new coupled hydro-thermal model which was developed based on the work of Comola et al. (2015). The aim of this model is to provide detailed stream temperature predictions at the hourly time scale, to be used in studies assessing the impacts of climate or land use change. My contribution consisted in completely reformatting the model code and incorporating new functionalities into it. Particular attention was paid to the quality of the new code, so as to facilitate its readability and ease of extension by future programmers. The added functionalities were meant to offer alternative ways of simulating certain parts of the hydrological cycle, such as the temperature of subsurface runoff or the routing of water in the stream channels. Application of the model over a test catchment in the Swiss Alps can be found at the end of Chapter 3.

Chapter 4 discusses various aspects common to both models and places the results in the context of the research questions mentioned above. The last chapter contains a summary of the present thesis as well as suggestions for potential future work.



## 2 Stream temperature prediction in ungauged basins

*This chapter has been published in 2015 as an open-access article in journal Hydrology and Earth System Sciences (HESS) under the title “Stream temperature prediction in ungauged basins: review of recent approaches and description of a new physics-derived statistical model.” The authors are, in order of publication: Aurélien Gallice, Bettina Schaefli, Michael Lehning, Marc B. Parlange and Hendrik Huwald. The on-line version of the article is freely accessible at <http://www.hydrol-earth-syst-sci.net/19/3727/2015>. Regarding the author contributions, A. Gallice performed the analysis, produced the figures and wrote the manuscript; B. Schaefli gave much appreciated guidance and impulse to the work; M. B. Parlange commented on the manuscript; and H. Huwald, M. Lehning and B. Schaefli helped write the manuscript and co-supervised the work.*

### 2.1 Introduction

Among the parameters affecting the ecological processes in streams, temperature occupies a predominant role. It influences the concentration of chemicals, such as dissolved oxygen, and may increase the toxicity of dissolved substances (Langford, 1990). It also affects the life cycle of many fish species, particularly the salmonids whose rate of spawning, timing of birth and rate of death are directly influenced by stream temperature (Caissie, 2006; Benyahya et al., 2007). Water temperature is also a relevant factor for many thermal power plants which rely on cooling by river water, and whose electricity production decreases when water temperature exceeds a certain limit (Haag and Luce, 2008).

As a result of the rising concern about climate change and water management impacts on aquatic life, stream temperature modelling has regained some interest over the past 10–15 years. This fostered the development of many stochastic and deterministic models (e.g. Mohseni et al., 1998; Segura et al., 2014; Chang and Psaris, 2013; DeWeber and Wagner, 2014; Meier et al., 2003; Westhoff et al., 2007). The former type relies on a statistical analysis to empirically relate stream temperature to climatic and physiographic variables, such as air temperature, discharge, altitude or channel width (see Benyahya et al., 2007, for a complete

review of this subject). Deterministic models, on the other hand, rely on a physically based formulation of the stream energy conservation to compute water temperature (Caissie, 2006). Both model types have usually been applied to a single stream reach or a limited number of catchments (e.g. Sinokrot and Stefan, 1993; Roth et al., 2010; Caissie et al., 2001; Caldwell et al., 2013; Grbić et al., 2013). As a response to the lack of stream temperature data, some studies have recently attempted to develop regionalized models. This effort was certainly encouraged by the incentive of the International Association of Hydrological Sciences (IAHS), which set the focus of the last decade on hydrological prediction in ungauged basins (Sivapalan et al., 2003; Hrachowitz et al., 2013). In the case of stream temperature, the difficulty in meeting the data requirements of the physically based models led the authors to mostly rely on statistical approaches to make predictions in ungauged catchments. However, the validity of these models for studying climate change impacts or water management techniques has not been assessed yet.

In this paper, more than 30 studies describing regionalized statistical models for stream temperature estimation were reviewed to put our work in a larger context (see Table 2.1). The extensive introduction below discusses several aspects of the reviewed literature which motivated the development of the novel stream temperature model described in the next section.

### 2.1.1 Predictions with limited precision

One recurring issue described in the reviewed literature is the difficulty in predicting stream temperature with a high level of precision. A typical example is the statistical model of Isaak et al. (2010) for the estimation of mean summer stream temperature (15 July–15 September) in the Boise River basin, Idaho. Despite considering a significant number of predictor variables and two different modelling approaches a priori, Isaak et al. (2010) could not reduce the root-mean-square error (RMSE) of their model below 1.5 °C. Prediction uncertainties of the same order of magnitude are reported e.g. by Wehrly et al. (2009), Ruesch et al. (2012), Moore et al. (2013) or Hill et al. (2013).

In general, it seems that the model error originates partly from the lack of appropriate field data, such as measures of riparian shading, groundwater infiltration or irrigation withdrawals (Moore et al., 2013). As noted by Hill et al. (2013), “these types of data are not readily available everywhere and will take time to develop”. In the meantime, they can in some circumstances be accounted for through indirect measures. For example, Tague et al. (2007) used the geological aquifer type as a proxy for the presence or absence of groundwater infiltration. Similarly, Hrachowitz et al. (2010) and Scott et al. (2002) estimated riparian shading based on riparian forest coverage, computed over buffer areas of various widths and lengths around the streams. In the absence of such proxies, the model cannot represent some known processes and must concede some increase in its prediction error (Moore et al., 2013). The size of the areas over which stream temperature is modelled—and hereby the diversity of encountered climatic

Table 2.1: List of reviewed publications about statistical stream temperature prediction in ungauged basins.

Reference	Geographic location	Model type <sup>a</sup>	Number of sites	Number of years <sup>b</sup>	Temporal scale	Model precision <sup>b,c</sup>
Arscott et al. (2001)	Italy	MLR	22	1	Season	$R^2 = 0.37-0.8$
Bogan et al. (2003)	Eastern USA	AE	596	30	Week	$R^2 = 0.80$ , $\sigma_e = 3.1^\circ\text{C}$
Chang and Psaris (2013)	Western USA	MLR/GWR	74	n/a	Week/year	$R^2 = 0.52-0.62$ , $\sigma_e = 2.0-2.3^\circ\text{C}$
Daigle et al. (2010)	West. Canada	Various	16	0.5	Month	$\sigma_e = 0.9-2.8^\circ\text{C}$
DeWeber and Wagner (2014)	Eastern USA	ANN	1080	31	Day	$\sigma_e = 1.8-1.9^\circ\text{C}$
Ducharme (2008)	France	MLR	88	7	Month	$R^2 = 0.88-0.96$ , $\sigma_e = 1.4-1.9$
Gardner and Sullivan (2004)	Eastern USA	NKM	72	1	Day	$\sigma_e = 1.4^\circ\text{C}$
Garner et al. (2014)	UK	CA	88	18	Month	n/a
Hawkins et al. (1997)	Western USA	MLR	45	$\geq 1$	Year	$R^2 = 0.45-0.64$
Hill et al. (2013)	Conterm. USA	RF	$\sim 1000$	1/site	Season/year	$\sigma_e = 1.1-2.0^\circ\text{C}$
Hrachowitz et al. (2010)	UK	MLR	25	1	Month/year	$R^2 = 0.50-0.84$
Imholt et al. (2013)	UK	MLR	23	2	Month	$R^2 = 0.63-0.87$
Isaak et al. (2010)	Western USA	MLR/NKM	518	14	Month/year	$R^2 = 0.50-0.61$ , $\sigma_e = 2.5-2.8^\circ\text{C}$
Isaak and Hubert (2001)	Western USA	PA	26	1/site	Season	$R^2 = 0.82$
Johnson (1971)	New Zealand	ULR	6	1	Month	n/a
Johnson et al. (2014)	UK	NLR	36	1.5	Day	$R^2 = 0.67-0.90$ , $\sigma_e = 1.0-2.4^\circ\text{C}$
Jones et al. (2006)	Eastern USA	MLR	28	3	Year	$R^2 = 0.57-0.73$
Kelleher et al. (2012)	Eastern USA	MLR	47	2	Day/week	n/a
Macedo et al. (2013)	Brazil	LMM	12	1.5	Day	$R^2 = 0.86$
Mayer (2012)	Western USA	MLR	104	$\geq 2$	Week/month	$R^2 = 0.72$ , $\sigma_e = 1.8^\circ\text{C}$
Miyake and Takeuchi (1951)	Japan	ULR	20	n/a	Month	n/a
Moore et al. (2013)	West. Canada	MLR	418	1/site	Year	$\sigma_e = 2.1^\circ\text{C}$
Nelitz et al. (2007)	West. Canada	CRT	104	1/site	Year	n/a
Nelson and Palmer (2007)	Western USA	MLR	16	3	Season	$R^2 = 0.36-0.88$
Ozaki et al. (2003)	Japan	ULR	5	8	Day	n/a
Pratt and Chang (2012)	Western USA	MLR/GWR	51	1/site	Season	$R^2 = 0.48-0.78$
Risley et al. (2003)	Western USA	ANN	148	0.25	Hour/season	$\sigma_e = 1.6-1.8^\circ\text{C}$
Rivers-Moore et al. (2012)	South Africa	MLR	90	1/site	Month/year	$R^2 = 0.14-0.50$
Ruesch et al. (2012)	Western USA	NKM	165	15	Year	$R^2 = 0.84$ , $\sigma_e = 1.5^\circ\text{C}$
Segura et al. (2014)	Conterm. USA	MLR	171	$\geq 1.5$	Week/month	$R^2 = 0.79$
Sponseller et al. (2001)	Eastern USA	MLR	9	1	Year	$R^2 = 0.81-0.93$
Scott et al. (2002)	Eastern USA	MLR	36	1/site	Season	$R^2 = 0.82$
Stefan and Preud'homme (1993)	Eastern USA	ULR	11	n/a	Day/week	$\sigma_e = 2.1-2.7^\circ\text{C}$
Tague et al. (2007)	Western USA	MLR	43	4	Day	$R^2 = 0.49-0.65$
Wehrly et al. (2009)	Eastern USA	Various	1131	1/site	Month	$\sigma_e = 2.0-3.0^\circ\text{C}$
Westenbroek et al. (2010)	Eastern USA	ANN	254	1/site	Day	$R^2 = 0.70$ , $\sigma_e = 1.8^\circ\text{C}$
Young et al. (2005)	New Zealand	MLR	23	1	Season	$R^2 = 0.75-0.93$

<sup>a</sup> AE: analytical expression; ANN: artificial neural network; CA: cluster analysis; CRT: classification and regression trees; GWR: geographically weighted regression; LMM: linear mixed model; MLR: multi-linear regression; NKM: networked kriging model; NLR: non-linear regression; PA: path analysis; RF: random forest; ULR: univariate linear regression.

<sup>b</sup> n/a: not available.

<sup>c</sup>  $\sigma_e$ : root-mean-square error;  $R^2$ : coefficient of determination (sometimes referred to as the Nash–Sutcliffe index).

and geomorphologic conditions—constitutes another factor potentially explaining the model uncertainties for some studies.

Regarding the impact of the modelling approach, Wehrly et al. (2009) investigated four different statistical model types and showed that their difference in prediction accuracy was relatively small. The same conclusion was reached by Daigle et al. (2010), who compared four other modelling techniques. Isaak et al. (2010) found that networked kriging regression performed better than multi-linear regression over the calibration data set, but this assertion became much less evident over the validation set. Similarly, Pratt and Chang (2012) and Chang and Psaris (2013) concluded that geographically weighted regression is slightly more accurate than multi-linear regression, but they did not validate their results on an independent data set. These studies tend to suggest that no significant decrease in the prediction errors should be awaited from a change in the statistical modelling technique.

Further comparisons between the different models reported in the literature are unfortunately hindered by the diversity of temperature metrics and error measures used by the authors. As mentioned in several studies already, we advocate here the systematic use of the different error measures that are RMSE, bias and coefficient of determination  $R^2$  for the evaluation of the model precision, possibly combined with a benchmark model (Schaepli and Gupta, 2007). It should be noted that  $R^2$  is also referred to as Nash–Sutcliffe efficiency by the hydrological community (Nash and Sutcliffe, 1970), and is defined as 1 minus the ratio of the model error variance over the variance of the observed data.

### 2.1.2 Few models can predict the stream temperature annual cycle

Inspecting Table 2.1, it can be seen that most regionalization efforts have concentrated on some particular periods of the year. For example, Jones et al. (2006), Isaak et al. (2010) and Chang and Psaris (2013) focused on the annual maximum of the 7-day moving average of the daily maximum temperature (MWMT). Similarly, both Pratt and Chang (2012) and Hill et al. (2013) aimed at estimating mean stream temperature in summer and winter. Very few studies have actually attempted to derive regional models to compute the complete annual cycle of stream temperature over several years.

Miyake and Takeuchi (1951) and Stefan and Preud'homme (1993) were probably the first authors to address this issue; they relied on linear regression against air temperature to simultaneously estimate stream temperature at multiple sites. However, their respective works are restricted to a limited number of rivers (20 and 11, respectively) and could probably not be applied to larger areas. In an attempt at generalizing these models, Ozaki et al. (2003) and Kelleher et al. (2012) separately regressed stream temperature against air temperature in each one of the catchments they considered, and subsequently regionalized the slopes of the regression lines. However, both studies were only partly successful in completing the regionalization step, since the modelled regression slopes had large prediction errors. They would additionally have had to model the intercepts of the regression lines to completely regionalize

the stream–air temperature relationship. In a similar fashion, Johnson et al. (2014) relied on the logistic equation introduced by Mohseni et al. (1998) to relate stream temperature to air temperature in each catchment. Also, they faced difficulties in regressing the equation parameters against geomorphological properties of the catchments. The two most complete works on the regionalization of the linear stream–air temperature relationship were recently conducted by Ducharne (2008) and Segura et al. (2014). These two studies attempted to regionalize both the slopes and intercepts of the regression lines between stream and air temperature. To this end, Ducharne (2008) grouped the streams according to their Strahler order and fitted a single line in each group. Segura et al. (2014), on the other end, expressed the slopes and intercepts as linear combinations of climatic and physiographic variables. The model of Ducharne (2008) had nominally a higher explanatory power ( $R^2 = 0.88\text{--}0.96$ , depending on the Strahler order) than Segura et al. (2014)'s model ( $R^2 = 0.79$ ), but was effectively based on about 10 times fewer rivers.

Instead of using air temperature as an independent variable, Bogan et al. (2003) relied on equilibrium temperature. This variable corresponds to the stream temperature at which the net energy flux at the air–water interface vanishes (e.g. Edinger et al., 1968). It was shown by Bogan et al. (2003) to be a fairly good estimator of stream temperature for almost 600 rivers in the eastern and central United States, with a prediction error of about 3 °C.

As an alternative to the above-mentioned studies, the annual cycle of stream temperature has been modelled by some authors as a function of time directly, rather than air or equilibrium temperature. Hrachowitz et al. (2010), Imholt et al. (2013) and Rivers-Moore et al. (2012) expressed water temperature as a linear combination of climatic and physiographic variables for each month of the year separately. Their models were derived for a particular year, but can be transferred to other years by estimating stream temperature at a few measurement points using Mohseni's logistic equation and fitting the multi-linear regression model to the resulting values (Hrachowitz et al., 2010). Based on a similar approach, Macedo et al. (2013) succeeded in deriving one single regression model to estimate daily mean stream temperature at 12 different sites in Brazil over 1.5 years. The performance of their model was not tested using data from subsequent years, though.

Johnson (1971) relied on another different technique to estimate the thermal regime of six rivers in New Zealand. He first fitted the stream temperature annual cycles with sine curves. In a second step, he identified the physiographic properties of the catchments which best correlated with the fit coefficients. The focus of his study being on the investigation of these physiographic properties, he did not evaluate the prediction error of his model. Although not intended for this purpose, the work of Garner et al. (2014) is based on a somewhat similar approach and may be used to get a first estimate of the annual cycle of temperature in UK streams. The authors classified rivers into several groups according to the shape and magnitude of their respective thermal regimes. Then, they investigated the similarities and dissimilarities of some geomorphological properties among and between the groups. This processing could be inverted to infer the thermal regime from the physiographic properties of

the catchments.

Finally, some studies have evaluated the possibility of modelling the time evolution of stream temperature using machine learning techniques. For example, DeWeber and Wagner (2014) trained an artificial neural network to reproduce daily mean temperature values from May to October over more than 30 years for 1080 streams in the eastern United States. Their approach could be easily extended so as to model the complete annual cycle of stream temperature each year.

### 2.1.3 Space-averaging of the predictor variables

Some of the reviewed publications on regional stream temperature modelling addressed the question of the spatial scale over which the predictor variables should be averaged. It is common knowledge that stream temperature is not only affected by local environmental conditions, but also by the conditions prevailing upstream. However, the exact extent of the area controlling the stream energy balance at a given point is not clear (Moore et al., 2005a).

Due to this uncertainty, different approaches have been used in the literature to average the predictor variables. Based on studies of the effect of forest harvesting on stream temperature (e.g. Moore et al., 2005a), some authors considered riparian buffer zones of various widths and lengths as averaging areas. This approach was usually applied to average the land cover characteristics only, particularly forest coverage (e.g. Sponseller et al., 2001; Scott et al., 2002; Macedo et al., 2013; Segura et al., 2014), but also in some cases to average most of the predictor variables, including elevation or slope (Hrachowitz et al., 2010; Imholt et al., 2013). Other authors considered larger portions of the catchments as averaging areas, sometimes extending far beyond the riparian zone. For example, Wehrly et al. (2009) used the whole area drained by the stream segment located directly upstream of the temperature measurement point. Whereas most studies relied on simple spatial averaging, a few of them applied a weighting scheme to give more emphasis to the conditions prevailing near the gauging point. As such, Isaak et al. (2010) and Hill et al. (2013) applied a weight  $w$  decreasing exponentially with the distance  $d$  to the catchment outlet,  $w = \exp(-d/L_c)$ , where the  $e$ -folding distance  $L_c$  controls the spatial extent of the averaging area.

In response to this diversity of methods, we could not find a general consensus in the reviewed literature concerning the extent of the spatial area which is relevant for stream temperature prediction. While some studies conclude that this area should have a length of about 1–4 km (Isaak et al., 2010; Hrachowitz et al., 2010; Chang and Psaris, 2013; Macedo et al., 2013), others tend to indicate that the catchment scale is the most appropriate one (Sponseller et al., 2001; Scott et al., 2002). Similarly, values between 30 and 200 m are assumed for the width of the riparian buffer affecting stream temperature at a given point (e.g. Jones et al., 2006; Scott et al., 2002; DeWeber and Wagner, 2014).

### 2.1.4 State-of-the-art in the European Alps

Of all the regional models reported in Table 2.1, less than a third were developed for stream temperature prediction outside of North America, and only one—the model developed by Arscott et al. (2001)—is applied over a European Alpine region. An unpublished attempt at developing another model for an Alpine country (Switzerland) was conducted by Rubin et al. (2012). They relied on the regionalization of the stream–air temperature relationship, but unfortunately did not evaluate the precision of their model. Other studies have sought to classify the thermal regimes of Alpine rivers (Jakob, 2010; Müller, 2011), sometimes with minimal success (see Schädler, 2008, for a review of the classification efforts before 2008). These authors grouped the streams according to the physiographic characteristics of their associated watershed, such as mean basin altitude, water origin (lake, artificial reservoir, deep aquifer or shallow subsurface groundwater), channel width or slope. They computed the characteristics of the typical thermal regime of each group. However, inter-annual variations of the thermal regime cannot be accounted for by this method.

### 2.1.5 Investigation of a new modelling approach

All the reviewed models rely on standard statistical techniques to estimate stream temperature. The range of methods encompasses traditional approaches such as multi-linear regression (e.g. Arscott et al., 2001; Mayer, 2012; Imholt et al., 2013) or linear mixed modelling (Macedo et al., 2013), but also more advanced techniques such as geographically weighted regression (Pratt and Chang, 2012; Chang and Psaris, 2013), networked kriging models (Gardner and Sullivan, 2004; Isaak et al., 2010; Ruesch et al., 2012) or machine learning techniques (e.g. Westenbroek et al., 2010; Hill et al., 2013; DeWeber and Wagner, 2014).

All these methods are general, in the sense that they can be used to model almost any possible relationship between given input and output variable(s). As a consequence of this generality, the user has to specify the set of predictor variables to be considered by the model. Although some objective methods can help to perform this selection (e.g. Burnham and Anderson, 2002), the original set of variables on which these methods act must initially be indicated by the user. In the end, the choice of predictor variables is necessarily affected to some extent by the training and experience of the authors, hereby introducing some diversity in the sets of predictor variables. Thus, in the case of stream temperature modelling in ungauged catchments, some studies consider only physiographic characteristics as predictor variables (e.g. Scott et al., 2002; Jones et al., 2006; Nelson and Palmer, 2007; Hrachowitz et al., 2010), while others also include climatic variables (e.g. Isaak et al., 2010; Ruesch et al., 2012; Moore et al., 2013), stream morphological factors such as channel width or bed gravel size (e.g. Hawkins et al., 1997; Arscott et al., 2001; Daigle et al., 2010), or even markers of anthropogenic activities (e.g. Pratt and Chang, 2012; Hill et al., 2013; Macedo et al., 2013). It should be mentioned that this diversity also largely results from the varying availability and reliability of data among different geographic areas. This is particularly true for riparian shading, which is never directly

measured and can only be estimated based on the data at one's disposal. For example, Isaak et al. (2010) approximated riparian shading using a sophisticated combination of satellite orthoimages and ground hemispherical canopy pictures, whereas DeWeber and Wagner (2014) could only rely on country-wide land-use data.

Although the generality of the standard statistical methods allows them to be applied to many problems, it prevents them from incorporating prior knowledge about the system dynamics into their structure. For example, a multi-linear model expresses the predictand as a linear combination of the predictors regardless of the problem at hand. This fact is also true for non-parametric methods such as artificial neural networks, which implicitly impose some (flexible) functional form onto the model. As advocated by Burnham and Anderson (2002), our idea is therefore to attempt to derive a statistical model whose structure includes known dynamics of the predictand variable of interest, namely stream temperature in the case at hand.

Our approach is strongly inspired by the physically based models which have been used for decades to predict water temperature along stream reaches (e.g. Brown, 1969; Sinokrot and Stefan, 1993; Westhoff et al., 2007). However, it differs from these models in the sense that we seek a much simpler expression for stream temperature, expressed as a function of variables which are readily available at the regional scale. To this end, we analytically solve a simplified version of the energy-balance equation over an entire stream network (see Sect. 2.3.1). The resulting expression involves variables whose value cannot be estimated based on the available spatial data sets. Due to our lack of knowledge regarding the nature of the relationships between the unknown variables and the available data, we choose to rely on multi-linear regression to estimate the former as a function of the latter. Although this step involves the subjective selection of predictor variables and assumes a linear relationship, we do not think that it entirely questions our incentive to incorporate physical considerations into the model structure. As a matter of fact, only the unknown variables are replaced in the analytical formula, letting the global form of the relationship be unaffected. Assuming that the major non-linearities are already captured by the global structure of the model, the specific form of the expressions used to approximate the unknown terms may be considered to have a minor effect. Moreover, our approach attributes a physical meaning to some of the terms appearing in the formula. These terms can be constrained to remain within physical bounds, hereby restricting the range of values that the calibration parameters can adopt.

The objectives of the present work are three-fold: (1) describe a new physics-inspired statistical model for the prediction of stream temperature in ungauged basins, allowing for the computation of the monthly resolved annual cycle and capturing inter-annual variability; (2) through proper calibration of the model, determine the length of the upstream area which controls stream temperature at a given point; and (3) compare the physics-inspired model with a more standard statistical approach over a set of various Swiss catchments, so as to evaluate the potential benefits of the incorporation of physical considerations into the model structure. The data set used to evaluate the performances of the models is presented in Sect. 2.2. The



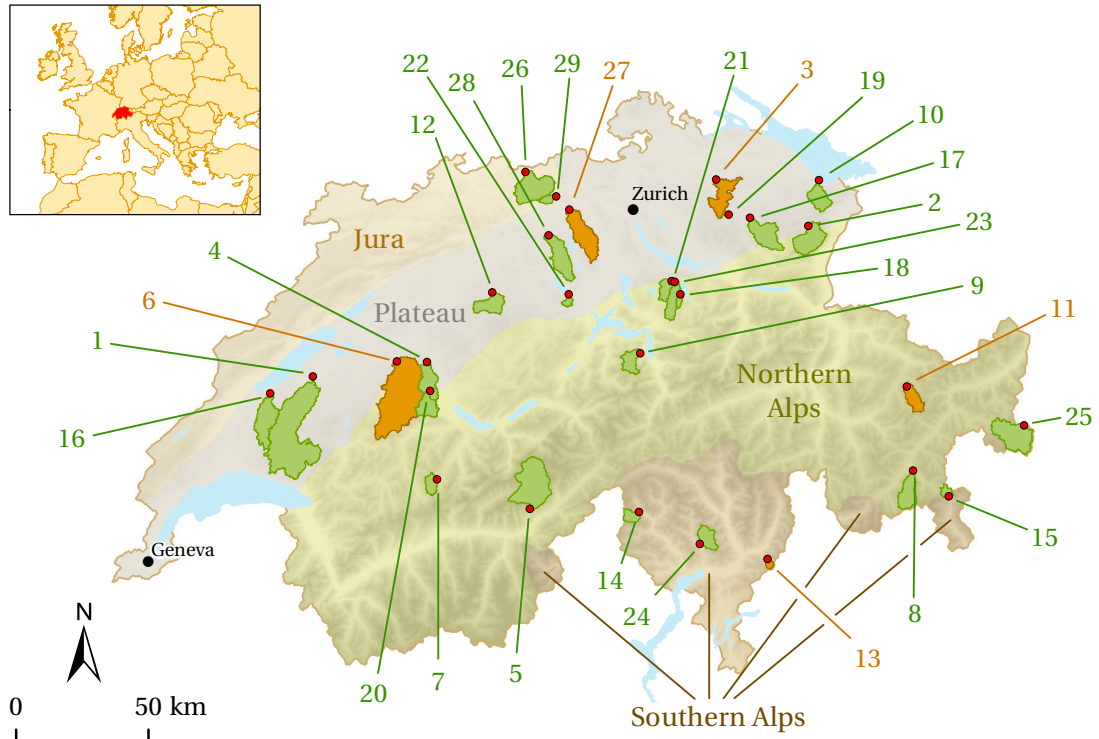


Figure 2.1: Locations of the gauging stations selected for the evaluation of the physics-inspired and standard statistical models. The stations are displayed as red points and their associated catchments as green or orange areas, depending on whether they are used to calibrate or validate the model. The four main climatic regions of Switzerland—the Jura mountains, Plateau, Northern Alps and Southern Alps—are displayed in different colours. The numbering corresponds to Table 2.2.

models are described in Sect. 2.3. Results are detailed in Sect. 2.4 and discussed in Sect. 2.5, followed by the conclusion.

## 2.2 Data description

### 2.2.1 Selected catchments for model evaluation

In order to test the two stream temperature models, catchments are selected in Switzerland such that (a) the natural regime of the river is as little affected by anthropogenic activities as possible, and (b) measurements of discharge and stream temperature are available for more than 1 year. This results in a set of 29 catchments, whose locations are depicted in Fig. 2.1 and physiographic properties are summarized in Table 2.2.

About half of the selected catchments are situated on the Swiss Plateau—a large area with little altitude variations between Lake Geneva in the south-west and Lake Constance in the north-east. The climate in this region is relatively mild, with precipitation mostly falling as rain

## Chapter 2. Stream temperature prediction in ungauged basins

Table 2.2: Physiographic properties of the 29 selected hydrological catchments in Switzerland. The three watersheds indicated in bold are not used for the model evaluation.

Basin number	Name	Area (km <sup>2</sup> )	Station altitude (m)	Mean altitude (m)	Glacier cover (%)	Hydrological regime <sup>a</sup>	Temperature measurement period	Data provider <sup>b</sup>
1	Broye at Payerne	392.0	441	710	0	Pluvial inferior	1976–2012	FOEN
2	Sitter at Appenzell	74.2	769	1252	0.1	Transition nival	2006–2012	FOEN
3	Murg at Wängi	78.0	466	650	0	Pluvial inferior	2002–2012	FOEN
4	Gürbe at Belp, Mülimatt	117.0	522	849	0	Transition pluvial	2007–2012	FOEN
<b>5</b>	<b>Massa at Blatten, Naters</b>	<b>195.0</b>	<b>1446</b>	<b>2945</b>	<b>65.9</b>	<b>Glacial</b>	<b>2003–2012</b>	<b>FOEN</b>
6	Sense at Thörishaus, Sense matt	352.0	553	1068	0	Pre-Alpine nivo-pluvial	2004–2012	FOEN
7	Allenbach at Adelboden	28.8	1297	1856	0	Alpine nival	2002–2012	FOEN
8	Rosegbach at Pontresina	66.5	1766	2716	30.1	Glacial	2004–2012	FOEN
<b>9</b>	<b>Grosstalbach at Isenthal</b>	<b>43.9</b>	<b>767</b>	<b>1820</b>	<b>9.3</b>	<b>Alpine nival</b>	<b>2005–2012</b>	<b>FOEN</b>
10	Goldach at Goldach, Bleiche	49.8	399	833	0	Pluvial superior	2005–2012	FOEN
11	Dischmabach at Davos, Kriegsmatte	43.3	1668	2372	2.1	Glacio-nival	2004–2012	FOEN
12	Langeten at Huttwil, Häberenbad	59.9	597	766	0	Pluvial inferior	2002–2012	FOEN
13	Riale di Roggiasca at Roveredo	8.1	980	1710	0	Meridional nivo-pluvial	2003–2012	FOEN
<b>14</b>	<b>Riale di Calneggia at Caviglioglio, Pontit</b>	<b>24</b>	<b>890</b>	<b>1996</b>	<b>3.0</b>	<b>Meridional nival</b>	<b>2002–2012</b>	<b>FOEN</b>
15	Poschiavino at La Rösä	14.1	1860	2283	0.4	Meridional nival	2004–2012	FOEN
16	Mentue at Yvonand, La Mauguettaz	105.0	449	679	0	Jurassian pluvial	2003–2012	FOEN
17	Necker at Mogelsberg, Aachsäge	88.2	606	959	0	Pluvial superior	2007–2012	FOEN
18	Grossbach at Gross, Säge	9.1	940	1276	0	Pre-Alpine nivo-pluvial	2003–2012	FOEN
19	Rietholzbach at Mosnang, Rietholz	3.3	682	795	0	Pluvial superior	2002–2012	FOEN
20	Gürbe at Burgistein, Pfandersmatt	53.7	569	1044	0	Pre-Alpine nivo-pluvial	2007–2008	FOEN
21	Biber at Biberbrugg	31.9	825	1009	0	Pluvial superior	2003–2012	FOEN
22	Sellenbodenbach at Neuenkirch	10.5	515	615	0	Pluvial superior	2003–2012	FOEN
23	Alp at Einsiedeln	46.4	840	1155	0	Transition pluvial	2003–2012	FOEN
24	Riale di Pincascia at Lavertezzo	44.4	536	1708	0	Meridional nivo-pluvial	2004–2012	FOEN
25	Rom at Müstair	129.7	1236	2187	0.1	Meridional nival	2003–2012	FOEN
26	Sissle at Eiken	123.0	314	529	0	Jurassian pluvial	2004–2012	Aargau
27	Bünz at Othmarsingen	110.6	390	526	0	Pluvial inferior	2005–2012	Aargau
28	Wyna at Unterkulm	92.1	455	643	0	Pluvial inferior	2005–2012	Aargau
29	Talbach at Schinznach-Dorf	14.5	358	559	0	Jurassian pluvial	2009–2012	Aargau

<sup>a</sup> According to the classification by Aschwanden and Weingartner (1985).

<sup>b</sup> FOEN: Swiss Federal Office for the Environment, Aargau: Department for Construction, Transport and Environment of Canton Aargau.

in winter and mean daily maximum air temperature hardly exceeding 30 °C in summer. The hydrological regimes of the catchments in the plateau depend on the precipitation patterns and are therefore strongly variable from year to year (Aschwanden and Weingartner, 1985). Discharge does not vary by more than a factor 2 over the year; it usually reaches its maximum during winter, when evapotranspiration is the lowest. As catchments gain in altitude, the discharge control mechanism changes from evapotranspiration to snowmelt: higher-altitude catchments present a discharge peak during the melt season, in April–May.

Only two catchments are found in the Jura mountains, a relatively low-altitude (< 1700 m) mountainous range with rigorous winters. This region is characterized by its karstic aquifers with preferential flow paths, generating fast and complex responses to precipitation events. Although more marked, the hydrological regimes of the Jura catchments are relatively similar to those of the watersheds in the plateau. A clear peak in discharge is noticeable in April for the highest catchments (Aschwanden and Weingartner, 1985).

The Alpine region of Switzerland is typically subdivided into its northern and southern parts, based on their difference in climate. The Southern Alps are influenced by Mediterranean weather, implying warmer winters and more precipitation in autumn than in the Northern Alps. The hydrological regimes of the catchments in the Northern Alps are strongly related to altitude. The month in which the peak of discharge is observed ranges from May for low-altitude watersheds to July–August for catchments partially covered by glaciers. Moreover, the ratio of annual maximum to annual minimum discharge increases with altitude. Similar hydrological regimes are observed in the Southern Alps, except for a second discharge peak in autumn due to rainfall (Aschwanden and Weingartner, 1985). As seen in Fig. 2.1, only three unperturbed catchments could be found in the Northern Alps, while five are located in the Southern Alps.

All in all, 10 of the 16 hydrological regimes identified by Aschwanden and Weingartner (1985) in Switzerland are present among the 29 selected catchments (see Table 2.2). The surface area distribution is quite large, with catchments ranging from 3.31 km<sup>2</sup> (Rietholzbach at Mosnang) to 392 km<sup>2</sup> (Broye at Payerne). The mean altitudes of the watersheds also span a wide range of values. Few catchments are partially covered by a glacier, with only two of them having a glacier cover fraction over 10 %.

### 2.2.2 Stream temperature data

The stream temperature data which are used in the present study were provided by the Swiss Federal Office for the Environment (FOEN). Advantage is taken of the present publication to describe this new data set, which is freely accessible for research purposes at the following address: <http://www.bafu.admin.ch/wasser/13462/13494/15076/index.html?lang=en>. A map displaying the position of all available hydrological stations which measure stream temperature can also be found on the website of the FOEN.<sup>1</sup>

<sup>1</sup>See [http://www.hydrodaten.admin.ch/en/messstationen\\_temperatur.html](http://www.hydrodaten.admin.ch/en/messstationen_temperatur.html)

## Chapter 2. Stream temperature prediction in ungauged basins

---

The FOEN operates an automatic network of stream gauging stations, continuously measuring water level and discharge at more than 180 locations in Switzerland. Water level is recorded using an ultrasonic distance sensor and converted into discharge values through a rating curve adapted each year. The water level values are validated against the measurements of a second instrument—a pressure probe—and rejected in case the difference between the two values is greater than 2 cm. A limited number of gauging stations has been equipped with a thermometer, the earliest starting in 1968. This number has increased greatly since 2002, with now more than 70 stations automatically probing water temperature every 10 min (Jakob, 2010). The measurement values are automatically uploaded and displayed in real time on the webpage of the FOEN (same page as for the map displaying the positions of the stations).

Among the watersheds in which temperature is monitored, 25 have been identified in the present study as being little affected by anthropogenic activities. In order to complete this data set, the temperature and discharge measurements of four additional gauging stations were obtained from the Department for Construction, Transport and Environment of Canton Aargau (see Table 2.2). The period in which water temperature was measured by each station is also indicated in Table 2.2.

The temperature data are usually not quality-proofed by the FOEN or Canton Aargau. As a validation procedure, we performed two different tests on the data at the hourly time step, on top of visual inspection.

- a. All temperature measurements lower than 0°C or greater than 30°C were removed, except for the values between –0.5 and 0°C, which were set to 0°C, and the values between 30 and 30.5°C which were set to 30°C. Although the limit of 30°C might be naturally reached in shallow areas, some temperature series showed clear evidence that such temperature was recorded as a result of the sensor being out of water. As a consequence, it was decided to remove all data points above 30°C, potentially discarding correct data.
- b. The temperature variation between consecutive time steps was checked to remain within physical bounds. In particular, it was verified that temperature varied by more than 0.01°C over 5 h, but less than 3°C within 1 h. Constant temperature values could result from a defect in the sensor, but also from the fact that the hourly values had been replaced with their daily mean in some cases. In order to distinguish between the two, the present quality control procedure was performed semi-manually.

After quality control, the hourly data were aggregated into monthly mean values.

### 2.2.3 Meteorological data

The two statistical models described in Sect. 2.3 use monthly mean air temperature and incoming solar radiation as predictor variables. Data for these variables were obtained from

the Swiss Meteorological Office (MeteoSwiss), which provides free access to them for research purposes. For each one of the selected catchments described in Sect. 2.2.1, the air temperature and incoming solar radiation values measured by all the meteorological stations located at less than 20 km from the catchment outlet were collected. In case fewer than three stations could be found within a 20 km radius, data from the three closest meteorological stations were retained. The value of 20 km was chosen so as to ensure that data interpolations would remain representative of the climatic conditions at the catchment outlet, while being based on three stations at least. In fact, 27 of the 29 selected catchments are entirely contained within the disk of radius 20 km centered on their respective outlet point (not shown). As such, the collected meteorological data can actually be considered as representative for the entire catchments, and not just for their outlet point.

We were provided with hourly mean data, which we aggregated into monthly mean values. We did not perform any quality checks on the data, since MeteoSwiss already follows strict quality control procedures.<sup>2</sup>

Among its network of operated meteorological stations, MeteoSwiss selected a subset of 14 stations which are considered to be representative of the climate diversity in Switzerland.<sup>3</sup> These stations, referred to as “reference stations” in the following, are used by the standard statistical model to estimate the monthly mean air temperature over the entire Swiss territory (see Sect. 2.3.2).

### 2.2.4 Thermal regime classification

A preliminary study of the selected catchments was performed, with the aim of classifying the rivers according to their thermal behaviour. This classification was intended to be used later in order to investigate whether the performance of the models was affected by the river thermal regime.

As a first attempt, we examined whether the catchments could be classified based on the shape of their stream temperature curve. To this end, we *z* scored (i.e. standardized) the monthly mean stream temperature values in each watershed similarly to Garner et al. (2014). However, as observed by these authors, we could identify only one single thermal regime (Fig. 2.2a). Only two catchments among the 29 did not to present the same thermal regime as the others, namely those labelled as 5 and 14 in Table 2.2.

As an alternative approach, we tested whether the characteristics of the stream–air temperature curve could be used to characterize the thermal regime of the catchments. For this purpose, monthly mean stream temperature was linearly regressed against monthly mean air temperature, excluding the points with negative air temperature values (e.g. Kelleher et al.,

<sup>2</sup>For more information, see <http://www.meteosuisse.admin.ch/home/systemes-de-mesure-et-de-prevision/gestion-des-donnees/preparation-des-donnees.html>; webpage only available in German, French or Italian.

<sup>3</sup>See <http://www.meteoswiss.admin.ch/home/climate/past/homogenous-monthly-data.html>; description only available in German, French or Italian.

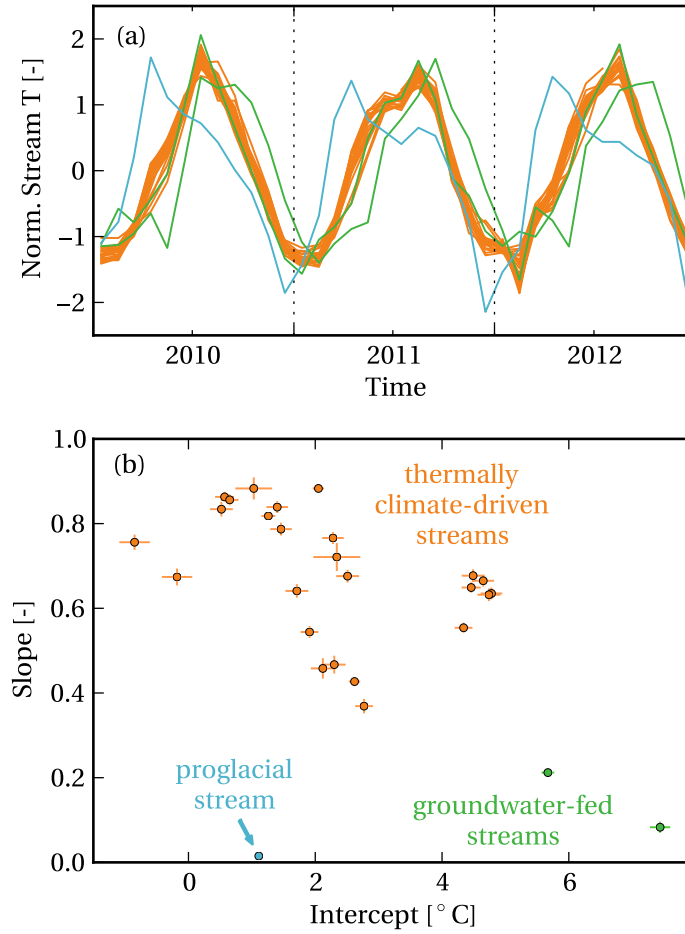


Figure 2.2: Classification of the thermal regimes of the selected catchments. Streams impacted by groundwater infiltration are shown in green, the proglacial stream in blue and the thermally climate-driven streams in orange. **(a)** Normalized monthly mean stream temperature curves over 3 consecutive years (2010–2012); all curves are  $z$  scored independently each year. **(b)** Slopes and intercepts of the regression lines fitted to the stream–air temperature points of the respective catchments. All points with negative air temperature values have been discarded prior to fitting. The bars indicate the standard error estimates.

2012). Based on the values of the slope and intercept of this relationship, three groups of catchments could be clearly identified (Fig. 2.2b). The first group contains the watersheds in which a significant portion of discharge originates from deep aquifer infiltration (watersheds 9 and 14 in Table 2.2, labelled as “groundwater-fed streams” in Fig. 2.2b). This group is characterized by low slope and high intercept values, as reported by many studies (e.g. Caissie, 2006; Webb et al., 2008). The second group of watersheds corresponds to the high-altitude basins with more than 50 % glacier cover. Both the slope and intercept of the stream–air temperature relationship are small for the members of this group, which is actually composed of only one catchment (watershed 5 in Table 2.2, denoted as “proglacial” in Fig. 2.2b). The vast majority

of the watersheds do not fall into any of the two aforementioned groups. These catchments, denoted as “thermally climate-driven”, are characterized by relatively low intercept and high slope values; i.e. their stream temperature is strongly correlated with air temperature.

Because of the predominance of the thermally climate-driven streams, only the latter will be considered for the testing of the physics-inspired and standard regression models. The inclusion of the groundwater-dominated streams in the test set would require the amount of groundwater discharging into the stream to be estimated. We tested several methods, including the derivation of the baseflow index from discharge measurements (e.g. Eckhardt, 2005; van Dijk, 2010) or from the TOPMODEL topographic index (e.g. Ducharne, 2009). However, none of the investigated techniques succeeded in predicting a larger baseflow index for the catchments labelled as “groundwater-fed” as compared to the others (not shown). Similarly, the consideration of the proglacial streams would imply the glacier cover fraction being included in the models. This addition of one calibration parameter was not considered justified given that this group contains only one catchment. In total, 26 catchments were used for the calibration and validation of the models, namely all those listed in Table 2.2 except watersheds 5, 9 and 14.

## 2.3 Formulations of the stream temperature models

The new physics-inspired statistical model for stream temperature prediction is derived in the following subsection. The standard statistical model used for comparison is presented in Sect. 2.3.2.

### 2.3.1 Physics-inspired statistical model

As mentioned above, the physics-inspired stream temperature model presented in this paper is based on the analytical solution to the stream energy-balance equation. This topic has been investigated extensively in the literature (e.g. Edinger et al., 1968; Theurer et al., 1984; Gosink, 1986; Polehn and Kinsel, 2000; Toffolon et al., 2010), although used only once for stream temperature prediction in ungauged basins (Bogan et al., 2003). In order to analytically solve the energy-balance equation, all studies relied on the linearization of the heat flux  $\phi_a$  at the air–water interface as a function of stream temperature  $T$ :  $\phi_a = -k(T - T_e)$ . Some of them assumed the heat transfer coefficient  $k$  to be constant and used prescribed functions of time, space or both to express the equilibrium temperature  $T_e$  (e.g. Gosink, 1986; Polehn and Kinsel, 1997; Daly, 2005). Other studies derived analytical formulations for  $k$  and  $T_e$  based on the physical expressions of the heat fluxes occurring at the stream–air interface (e.g. Edinger et al., 1968; Bogan et al., 2003; Caissie et al., 2005; Bustillo et al., 2014). While a minority of authors considered the temperature distribution to be spatially homogeneous (Edinger et al., 1968; Caissie et al., 2005; Bustillo et al., 2014), most of them assumed the stream to be in a steady state or, equivalently, the stream celerity to be constant. In addition, they all assumed the river width to remain constant along the stream so as to analytically solve the

energy-balance equation. Very few studies accounted for the heat exchange with the stream bed or the heat advected by lateral inflow of water (Bogan et al., 2004; Herb and Stefan, 2011). Bogan et al. (2003) were the only authors to evaluate their analytical expression over ungauged basins. They tested their model in the central and eastern United States, since this region has a topography flat enough for a meteorological station located even at more than 100 km from a given point to be still representative of the climate at that point. Their work is therefore hardly transferable to Switzerland, where the mountainous landscape prevents the proper interpolation of variables such as air humidity or wind speed, which are required as input by the model.

### Derivation of the analytical solution to the energy-balance equation

Assuming a well-mixed water column and a negligible longitudinal heat dispersion, the mass and energy-balance equations along a stream reach read (adapted from Westhoff et al., 2007)

$$\frac{\partial A}{\partial t} + \frac{\partial Q}{\partial x} = q_\ell, \quad (2.1)$$

$$\frac{\partial(AT)}{\partial t} + \frac{\partial(QT)}{\partial x} = \frac{w\phi_a + p\phi_b}{\rho c_p} + q_\ell T_\ell - Q \frac{g}{c_p} \frac{\partial z}{\partial x}, \quad (2.2)$$

where  $w$  (m),  $p$  (m),  $A$  (m<sup>2</sup>),  $Q$  (m<sup>3</sup> s<sup>-1</sup>) and  $T$  (°C) denote the width, wetted perimeter, cross-sectional area, discharge and temperature of the stream, respectively;  $t$  (s) refers to time,  $x$  (m) to the downstream distance,  $z$  (m) to altitude, and  $g$  (m s<sup>-2</sup>) to the gravitational acceleration. The water mass density  $\rho$  (kg m<sup>-3</sup>) and the specific heat capacity of water  $c_p$  (J °C<sup>-1</sup> kg<sup>-1</sup>) are both assumed constant. The quantities  $\phi_a$  (W m<sup>-2</sup>) and  $\phi_b$  (W m<sup>-2</sup>) refer to the energy fluxes at the stream–air and stream–bed interfaces, respectively. The lateral heat fluxes due to the inflow of surface, fast subsurface and slow subsurface runoffs into the stream are merged into a single term,  $q_\ell T_\ell$ , where  $q_\ell$  (m<sup>2</sup> s<sup>-1</sup>) denotes the sum of these three runoffs per unit stream length and  $T_\ell$  (°C) stands for their mean temperature. The last term on the right-hand side of Eq. (2.2) corresponds to friction, which is usually neglected in stream temperature models (e.g. Sinokrot and Stefan, 1993; Westhoff et al., 2007), but has been shown by Hannah et al. (2004) and Leach and Moore (2014) to be an important term in the energy balance of small streams during winter.

The present study builds mainly upon the work of Theurer et al. (1984), which is one of those considering the less restrictive approximations for the derivation of the solution to Eqs. (2.1)–(2.2). Our own assumptions are the following.

- (i) At the timescale of the month, the stream temperature is assumed to be in a steady state.
- (ii) The energy flux at the stream–air interface is expressed as

$$\phi_a = \phi_r + k(T_a - T), \quad (2.3)$$



### 2.3. Formulations of the stream temperature models

where  $\phi_r$  ( $\text{Wm}^{-2}$ ) denotes the net radiative heat flux, incorporating both the short-wave and long-wave components. The second term on the right-hand side accounts for both the latent and sensible heat fluxes (e.g. Polehn and Kinsel, 1997; Toffolon et al., 2010), where the bulk heat transfer coefficient  $k$  ( $\text{Wm}^{-2}\text{°C}^{-1}$ ) between water and air is assumed to be constant, and  $T_a$  ( $\text{°C}$ ) refers to the air temperature.

- (iii) The energy flux at the stream–bed interface is neglected; i.e.  $\phi_b = 0$  (e.g. Bogan et al., 2003; Caissie et al., 2005; Bustillo et al., 2014).
- (iv) The lateral inflow of water  $q_\ell$  is assumed to be spatially constant (e.g. Biswal and Marani, 2010; Mutzner et al., 2013).
- (v) The ratio of stream width to discharge  $w/Q$  is assumed to be spatially constant, as opposed to Theurer et al. (1984) and Polehn and Kinsel (2000), who both assumed a constant stream width. This approximation also differs from the typical relationship used in fluvial geomorphology, which expresses stream width as a power-law function of discharge with exponent  $\sim 0.5$  (see e.g. Knighton, 1998). It allows for the definition of a characteristic stream length  $L_c$  (m),

$$L_c = \frac{c_p \rho Q}{w k}. \quad (2.4)$$

- (vi) All sources in the network are supposed to have the same discharge, denoted as  $Q_s$  in the following. This approximation is discussed in more detail later in this section.

Using the above assumptions, the mass and energy-balance equations simplify to Eqs. (2.5)–(2.6),

$$\frac{dQ}{dx} = q_\ell, \quad (2.5)$$

$$\frac{dT}{dx} = \frac{1}{L_c} (\gamma \phi_r + T_a - T) + \frac{q_\ell}{Q} (T_\ell - T) - \frac{g}{c_p} \frac{dz}{dx}, \quad (2.6)$$

where  $\gamma = 1/k$ . The reader is referred to Appendix A for the complete derivation of the analytical solution to these equations. Only the final expressions for discharge  $Q_{\text{out}}$  and stream temperature  $T_{\text{out}}$  at the outlet of a catchment are reported here,

$$Q_{\text{out}} = n_s Q_s + L_{\text{tot}} q_\ell, \quad (2.7)$$

$$T_{\text{out}} = \omega_1 \overline{T_s} + \omega_2 \langle T_\ell \rangle_{\mathcal{L}} + \omega_3 \langle \gamma \phi_r + T_a - L_c \frac{g}{c_p} \frac{dz}{dx} \rangle_{\mathcal{L}}, \quad (2.8)$$

with

$$\omega_1 = (1 - \eta) \delta_s, \quad (2.9)$$

$$\omega_2 = \eta \delta_\ell, \quad (2.10)$$

$$\omega_3 = 1 - \omega_1 - \omega_2. \quad (2.11)$$

In the above equations,  $L_{\text{tot}}$  and  $n_s$  correspond to the total length of the river network and the number of sources in the catchment, respectively. The operator  $\langle \cdot \rangle_{\mathcal{L}}$  refers to the distance-weighted average; it computes the average of its operand over the entire stream network using a weight equal to  $\exp(-d/L_c)$ , where  $d$  denotes the distance to the catchment outlet. This operator gives much more emphasis to the points located near to the catchment exit. It should be noted that the spatial extent of the area over which the average is computed is controlled by the characteristic length  $L_c$ : the smaller  $L_c$ , the smaller the contributing area. The quantity  $\overline{T_s}$  appearing in Eq. (2.8) denotes the weighted average of water temperature at the network sources. The latter are weighted by a factor  $\exp(-d_{s,i}/L_c)$ , where  $d_{s,i}$  is the distance along the stream between the  $i$ th source point and the catchment outlet. The weights  $\omega_1$ ,  $\omega_2$  and  $\omega_3$  are all in the interval  $[0, 1]$ . In Eqs. (2.9)–(2.10), the factor  $\eta$  refers to the fraction of discharge at the catchment outlet originating from lateral inflow of water along the stream network—i.e. excluding the fraction coming from the sources,

$$\eta = \frac{q_{\ell} L_{\text{tot}}}{Q_{\text{out}}} = 1 - \frac{n_s Q_s}{Q_{\text{out}}}. \quad (2.12)$$

The two factors  $\delta_s$  and  $\delta_{\ell}$  are defined as

$$\delta_s = \frac{1}{n_s} \sum_{i=1}^{n_s} e^{-d_{s,i}/L_c}, \quad (2.13)$$

$$\delta_{\ell} = \frac{L_c}{L_{\text{tot}}} \sum_{k=1}^{n_r} e^{-d_k/L_c} (1 - e^{-L_k/L_c}), \quad (2.14)$$

where  $n_r$  denotes the number of reaches in the stream network,  $d_k$  the streamwise distance between the downstream point of stream reach  $k$  and the catchment outlet, and  $L_k$  the length of stream reach  $k$ . The factor  $\delta_s$  corresponds to the average of the weight  $\exp(-d(x)/L_c)$  over all the network sources, and the factor  $\delta_{\ell}$  refers to the average of the same weight over the set of all stream reaches in the catchment. It follows that both  $\delta_s$  and  $\delta_{\ell}$  decrease roughly exponentially as a function of the network length.

Equation (2.8) expresses stream temperature as a linear function of air temperature, the slope of the regression line between the two being equal to  $\omega_3 = 1 - \omega_1 - \omega_2$ . Assuming  $\eta$  to vary only slightly along the network, it can be seen in Eqs. (2.9) and (2.10) that  $\omega_1$  and  $\omega_2$  decrease roughly exponentially with the stream network length. As a consequence, the present model predicts  $\omega_3$  to tend towards 1 as the catchment size increases, a fact which has been observed at many locations (e.g. Ozaki et al., 2003; Ducharne, 2008; Kelleher et al., 2012; Chang and Psaris, 2013; Segura et al., 2014).

The present expression for  $T_{\text{out}}$  differs from those reported previously in the literature in at least two aspects (see Sect. 2.1 for a review of the analytical solutions to the energy-balance equation published to date). First, the terms on the right-hand side of Eq. (2.6) were not assumed to be spatially homogeneous when integrating them. This explains the presence of the spatial averaging operator  $\langle \cdot \rangle_{\mathcal{L}}$  in Eq. (2.8), which in turn translates the fact that stream

### 2.3. Formulations of the stream temperature models

temperature is not impacted by local conditions only. This operator has already been used for the computation of predictor variables in regression-based stream temperature models (Isaak et al., 2010; Hill et al., 2013), but never in association with analytical solutions to the energy-balance equation. Second, the source and lateral inflow terms have not been neglected. These two terms are weighted by the factors  $\omega_1$  and  $\omega_2$  in Eq. (2.8), respectively, and tend to decrease exponentially with the stream length (see discussion above). Although negligible in large catchments, they might be of the same order of magnitude as the heat exchange term in small watersheds. Only a few studies relying on an analytical expression for stream temperature modelling have considered the lateral inflow term to date (Bogan et al., 2004; Herb and Stefan, 2011), and none has retained the source term.

As noted above, the extent of the zone over which  $\langle \cdot \rangle_{\mathcal{L}}$  averages its operand is controlled by the characteristic length  $L_c$ . Given that this length is a function of the river discharge-to-width ratio  $Q/w$  (see Eq. (2.4)) and that the stream celerity is assumed here to be constant,  $L_c$  is approximately proportional to the water height. Its value should therefore be expected to change over the course of the year. Based on a formula similar to Eq. (2.4), Herb and Stefan (2011) have estimated  $L_c$  to vary between 3 and 45 km for discharge values between 0.4 and 5.8 m<sup>3</sup> s<sup>-1</sup> in the case of the Vermillion River in Minnesota. As most of the catchments considered in the present study have discharges contained within this range, we should expect a marked variation in the values of  $L_c$  both during the course of the year and across catchments. However, since the characteristic length will be treated as a calibration parameter here (see Sect. 2.3.1), only its seasonal variability will be investigated. A single value will be assumed in each season for all the catchments (see Sect. 2.4), for otherwise  $L_c$  would have to be calibrated independently for each catchment, which would prevent prediction in ungauged basins. We acknowledge this as a limitation of our model.

#### Parametrization of the unknown terms

Equation (2.8) contains several unknown quantities. The procedure used to calculate their respective values is detailed below.

The channel slope  $dz/dx$  is computed along the centre line of each stream. A vector representation of the centre lines was extracted from a land cover map at scale 1 : 25 000.<sup>4</sup> This map was overlaid with a digital elevation model of Switzerland with 2 m horizontal resolution produced by the Swiss Federal Office of Topography<sup>5</sup> in order to extract the altitude of each point. As an alternative approach, a geomorphological analysis of the stream watersheds could have been performed so as to automatically extract the stream networks. However, it was observed that the results of this analysis did not match with the land cover map in some basins (not shown).

The monthly mean air temperature  $T_a$  along the streams is computed based on the values measured by the neighbouring meteorological stations (see Sect. 2.2.3). Within each catchment  $i$ ,

<sup>4</sup>See <http://www.swisstopo.admin.ch/internet/swisstopo/en/home/products/maps/national/25.html>

<sup>5</sup>See <http://www.swisstopo.admin.ch/internet/swisstopo/en/home/products/height/swissALTI3D.html>

air temperature  $T_{a,i}$  is assumed to be a linear function of altitude only,

$$T_{a,i}(z) = a_{T,i}(z - z_i) + b_{T,i}, \quad (2.15)$$

where  $z_i$  (m) refers to the altitude of the gauging station. The lapse rate  $a_{T,i}$  ( $^{\circ}\text{Cm}^{-1}$ ) is computed each month separately by regressing the air temperature measurements of the neighbouring meteorological stations against the station altitudes. In case the coefficient of determination  $R^2$  of the regression line is lower than 0.6,  $a_{T,i}$  is set equal to 0. The intercept  $b_{T,i}$  ( $^{\circ}\text{C}$ ) is computed each month as the inverse-distance-weighted average of the same air temperature measurements, which are first corrected for the altitude effect by virtually transferring them to altitude  $z_i$  using the lapse rate  $a_{T,i}$ .

The quantity  $\gamma\phi_r$ , which accounts for the effect of the net radiation heat flux at the air–water interface, cannot be readily computed based on the available data. As a matter of fact, long-wave radiation and reflected short-wave radiation measurements are performed by MeteoSwiss at a few locations only. Incoming short-wave radiation  $\phi_{\text{isw}}$  ( $\text{Wm}^{-2}$ ), on the other hand, is a commonly measured variable which can be interpolated along the stream networks. To this end, it is assumed that the incoming short-wave radiation  $\phi_{\text{isw},i}$  in each catchment  $i$  is a function of altitude only,

$$\phi_{\text{isw},i}(z) = a_{\phi,i}(z - z_i) + b_{\phi,i}, \quad (2.16)$$

where the lapse rate  $a_{\phi,i}$  ( $\text{Wm}^{-3}$ ) and the intercept  $b_{\phi,i}$  ( $\text{Wm}^{-2}$ ) are computed similarly to  $a_{T,i}$  and  $b_{T,i}$  in Eq. (2.15). An attempt is made to correct the values computed using Eq. (2.16) in order to account for riparian shading. As discussed in Sect. 2.1.5 above, very few spatial data sets exist for riparian shading, which in practice often has to be estimated using proxy variables. In the present case, riparian shading at a given stream point is approximated based on the stream orientation  $\theta$  and riparian forest cover  $f_i$  at that point. Using the land cover map at scale 1 : 25 000 mentioned above,  $\theta$  is computed as the cosine of the angle between north and the stream flow direction; it is a measure of northing, i.e. values close to 1 indicate a catchment that is oriented towards north and values close to  $-1$  a catchment that is south-oriented. The riparian forest cover  $f_i$  is defined here as the fraction of the riparian zone which is covered with forests according to the land cover map. As the extent of the riparian zone affecting stream temperature is unclear (Moore et al., 2005a), the forest cover fraction is computed over riparian buffers with different widths: 25, 50 and 100 m on each side of the centre line of the streams (total buffer widths are 50, 100 and 200 m, respectively). The map does unfortunately not allow for the distinction between coniferous and deciduous forests. In addition to  $\theta$  and  $f_i$ , topographical shading  $f_s$  is also computed in order to correct the incoming solar radiation values estimated from Eq. (2.16).  $f_s$  is expressed at each point along the streams as a value between 0 and 1, 1 indicating complete shading. It is derived from the above-mentioned 2 m digital elevation map of Switzerland at nine different hours of day time—corresponding to the fractions 0.1–0.9 of the day-time period—on the 15th day of each month of the year. These values are then averaged at each grid cell and in each season to obtain the spatial distribution

### 2.3. Formulations of the stream temperature models

of  $f_s$ . Since shading by topography and by the riparian forest does not only affect incoming solar radiation, but also incoming long-wave radiation, it was decided not to use the variables  $\theta$ ,  $f_f$  and  $f_s$  to directly modify the values of  $\phi_{\text{isw}}$ . Instead, it is the unknown term  $\gamma\phi_r$  which is approximated as a linear combination of  $\phi_{\text{isw}}$ ,  $\theta$ ,  $f_f$  and  $f_s$ :

$$\gamma\phi_r = a_{\phi,\text{isw}}\phi_{\text{isw}} + a_{\phi,s}f_s + a_{\phi,\theta}\theta + a_{\phi,f}f_f + b_\phi. \quad (2.17)$$

As discussed in Sect. 2.1.5, the choice of a linear relationship is motivated by our wish to keep the model simple and by our ignorance of the actual form of the function linking  $\gamma\phi_r$  to the above-mentioned predictor variables. A linear relationship also significantly simplifies the computation of the distance average of  $\gamma\phi_r$  using the operator  $\langle \cdot \rangle_{\mathcal{L}}$ . Equation (2.17) requires the calibration of five unknown coefficients, namely  $\{a_{\phi,x}\}_{x=\text{isw},s,\theta,f}$  and  $b_\phi$ . In order to limit the number of model parameters, this expression is not directly used as is, but more parsimonious formulations are evaluated instead. All possible sub-expressions involving any combination of either one or two of the predictor variables  $\{\phi_{\text{isw}}, \theta, f_f, f_s\}$  is considered for approximating  $\gamma\phi_r$ . It should be mentioned that the choice to consider expressions with at most two terms (plus the intercept) is arbitrary and only introduced to avoid equifinality issues (Beven, 2012). In total, 11 different models are tested for  $\gamma\phi_r$ —including the constant expression with only  $b_\phi$  as calibration parameter.

The two weights  $\omega_1$  and  $\omega_2$  cannot be readily estimated from Eqs. (2.9) and (2.10). While the values of the factors  $\delta_s$  and  $\delta_\ell$  can be easily derived from the vector representation of the stream network described above, the parameter  $\eta$  requires additional assumptions. It should be remembered that this parameter corresponds to the fraction of the outlet discharge which originates from lateral inflow. Assuming a typical power-law relationship between drainage area and discharge (e.g. Mutzner et al., 2013),  $\eta$  could in principle be approximated as the ratio between the area  $A_{\text{net}}$  drained by the network (excluding the area drained by the sources) and the total catchment area  $A_{\text{tot}}$ , raised to some power  $\alpha$ :  $\eta \sim (A_{\text{net}}/A_{\text{tot}})^\alpha$ . However, the computation of  $A_{\text{net}}$  would require a geomorphological analysis, which was discarded based on the discrepancy between the stream network predicted by this analysis and the observed one (see above). As alternative methods, we consider two different techniques for estimating  $\eta$ . The simplest approach assumes a constant single value for  $\eta$ , calibrated over all catchments. The second approach relies on the analytical expression for  $\eta$  presented in Eq. (2.12), in which the ratio  $Q_s/Q_{\text{tot}}$  is replaced with  $(A_s/A_{\text{tot}})^\alpha$ :

$$\eta = 1 - n_s \left( \frac{A_s}{A_{\text{tot}}} \right)^\alpha. \quad (2.18)$$

The calibration parameters of this second method correspond to the area  $A_s$  drained by a single source and the exponent  $\alpha$ .

In order to compute  $\overline{T_s}$  and  $\langle T_\ell \rangle_{\mathcal{L}}$  in Eq. (2.8), two different methods for the estimation of the source and lateral inflow temperatures are considered. In a first approximation, these two temperatures are assumed to be both constant and equal. The second method considers

## Chapter 2. Stream temperature prediction in ungauged basins

them to be linearly related to air temperature as measured at their respective altitudes. In other words, it expresses the temperature  $T_{s,i}$  of each source  $i = 1 \dots n_s$  and the lateral inflow temperature  $T_\ell(z)$  at any point with altitude  $z$  along the network as

$$T_{s,i} = a_w T_a(z_{s,i}) + b_w, \quad (2.19)$$

$$T_\ell(z) = a_w T_a(z) + b_w, \quad (2.20)$$

where  $z_{s,i}$  (m) denotes the altitude of source  $i$ , and  $a_w$  ( $^{\circ}\text{C}^{\circ}\text{C}^{-1}$ ) and  $b_w$  ( $^{\circ}\text{C}$ ) are two parameters to be calibrated over the set of all catchments. Notice that the same slope  $a_w$  and intercept  $b_w$  are used to derive both  $T_{s,i}$  and  $T_\ell$  from air temperature, hereby assuming that the source and lateral inflows originate from the same hydrological processes. Moreover, since these two parameters are the same for all catchments, it is implicitly supposed that the ratio of surface runoff to subsurface runoff is the same in all watersheds. As discussed in Sect. 2.2.4, this requires catchments to be classified by hydrological regime before  $a_w$  and  $b_w$  can be calibrated separately for each regime. In Eqs. (2.19)–(2.20), the monthly mean air temperature is computed in each catchment using Eq. (2.15).

The distance average of variables  $T_\ell$ ,  $\gamma\phi_r$ ,  $T_a$  and  $dz/dx$  are computed by discretizing the operator  $\langle \cdot \rangle_{\mathcal{L}}$  over the stream segments,

$$\langle f \rangle_{\mathcal{L}} = \frac{\sum_{k \in \Gamma} e^{-(d_k + L_k/2)/L_c} L_k f_k}{\sum_{k \in \Gamma} e^{-(d_k + L_k/2)/L_c} L_k}, \quad (2.21)$$

where  $f_k$  denotes the unweighted mean value of variable  $f$  along stream segment  $k$ ; the other quantities have been defined previously in Sect. 2.3.1. Except for the riparian forest cover  $f_r$ , which is derived over buffers of widths 25, 50 and 100 m, the unweighted means of all other quantities (namely  $\phi_{\text{isw}}$ ,  $f_s$ ,  $T_a$  and  $dz/dx$ ) along each stream segment are computed over a 20 m wide buffer centered around the centre line of the segment, as extracted from the vector representation of the stream network at scale 1 : 25 000 (see above). The value of 20 m is considered to be typical for the width of the streams investigated in the present study; although only this value has been tested, it is expected to have little impact on the computed averages. It should be noted that the expressions for  $\langle T_a \rangle_{\mathcal{L}}$  and  $\langle \phi_{\text{isw}} \rangle_{\mathcal{L}}$  both reduce to linear functions of the distance-weighted average of altitude along the stream network  $\langle z \rangle_{\mathcal{L}}$  as per Eqs. (2.15) and (2.17). The length  $L_k$  of stream reach  $k$  and the distance  $d_k$  between the downstream end of reach  $k$  and the catchment outlet are derived from the vector map of the stream network.

Replacing the terms in Eq. (2.8) with their above expressions, the stream temperature model reads

$$T_{\text{out}} = (1 - \eta)\delta_s(a_w \overline{T_a} + b_w) + \eta\delta_\ell(a_w \langle T_a \rangle_{\mathcal{L}} + b_w) + (1 - \delta_s - \eta\delta_s - \eta\delta_\ell)\langle T_{\text{eq}} \rangle_{\mathcal{L}}, \quad (2.22)$$

## 2.3. Formulations of the stream temperature models

Table 2.3: Calibration parameters of the physics-inspired statistical model.

Parameter	Defined in	Units	Calibration range	Physical constraints
$a_w$	Eqs. (2.19)–(2.20)	(°C °C <sup>-1</sup> )	Chosen so as to constrain $T_{s,i}$ and $T_\ell$ to the range 0–25 °C	Must be positive
$b_w$		(°C)		None
$a_{\phi, \text{isw}}$	Eq. (2.17)	(°C m <sup>2</sup> W <sup>-1</sup> )	Chosen so as to constrain $\gamma\phi_r$ to the range –20–20 °C	Must be positive
$a_{\phi, s}$		(°C)		Must be negative
$a_{\phi, \theta}$		(°C)		Must be negative
$a_{\phi, f}$		(°C)		None
$b_\phi$		(°C)		None
$\eta$	Eqs. (2.9)–(2.10)	(–)	0–1	None
$A_s$	Eq. (2.18)	(m <sup>2</sup> )	Chosen so as to constrain $\eta$ to the range 0–1	Must be positive
$\alpha$		(–)	0–3	None

where

$$T_{\text{eq}} = a_{\phi, \text{isw}} \langle \phi_{\text{isw}} \rangle_{\mathcal{L}} + a_{\phi, s} \langle f_s \rangle_{\mathcal{L}} + a_{\phi, \theta} \langle \theta \rangle_{\mathcal{L}} + a_{\phi, f} \langle f_f \rangle_{\mathcal{L}} + \langle T_a \rangle_{\mathcal{L}} - L_c \frac{g}{c_p} \left\langle \frac{dz}{dx} \right\rangle_{\mathcal{L}} + b_\phi. \quad (2.23)$$

The calibration parameters of the model are listed in Table 2.3. When testing a constant parametrization for the source and lateral inflow temperatures,  $a_w$  should be set to 0. Similarly, at least two of the coefficients  $\{a_{\phi, x}\}_{x=\text{isw}, s, \theta, f}$  are assumed equal to 0, as per the parametrization of the radiation term discussed above. Thus, between three and eight parameters must be calibrated, depending on the methods used to approximate the respective unknown variables in Eq. (2.8). Advantage is taken of the fact that each parameter can be interpreted from a physical point of view to restrict its associated calibration range (see Table 2.3). For example,  $\eta$  is imposed to adopt a value between 0 and 1 as per Eq. (2.12), and only positive values are considered for  $a_{\phi, \text{isw}}$  based on the fact that solar radiation is contributing positively to the net radiation heat flux. Moreover, six different values are tested for the characteristic length  $L_c$  used in the definition of  $\langle \cdot \rangle_{\mathcal{L}}$ : 1, 2, 4, 8, 16 and 32 km (see Sect. 2.4.2). All possible combinations of the different parametrizations of the model terms are tested for each one of these values of  $L_c$ . The model associated with the lowest value of the modified Akaike information criterion (AICc) is considered to be the best one among the tested set (e.g. Burnham and Anderson, 2002). As mentioned in Sect. 2.3.1, the model is calibrated in each season separately to account for the fact that the value of the parameter  $L_c$  varies over the year.

### 2.3.2 Standard regression model

In order to assess its performances, the physics-inspired statistical model described by Eq. (2.22) is compared with a more classical regression model which we developed based on a combination of some of the standard statistical approaches reviewed in Sect. 2.1. The regres-

sion model takes advantage of the fact that most stream temperature curves have a similar shape (see Sect. 2.2.4). This shape is first estimated by the model based on air temperature, before being mapped to the respective stream temperature curves of the catchments using a linear transformation.

The model assumes all streams to have the same  $z$  scored (i.e. standardized) temperature  $\hat{T}$  (–). The latter is related to the monthly mean temperature  $T_i$  of each individual catchment  $i$  through (see e.g. Garner et al., 2014)

$$T_i = \sigma_i \hat{T} + \bar{T}_i, \quad (2.24)$$

where  $\bar{T}_i$  (°C) and  $\sigma_i$  (°C) correspond to the annual mean and standard deviation of monthly mean stream temperature in catchment  $i$ , respectively. These two quantities are estimated each year independently using multi-linear regression (MLR) models. Although more sophisticated techniques could have been used, Wehrly et al. (2009) and Daigle et al. (2010) showed that MLR performs at least as well as several more complicated statistical methods for stream temperature prediction. The MLR models were constructed using similar predictor variables as in the physics-inspired statistical model, namely the annual mean and standard deviation of both air temperature and incoming short-wave radiation, the riparian forest cover fraction, stream channel slope, stream orientation, the difference in topographical shading between summer and winter, the number of sources in the network and the watershed area. All multi-linear models based on any possible subset of these variables were tested, with a maximum number of terms per model arbitrarily fixed to six. This limitation was introduced in order to avoid over-parametrization, but also to ensure that the number of parameters in the final standard regression model was about the same as in the physics-inspired model, hereby guaranteeing a more even comparison between the two. Multicollinearity issues were avoided by discarding MLR models whose variance inflation factor (VIF) exceeded 5. Each predictor variable was distance-averaged over the stream networks using the operator  $\langle \cdot \rangle_{\mathcal{L}}$ , as in the case of the physics-inspired statistical model. Different values of  $L_c$  were considered when applying this operator as per Eq. (2.21): 1, 2, 4, 8, 16 and 32 km. The best predicting MLR models for  $\bar{T}_i$  and  $\sigma_i$  were selected based on AICc.

In Eq. (2.24), the  $z$  scored stream temperature is computed each month based on a non-linear relationship with air temperature,

$$\hat{T} = \mu + \frac{\alpha - \mu}{1 + \exp\left(-\kappa(\hat{T}_a - \beta)\right)}, \quad (2.25)$$

where  $\mu$  (°C),  $\alpha$  (°C),  $\beta$  (°C) and  $\kappa$  (°C<sup>-1</sup>) are coefficients obtained through ordinary least squares regression, and  $\hat{T}_a$  (–) denotes the mean  $z$  scored air temperature over Switzerland.  $\hat{T}_a$  is obtained by averaging the  $z$  scored measurements of the 14 MeteoSwiss reference meteorolo-



logical stations (see Sect. 2.2.3),

$$\hat{T}_a = \frac{1}{14} \sum_{k=1}^{14} \frac{T_{a,k} - \bar{T}_{a,k}}{\sigma_{a,k}}. \quad (2.26)$$

In the above equation,  $T_{a,k}$  (°C) denotes the monthly mean air temperature measured at reference station  $k$ , and  $\bar{T}_{a,k}$  (°C) and  $\sigma_{a,k}$  (°C) refer to the annual average and standard deviation of  $T_{a,k}$  computed each year independently, respectively.

In summary, the standard regression model proceeds as follows to estimate stream temperature in an ungauged basin: (a) it first computes the mean  $z$  scored air temperature over Switzerland according to Eq. (2.26), based on the measurements of 14 meteorological stations, (b) it then uses  $\hat{T}_a$  to estimate the  $z$  scored stream temperature in any catchment as per Eq. (2.25), and finally (c) it converts  $\hat{T}$  to the actual stream temperature using Eq. (2.24), where the scaling coefficients  $\bar{T}_i$  and  $\sigma_i$  are estimated for the catchment of interest using MLR models. These different steps will be illustrated in more detail in Sect. 2.4.4.

## 2.4 Model evaluation

In order to rigorously evaluate the performance of the two models described in the previous section, 5 of the 26 selected catchments were removed from the data set to create an independent validation set (watersheds 3, 6, 11, 13 and 27, displayed in orange in Fig. 2.1). Caution was given to single out basins with different size, mean elevation and geographic location. Among the four climatic regions of Switzerland, only the Jura could not be represented in the validation set, given that only 1 station (number 26) among the 26 available was located in this area. A bootstrap on the validation stations was not possible because of too high computational requirements. Indeed, Burnham and Anderson (2002) recommend using at least 10 000 bootstrap samples, which led to a prohibitively high number of model evaluations in our case.

The measurement time period is also split into a calibration (2007–2012) and validation (all dates before and including 2006) period. Only the measurements performed by the calibration stations—whose drainage area is marked in green in Fig. 2.1—during the period 2007–2012 are used to calibrate the models. Four different validation sets can be formed with the remaining station months.

1. The data set containing the measurements of the validation stations during the calibration period. This set can be used to evaluate the ability of the models to make predictions in ungauged basins.
2. The data set containing the measurements of the calibration stations during the validation period. This set will be used to evaluate the precision of the models when predicting stream temperature in past or future years.

3. The data set formed by the measurements of the validation stations during the validation period. This set serves to evaluate the performance of the models when predicting stream temperature both in ungauged basins and in ungauged years.
4. The data set corresponding to the union of all three previous validation sets, which may be used to obtain a synthetic evaluation of the precision of the models.

The complete data set is almost equally subdivided into its calibration and validation parts, with the former containing 1223 station months and the validation sets 1–4 regrouping 360, 705, 204 and 1269 station months, respectively.

As mentioned in Sect. 2.3.1, the value of the characteristic stream length  $L_c$  is expected to change over the course of the year. In order to ease capturing of this variability, the physics-inspired statistical model is calibrated over each season separately. As such, the calibration and validation data sets are each subdivided into four groups, corresponding to winter (January–March), spring (April–June), summer (July–September) and autumn (October–December), respectively. Each one of these subgroups contains approximately one-fourth of the station months originally belonging to the parent group. The standard regression model is calibrated over all seasons at once, but is evaluated in each season separately so as to investigate a potential effect of the period of the year on its precision.

Since the physics-inspired model expresses stream temperature as a linear function of air temperature, it cannot reproduce the asymptotic behaviour of the former as the latter drops below 0 °C. Consequently, data points associated with negative air temperature values are removed from the data set before calibration (Kelleher et al., 2012). When evaluating the model over the validation sets, all stream temperatures predicted to be negative are replaced with 0 °C values.

In the following, the best seasonal formulations of the physics-inspired model are presented first. The precision of this model is then evaluated, and the influence of the stream network resolution on the model results investigated. Finally, comparison is made with the standard regression model. All the results presented in this section will be discussed and analysed in Sect. 2.5.

### 2.4.1 Model formulations

As mentioned in Sect. 2.3.1, the different possible formulations of the physics-inspired statistical model are ranked in each season according to their respective AICc value. AICc is preferred here over the classical definition of the Akaike information criterion (AIC) since it includes a correction term for finite-sized data sets (Burnham and Anderson, 2002). It should be mentioned that, following Burnham and Anderson (2002), AICc is computed by calibrating the models not over the calibration set only, but rather over the entire data set (i.e. both the calibration set and validation set 4). Only in a second time is each model calibrated over just

the calibration set, so as to evaluate its performances in terms of RMSE,  $R^2$  and bias.

Table 2.4 presents the best model formulations selected in each season, ranked according to their respective Akaike weights  $w_i$ . The latter corresponds to the probability of each model being a better descriptor of the observed data (according to information theory) as compared to the model with the minimum AICc value (Burnham and Anderson, 2002; Wagenmakers and Farrell, 2004). Considering models with  $w_i \leq 0.1$  to be statistically insignificant, it can be observed that only a few formulations were identified in each season as being relevant for stream temperature prediction. The characteristic stream length  $L_c$  is found to be consistent among these formulations, with a value of 4 km in spring, summer and autumn, and 8 km in winter, regardless of the formulation.

The model selection reveals the radiation term  $\gamma\phi_r$  to be preferentially expressed as a function of topographical shading  $f_s$  and riparian forest cover fraction  $f_r$ , or as a function of  $f_s$  alone. Among the tested buffer widths used to compute  $f_r$ , none of the three values 50, 100 or 200 m prevails significantly over the others. The order in which they appear in the ranked models varies depending on the season; for example in winter, forest cover computed over a 100 m wide buffer is expected to be a better predictor of  $\gamma\phi_r$  than forest cover over a 50 m wide buffer, whereas the opposite is true in spring. Focusing on each season separately, the linear coefficient associated with any given term is observed to have a fairly constant value among the different expressions tested for  $\gamma\phi_r$ . For example, the coefficient multiplying  $f_s$  remains within a narrow range (at most 1 °C large) in each season.

This behaviour is even more pronounced in the case of the term associated with the source and lateral inflow temperatures ( $T_s$  and  $T_\ell$ ). This term is expressed as a linear function of air temperature, whose slope  $a_w$  and intercept  $b_w$  are constant among the various model formulations in a given season (see Table 2.4). The values of  $a_w$  are observed to be rather low independently of the period of the year, which indicates a weak coupling between the stream source (or lateral inflow) temperature and air temperature. Moreover,  $a_w$  and  $b_w$  differ among the seasons in such a way that  $T_s$  and  $T_\ell$  are the least coupled to air temperature in winter and the most in summer.

The model ranking based on AICc also identified a single expression for  $\eta$  in each season. This parameter is found equal to 1 in summer and autumn, and 0 in winter. Its expression is slightly more complicated in spring, where the selected formulation is the one based on the source drainage area (see Sect. 2.3.1).

### 2.4.2 Model performance

The RMSE,  $R^2$  and bias of the best selected model formulation in each season—i.e. the one with  $w_i = 1$ —are reported in Table 2.5. Based on the results of the evaluation over validation set 4, the model precision is observed to be rather satisfactory. Its RMSE and  $R^2$  are relatively constant over the year (about 1.3 °C and 0.87, respectively), except in winter where the value of

## Chapter 2. Stream temperature prediction in ungauged basins

Table 2.4: Formulations of the physics-inspired statistical model selected in each season based on their corresponding AICc value. The Akaike weights are denoted as  $w_i$ . Only the model formulations with  $w_i \geq 0.1$  are presented here. The widths of the buffers used to compute the riparian vegetation cover are indicated as subscripts of the variable  $f_f$  (the indicated values correspond to the total buffer widths, i.e. accounting for both sides of the stream centre line).

Season	$w_i$	$L_c$ (km)	Formulation of $\gamma\phi_r$	Formulation of $T_s$ and $T_\ell$	Formulation of $\eta$
Winter	1	8	$\gamma\phi_r = a_{\phi,s}f_s + a_{\phi,f}f_{f,100m} + b_\phi$ , with $a_{\phi,s} = 18.2^\circ\text{C}$ , $a_{\phi,f} = -2.9^\circ\text{C}$ and $b_\phi = -12.1^\circ\text{C}$	$T_s = a_w T_a + b_w$ , with $a_w = 0.15$ and $b_w = 3.1^\circ\text{C}$	$\eta = 0$ (constant)
	0.25		$\gamma\phi_r = a_{\phi,s}f_s + b_\phi$ , with $a_{\phi,s} = 19.4^\circ\text{C}$ and $b_\phi = -14.1^\circ\text{C}$		
	0.15		$\gamma\phi_r = a_{\phi,s}f_s + a_{\phi,f}f_{f,50m} + b_\phi$ , with $a_{\phi,s} = 19.3^\circ\text{C}$ , $a_{\phi,f} = -0.4^\circ\text{C}$ and $b_\phi = -13.9^\circ\text{C}$		
Spring	1	4	$\gamma\phi_r = a_{\phi,s}f_s + a_{\phi,f}f_{f,50m} + b_\phi$ , with $a_{\phi,s} = 12.9^\circ\text{C}$ , $a_{\phi,f} = -3.7^\circ\text{C}$ and $b_\phi = -11.3^\circ\text{C}$	$T_s = a_w T_a + b_w$ , with $a_w = 0.27$ and $b_w = 5.3^\circ\text{C}$	$\eta = 1 - n_s(A_s / A_{\text{tot}})^\alpha$ , with $A_s = 0.13 \text{ km}^2$ and $\alpha = 1$
	0.86		$\gamma\phi_r = a_{\phi,s}f_s + a_{\phi,f}f_{f,200m} + b_\phi$ , with $a_{\phi,s} = 13.1^\circ\text{C}$ , $a_{\phi,f} = -3.4^\circ\text{C}$ and $b_\phi = -11.6^\circ\text{C}$		
	0.53		$\gamma\phi_r = a_{\phi,s}f_s + b_\phi$ , with $a_{\phi,s} = 13.1^\circ\text{C}$ and $b_\phi = -12.7^\circ\text{C}$		
	0.31		$\gamma\phi_r = a_{\phi,s}f_s + a_{\phi,f}f_{f,100m} + b_\phi$ , with $a_{\phi,s} = 13.4^\circ\text{C}$ , $a_{\phi,f} = -2.2^\circ\text{C}$ and $b_\phi = -12.3^\circ\text{C}$		
Summer	1	4	$\gamma\phi_r = a_{\phi,s}f_s + a_{\phi,f}f_{f,100m} + b_\phi$ , with $a_{\phi,s} = 13.4^\circ\text{C}$ , $a_{\phi,f} = -0.3^\circ\text{C}$ and $b_\phi = -13.0^\circ\text{C}$	$T_s = a_w T_a + b_w$ , with $a_w = 0.33$ and $b_w = 6.6^\circ\text{C}$	$\eta = 1$ (constant)
	0.15		$\gamma\phi_r = a_{\phi,s}f_s + b_\phi$ , with $a_{\phi,s} = 13.4^\circ\text{C}$ and $b_\phi = -13.1^\circ\text{C}$		
Autumn	1	4	$\gamma\phi_r = a_{\phi,s}f_s + b_\phi$ , with $a_{\phi,s} = 10.4^\circ\text{C}$ and $b_\phi = -5.9^\circ\text{C}$	$T_s = a_w T_a + b_w$ , with $a_w = 0.25$ and $b_w = 5.1^\circ\text{C}$	$\eta = 1$ (constant)
	0.54		$\gamma\phi_r = a_{\phi,s}f_s + a_{\phi,f}f_{f,100m} + b_\phi$ , with $a_{\phi,s} = 10.0^\circ\text{C}$ , $a_{\phi,f} = -2.8^\circ\text{C}$ and $b_\phi = -4.7^\circ\text{C}$		
	0.48		$\gamma\phi_r = a_{\phi,s}f_s + a_{\phi,f}f_{f,200m} + b_\phi$ , with $a_{\phi,s} = 10.1^\circ\text{C}$ , $a_{\phi,f} = -2.9^\circ\text{C}$ and $b_\phi = -4.7^\circ\text{C}$		
	0.4		$\gamma\phi_r = a_{\phi,s}f_s + a_{\phi,f}f_{f,50m} + b_\phi$ , with $a_{\phi,s} = 10.2^\circ\text{C}$ , $a_{\phi,f} = -2.2^\circ\text{C}$ and $b_\phi = -5.1^\circ\text{C}$		

Table 2.5: Performance of the best ( $w_i = 1$ ) physics-inspired statistical model in each season in terms of RMSE,  $R^2$  and bias, depending on the validation set. Columns 1 to 4 below each error measure refer to the different validation sets (see beginning of Sect. 2.4).

Season	RMSE (°C)				$R^2$ (-)				Bias (°C)			
	1	2	3	4	1	2	3	4	1	2	3	4
Winter	1.34	1.34	1.58	1.38	0.68	0.40	0.52	0.55	-0.58	-0.30	-0.84	-0.47
Spring	1.51	1.29	1.57	1.40	0.87	0.90	0.86	0.88	0.24	0.02	0.36	0.14
Summer	1.07	1.47	1.13	1.31	0.91	0.84	0.90	0.87	-0.04	0.01	-0.01	-0.01
Autumn	1.16	1.22	1.47	1.25	0.89	0.87	0.84	0.87	-0.49	0.15	-0.34	-0.11
All year	1.28	1.33	1.45	1.34	0.94	0.94	0.93	0.94	-0.22	-0.03	-0.21	-0.11

the coefficient of determination is much lower (0.55). Similarly, the bias is small in all seasons ( $-0.11$  to  $0.14$  °C) apart from winter ( $-0.47$  °C).

Regarding the different validation sets, it can be observed in Table 2.5 that the model performs better when predicting in ungauged catchments as compared to simulating past or future years. Indeed, the RMSE values computed using validation set 1 are smaller than those based on set 2, particularly in winter, autumn and summer. Similarly, the values of  $R^2$  are higher over set 1 than over set 2, despite the fact that the model bias is larger over the former set as compared to the latter. As expected, the weakest model performances are generally associated with validation set 3, which contains the measurements performed by the validation stations during the validation period. The only noticeable exception is in summer, where the model evaluation over set 3 provides satisfactory results (RMSE =  $1.13$  °C,  $R^2 = 0.90$ , bias =  $-0.01$  °C).

### 2.4.3 Influence of the stream network resolution

The results reported above are based on the stream network geometries extracted from the land cover map at scale 1 : 25 000 (see Sect. 2.3.1). These geometries directly affect the values of the distance-averaged predictor variables, since the operator  $\langle \cdot \rangle_{\mathcal{L}}$  averages over the entire stream network. As a consequence, modifying the network resolution is expected to impact the model performance.

To test this hypothesis, two additional stream networks with a coarser resolution than the original one were investigated. These networks were obtained by removing stream segments with Strahler order 1, and those with Strahler order 1 and 2, respectively. Through this procedure, the mean drainage density of the 26 selected catchments decreased from  $2.1 \text{ km km}^{-2}$  for the original network to  $0.5 \text{ km km}^{-2}$  for the coarsest one, passing through  $1.0 \text{ km km}^{-2}$  for the intermediate-resolution network. The different model formulations were evaluated over the two additional networks using the same procedure as described in the previous section. Although the results are not reported here, it was essentially observed that the network resolution had little influence on the ranking of the model formulations based on AICc in each season. Almost all selected models were associated with a characteristic stream length

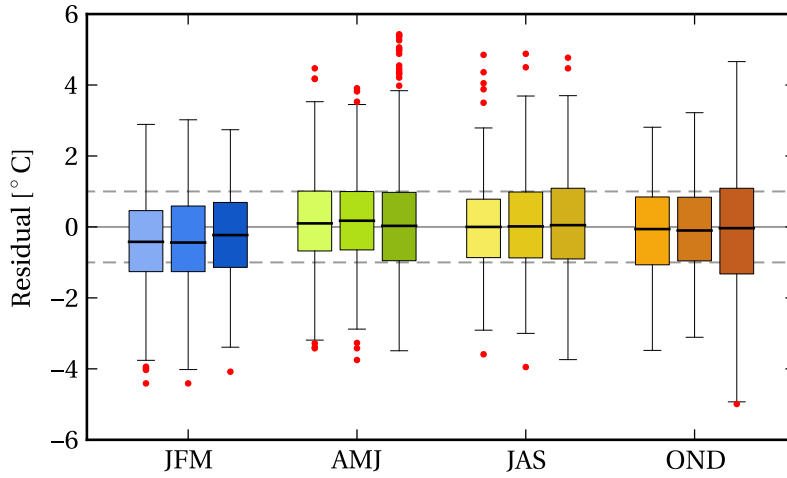


Figure 2.3: Prediction error of the physics-inspired statistical model for different resolutions of the stream network. The boxes extend from the first to the third quartile of the error distribution. Outliers are displayed as red dots. In each season, the network resolution decreases from left to right: the left box corresponds to the network with all stream reaches, whereas the central and right boxes contain only the stream segments whose Strahler order is greater than or equal to 2 and 3, respectively. The error values 0,  $-1$  and  $+1$  °C are displayed as a solid grey line and two dashed grey lines.

$L_c = 4$  or  $8$  km, as in the case of the original stream network. The parametrization of the net radiation heat flux  $\gamma\phi_r$  was also similar to the one reported in Table 2.4. Topographical shading and riparian forest cover remained the two most statistically significant predictors for this term, except during winter, where stream orientation appeared as a relevant variable. The values of the coefficients  $a_w$  and  $b_w$  were noted to vary little among the selected model formulations in a given season. Finally, the parameter  $\eta$  was preferentially expressed as a constant term. Its value was identified as being 0 in all seasons except summer in the case of the intermediate-resolution stream network, whereas its parametrization was close to the one described in Table 2.4 in the case of the coarser network.

As a consequence of the little influence of the network resolution on the model parametrization, few variations in the model precision were observed between the three stream networks. As seen in Fig. 2.3, no clear tendency can be identified among the residuals. At most, a small increase in the model prediction error can be detected for the coarsest network as compared to the first two, especially in autumn. The largest absolute residuals are also observed to be generated by this network. On the other hand, the strong bias previously noted in winter is present in the case of the intermediate resolution network, but less so in the case of the coarsest resolution one.

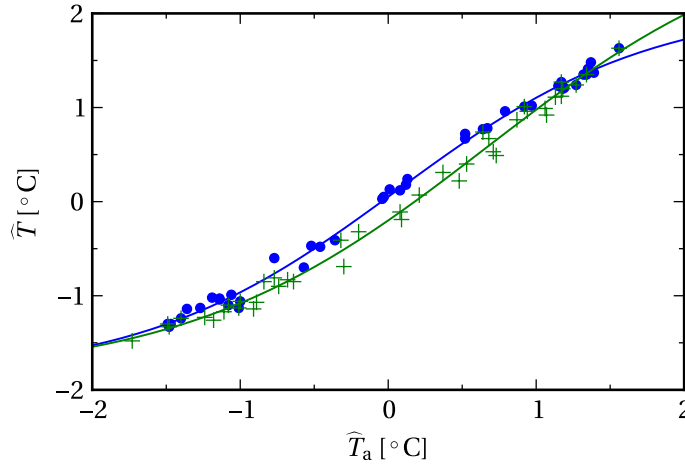


Figure 2.4: Non-linear relationship between the  $z$  scored stream temperature  $\hat{T}$  and the  $z$  scored air temperature  $\hat{T}_a$  averaged over 14 reference meteorological stations. The values of  $\hat{T}$  are obtained by averaging in each month the  $z$  scored stream temperatures measured at the 21 calibration stations. Each point corresponds to a single month of the calibration period 2007–2012. Months from January to June are displayed as green crosses, and those from July to December as blue dots. The two solid lines correspond to the respective fits of the data points in the two year halves (see Eqs. 2.27–2.28).

#### 2.4.4 Comparison with the standard regression model

This section describes the characteristics of the calibrated standard regression model first, before presenting the results of its evaluation in a second step. Figure 2.4 pictures the observed monthly mean stream temperature,  $z$  scored and averaged over the 21 calibration stations, as a function of  $\hat{T}_a$  over the period 2007–2012. As can be observed, the relationship between these two quantities displays a small hysteresis effect, which can be explained by stream cooling due to snowmelt in spring (Mohseni et al., 1998). The logistic equation introduced by Mohseni et al. (1998) is fitted to each one of the hysteresis branches separately,

$$\hat{T} = -1.87 + \frac{4.88}{1 + e^{-0.99 \cdot (\hat{T}_a - 0.66)}} \quad (\text{in January–June}), \quad (2.27)$$

$$\hat{T} = -1.86 + \frac{3.96}{1 + e^{-1.16 \cdot (\hat{T}_a - 0.06)}} \quad (\text{in July–December}). \quad (2.28)$$

It should be noted that the parameters corresponding to the lower and upper asymptotic values of the logistic curve are particularly sensitive to the data points located at both ends of the hysteresis. To limit inaccuracy errors, the temperatures measured in January and July were used to fit both branches of the hysteresis, as they usually correspond to the annual extreme values. Equations (2.27)–(2.28) are those used in the model to determine the  $z$  scored stream temperature  $\hat{T}$  at any location based on  $\hat{T}_a$  (see Sect. 2.3.2).

The multi-linear regression models which were selected to estimate the annual mean  $\bar{T}_i$  and

## Chapter 2. Stream temperature prediction in ungauged basins

Table 2.6: Best multi-linear regression models for the prediction of annual mean  $\bar{T}_i$  and standard deviation  $\sigma_i$  of the monthly mean stream temperature in a given year. All predictor variables are averaged over the stream networks using the operator  $\langle \cdot \rangle_{\mathcal{L}}$ .

Predictand	Predictors* (with coefficients)	$L_c$ (km)
$\bar{T}_i$ (°C)	$f_{f,25m}$ ( $-1.86$ °C), $\theta$ ( $0.60$ °C), $A_{tot}$ ( $1.6 \times 10^{-3}$ °C km $^{-2}$ ), $\Delta f_s$ ( $-4.90$ °C), $\bar{T}_{a,i}$ ( $0.75$ °C °C $^{-1}$ ), intercept ( $3.88$ °C)	4
$\sigma_i$ (°C)	$ dz/dx $ ( $6.03$ °C), $f_{f,25m}$ ( $6.70$ °C), $\theta$ ( $0.93$ °C), $n_s$ ( $1.6 \times 10^{-3}$ °C), $\Delta f_s$ ( $-12.8$ °C), $\sigma_{a,i}$ ( $0.39$ °C °C $^{-1}$ ), intercept ( $0.34$ °C)	32

\*  $\Delta f_s$  denotes the difference in topographical shading between summer and winter,  $\bar{T}_{a,i}$  and  $\sigma_{a,i}$  refer to the annual mean value and standard deviation of air temperature in the year of interest, respectively,  $A_{tot}$  denotes the watershed area and  $|dz/dx|$  the channel slope. The other variables have been defined in the text.

Table 2.7: Performance of the standard regression model in terms of RMSE,  $R^2$  and bias computed over the validation set 4 in each season. The stream network used to evaluate the model corresponds to the original one derived from the map at scale 1 : 25 000.

Season	RMSE (°C)	$R^2$	Bias (°C)
Winter	1.18	0.67	-0.27
Spring	1.06	0.93	-0.09
Summer	1.18	0.90	0.11
Autumn	1.03	0.91	0.02
All year	1.12	0.96	-0.06

the standard deviation  $\sigma_i$  of stream temperature in a given year are presented in Table 2.6. They correspond to the models associated with the lowest AICc values among the tested formulations (see Sect. 2.3.2). As observed in the table, the characteristic stream length used by the operator  $\langle \cdot \rangle_{\mathcal{L}}$  to average the predictor variables over the stream networks is significantly different in the two cases:  $L_c = 4$  km for the  $\bar{T}_i$  model, whereas  $L_c = 32$  km for the  $\sigma_i$  one.

Table 2.7 summarizes the prediction errors of the standard stream temperature regression model when evaluated over validation set 4 using the original stream network. Comparison with Table 2.5 reveals that its precision is greater than the one of the physics-inspired model. Its RMSE is about  $0.2$  °C lower, its  $R^2$  about  $0.03$  to  $0.12$  larger, and its absolute bias  $0.05$  to  $0.20$  °C smaller, depending on the season. However, its performance worsens when using the two stream networks with coarser resolution: its yearly average RMSE increases to  $1.26$  °C in the case of the intermediate resolution network, and even  $1.29$  °C for the coarsest network, which is close to the value obtained with the physics-inspired model.



## 2.5 Discussion

The formulations of the physics-inspired model selected by AICc ranking are consistent among the different seasons. In particular, topographical shading systematically appears to be the strongest predictor of the net radiation heat flux  $\gamma\phi_r$ . This observation is not particularly surprising in a mountainous country like Switzerland, where some valleys are steep enough for their bottom not to be illuminated by direct sunlight for some period of the year. The basins referred to as numbers 14 and 24 in Table 2.2 are examples of such watersheds, both having a mean catchment slope larger than  $35^\circ$ . Riparian forest cover fraction corresponds to the second most important predictor for the net radiation heat flux term. It was rather unexpected to identify this parameter as relevant during autumn and winter, especially since more than half of the selected catchments are mainly covered with deciduous forests due to their relatively low mean elevation ( $< 1000$  m). This result has to be balanced with the fact that a given fraction increase in riparian forest cover is predicted by the model to have an effect on  $\gamma\phi_r$  about 4 to 6 times smaller in magnitude than the same fraction increase in topographical shading. It should also be remembered that the precision of the model is rather low in winter, hereby questioning the validity of its parametrization in this season. Certainly more unexpected is the absence of solar radiation among the predictors of  $\gamma\phi_r$ , which will be explained below. Regarding the parametrization of the discharge fraction due to lateral water inflow  $\eta$ , the model predicts the water in the stream channel to originate principally from surface and subsurface runoff during summer and autumn ( $\eta = 1$ ). This partly matches our expectations, since the fraction of discharge originating from the sources is expected to decrease when moving downstream along a given network. The characteristic catchment size defining the transition from source-water-dominated to lateral-inflow-dominated discharge is controlled here by  $L_c$ , which is equal to 4 km in summer and autumn. This value is smaller than the main channel length in more than 90 % of the selected watersheds (not shown), hereby strengthening our confidence in the parametrization of  $\eta$  during these two seasons. On the other hand, a value of 1 for  $\eta$  in all catchments may appear as a too simplified approach (see below). The questioning of the parametrization of  $\eta$  is all the more true in winter, where its value is predicted to be 0. Only in spring did the model ranking select the more physically based formulation for  $\eta$ , expressed as a function of the area drained by each source. Concerning the parametrization of the source and lateral inflow temperatures, it should be mentioned that the linear expression as a function of air temperature was systematically preferred over the constant term. This certainly results from the large altitudinal range covered by the selected catchments, which does not allow for a constant inflow temperature to reflect the diversity of encountered climatological conditions, and mainly air temperature.

As defined in Eq. (2.22), the physics-inspired model linearly relates air temperature to stream temperature through the proportionality coefficient  $\omega_3$ . The latter is compared in Fig. 2.5 with its actual observed value, namely the slope of the regression line between the monthly mean temperature measurements of the stream and air. As seen in the figure, the model systematically overestimates the value of  $\omega_3$ , particularly in winter and summer, where the

mean bias equals 0.2. Referring to Eq. (2.22), this implies that  $\omega_1$  and  $\omega_2$  are globally underestimated by the model, hereby indicating that the parametrization of the factor  $\eta$  could possibly be improved. As noted in Sect. 2.3.1, a more physically based expression could be used to compute  $\eta$ , as long as a geomorphological analysis of the river watersheds can be performed. This approach was not investigated here for the reasons mentioned earlier.

The overestimation of  $\omega_3$  is probably at the origin of the fact that solar radiation is unexpectedly missing from the selected expressions for the net radiation heat flux  $\gamma\phi_r$  (see Table 2.4). Contrary to the standard regression model, the physics-inspired model presents the advantage that the calibration range of most of its parameters can be restricted based on physical considerations (see Table 2.3). An attempt was made to remove these constraints, which resulted in incoming short-wave radiation being present in almost all models for  $\gamma\phi_r$ , but associated with a negative coefficient. It was concluded that the unconstrained model takes advantage of the fact that the annual cycles of air temperature and solar radiation have a similar shape to artificially reduce the value of air temperature by subtracting a fraction of solar radiation, hereby compensating for the too large value of  $\omega_3$ . This observation argues once more in favour of a better parametrization of the factor  $\eta$ .

As mentioned in Sect. 2.4, the characteristic stream length  $L_c$  is found to be of the order of 4–8 km regardless of the season or the stream network resolution in the case of the physics-inspired model. This range is in agreement with the findings of Isaak et al. (2010) and Macedo et al. (2013). Hrachowitz et al. (2010) and Chang and Psaris (2013) rather concluded that  $L_c$  was around 1 km; however, they did not investigate values for  $L_c$  larger than 1 km. Contrary to our expectations, we do not observe a marked variation of  $L_c$  across seasons, probably due to the fact that we assumed a single value for all the catchments. The annual cycle of  $L_c$  may have been better captured by separately calibrating this parameter in each catchment individually, but this would have contradicted our aim to derive a regional model. It should be emphasized that the absence of an observed annual cycle for  $L_c$  does not question the decision to calibrate the physics-inspired model on a seasonal basis, since the source temperature parametrization is observed to vary significantly over the year (see Table 2.4).

Our model is rather equivocal regarding the width of the riparian buffer which is relevant for the determination of stream temperature at a given point. As a matter of fact, none of the tested buffer widths appears to prevail over the other ones in the retained parametrizations of  $\gamma\phi_r$ . This ambiguity reflects the range of buffer widths used in the literature, which extends from 30 m (e.g. Jones et al., 2006; Macedo et al., 2013) to 200 m (e.g. Scott et al., 2002; Segura et al., 2014). This also points to the difficulty in adequately accounting for the effect of riparian vegetation using the available spatial data sets, which often lack important details such as the distinction between deciduous and coniferous forest.

The precision of the physics-inspired model was reported in the previous section to be rather low in January–March. This can be explained by the fact that the non-linearity of the stream–air temperature relationship at low air temperature values is not captured by the model. The

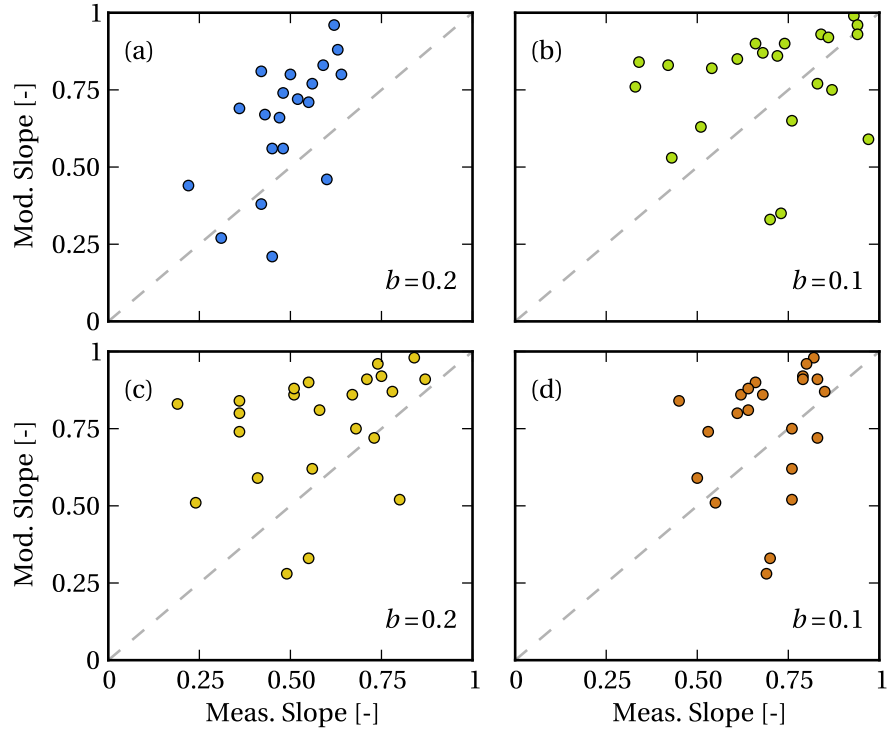


Figure 2.5: Comparison of modelled against measured slopes of the regression line between stream and air temperatures. The panels correspond to the different seasons: (a) January–March, (b) April–June, (c) July–September, and (d) October–December. The bias  $b$  corresponds to the average, in each season, of the difference between the modelled and measured regression slopes over all the selected stations and years (i.e. belonging to both the calibration set and validation set 4). The 1 : 1 line is indicated as a dashed grey curve.

latter rather simulates a sharp transition from the linear regime to a constant one, since the stream temperature values predicted to be negative are systematically replaced with  $0^{\circ}\text{C}$ . This implies a faster decrease towards  $0^{\circ}\text{C}$ , which is at the origin of the strong negative model bias in winter.

As is noticeable in Table 2.5, the model RMSE is larger in spring as compared to the other seasons. This is attributable to the fact that many of the selected watersheds are impacted by snowmelt in spring. Since the snow cover conditions are strongly variable both spatially and temporally, a large dispersion of the stream temperature values is typically observed in spring. The model performs nonetheless relatively well in this season, for its  $R^2$  value is of the same magnitude in spring as during the rest of the year.

Advantage can be taken of the physics integrated into the model structure to investigate some aspects of the stream temperature dynamics. For example, Fig. 2.6 displays the respective values of the factors  $\omega_1$ ,  $\omega_2$  and  $\omega_3$  appearing in Eq. (2.22) as a function of the season. These factors correspond to the weights associated with the mean source temperature  $\bar{T}_s$ , average

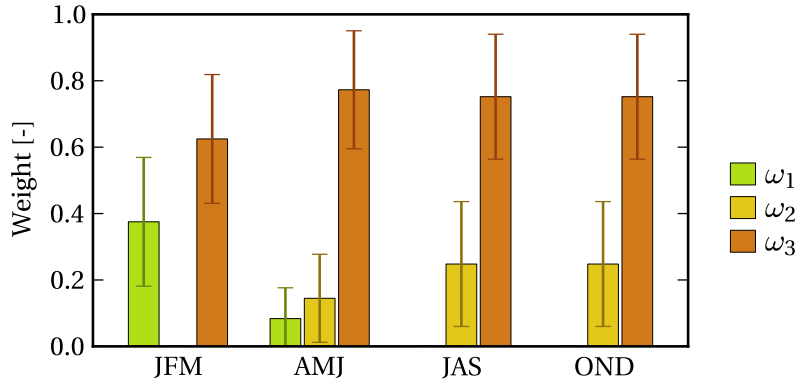


Figure 2.6: Seasonal values of the factors  $\omega_1$ ,  $\omega_2$  and  $\omega_3$  weighting the different terms in Eq. (2.8). The values of these weights are evaluated over the entire data set, i.e. both the calibration set and validation set 3. The error bars indicate the confidence interval centered around the mean and extending over 1 standard deviation on each side.

lateral inflow temperature along the network  $\langle T_\ell \rangle_{\mathcal{L}}$  and average equilibrium temperature along the network  $\langle T_e \rangle_{\mathcal{L}}$ , respectively. As seen in the figure,  $\omega_3$  is the largest factor of the three in all seasons, with a value of about 0.6–0.8. This results from the fact that stream temperature is primarily impacted by the atmospheric conditions. The other two factors are nonetheless non-negligible, with  $\omega_1$  being of the order of 0.4 in winter and  $\omega_2$  being approximately equal to 0.2 from April to December. The value of  $\omega_1$  has to be put into perspective with respect to the fact that our confidence in the model parametrization is relatively low in winter. Moreover, following the above discussion about the computation of the factor  $\eta$ , the values reported here for  $\omega_2$  should be considered as a lower limit. It therefore appears that not only the net total heat flux at the air–water interface is important in determining stream temperature, but also the heat flux associated with the lateral inflow of water. This conclusion is in agreement with the findings of Bogan et al. (2004), who found that the precision of their stream temperature model was improved by including a term accounting for the lateral water inflow. Similarly, Herb and Stefan (2011) mention that the heat input associated with groundwater infiltration may be of the same order of magnitude as the heat flux due to atmospheric forcing in some cases. This effect seems to be largely underestimated in the literature, since the lateral inflow of water has often been neglected in previous stream temperature models (e.g. Edinger et al., 1968; Bogan et al., 2003; Caissie et al., 2005; Bustillo et al., 2014).

The simplifying assumptions (i)–(vi) reported in Sect. 2.3.1 are likely to have limited the performance of the physics-inspired model. In particular, the assumption of a spatially homogeneous lateral inflow rate  $q_\ell$  is expected to fail in most catchments. For example, only the highest regions of low-altitude catchments experience snowmelt in spring. In higher-altitude catchments, snowmelt leads to an increase in  $q_\ell$  only at low altitudes at the beginning of spring, and only at higher altitudes later in the season. These mechanisms introduce an altitude dependence in  $q_\ell$  which contradicts our assumption and may partly explain the higher RMSE of the model in spring. Similarly, assumption (v) expresses stream width as a

linear function of discharge. As compared to the typical power-law relationship used in fluvial geomorphology (Knighton, 1998), this simplification may lead to an overestimation of stream width at low discharge rates—i.e. in small catchments—and to an underestimation of stream width at high discharge rates—i.e. in large catchments. This may in turn decrease the ability of the model to simulate catchments of various sizes, hereby increasing its prediction error. Assumption (vi), stating that all sources in a given catchment have the same discharge rate, is also disputable. This is particularly true for small catchments, where the short distance to the outlet and the low number of sources do not allow the averaging effect to be significant enough to compensate for the introduced error.

In addition to the simplifying assumptions discussed above, the parametrizations of the unknown terms in the analytical solution might also have impacted the model precision. Indeed, the estimation of the source and lateral inflow temperatures using only air temperature has recently been questioned, particularly for the catchments impacted by snowmelt or glacier melt (Leach and Moore, 2015). This simplification may notably have contributed to increase the model RMSE in spring. Regarding the parametrization of the term accounting for the net radiation heat flux at the air–water interface, the use of a linear expression may appear as limiting. We actually tested a power-law function as well, but did not succeed in calibrating the model due to convergence issues. We also considered an alternative expression based on an estimation of the incoming atmospheric radiation and a first-order approximation of the long-wave radiation emitted by the stream (not shown). Rather than an improvement, this parametrization actually led to a decrease in the model precision, as a result of its inability to compensate for the overestimation of  $\omega_3$  (see above).

As opposed to the physics-inspired model, the parameter values of the standard regression model could not be constrained using physical considerations. As a result, the sign of some of the linear coefficients relating the predictor variables to  $\bar{T}_i$  and  $\sigma_i$  are in contradiction with our understanding of stream temperature dynamics (see Table 2.6). For example, the stream orientation  $\theta$ , measured as the cosine of the angle between north and the channel direction, is positively related to the annual mean stream temperature  $\bar{T}_i$ . It was rather expected that north-oriented catchments receive less radiation from the sun, hereby implying lower stream temperatures. The same observation is true for the riparian forest cover fraction, which is positively associated in the model with the annual standard deviation  $\sigma_i$  of stream temperature. However, experimental observations tend to conclude that riparian shading has a buffering effect on stream temperature, therefore dampening the amplitude of the variations of the latter (see e.g. Moore et al., 2005a). Despite these inconsistencies, the standard regression model performs better than the physics-inspired one in terms of RMSE,  $R^2$  and bias. This fact questions further the validity of the parametrization of the physics-inspired model, which could certainly be improved (see Sect. 2.6). On the other hand, the standard regression model appears to be much more sensitive to the stream network resolution as compared to its counterpart, possibly as a consequence of its lack of physical elements in its structure. This lack also does not allow for the investigation of the physics governing stream temperature, as can be done with the physics-inspired model (see Fig. 2.6).

### 2.6 Conclusions

This study aimed to present a new statistical model for the prediction of monthly mean stream temperature in ungauged basins. As opposed to the standard statistical methods, this model is devised so as to incorporate physical considerations into its structure. To this end, it is built upon the analytical solution to a simplified version of the one-dimensional heat advection equation. Contrary to previously reported analytical solutions, the present one is obtained by solving the equation over an entire stream network instead of a single stream each. Moreover, the various terms of the equation are not supposed to be spatially homogeneous, which leads to the apparition of a space averaging operator  $\langle \cdot \rangle_{\mathcal{L}}$  applied to most terms of the solution. This operator uses a weight which decreases exponentially with the distance to the catchment outlet, hereby giving more emphasis to the points located near the gauging station. Both the source and the lateral inflow terms—which are usually neglected—are retained in the final solution to the heat advection equation. This notably enables the model to be applied in small watersheds, where the influence of source temperature on the value of stream temperature measured at the catchment outlet cannot be discarded.

While most terms of the analytical expression can be evaluated using meteorological observations or topographic maps, some require data which are not available. These terms are replaced with approximations based on the spatial data sets at hand. In particular, the net radiation heat flux at the air–water interface is expressed as a linear combination of several physiographic variables. Similarly, the source and lateral inflow temperatures are approximated as a linear function of air temperature measured at the source location and along the stream, respectively. Finally, the fraction  $\eta$  of discharge at the catchment outlet originating from lateral water inflow along the network is estimated based on the number of sources in the watershed. As a consequence of these approximations, the resulting model is statistical in nature, but nevertheless retains physical aspects due to its global structure being derived from the heat-balance equation.

The performance of the model is quite satisfactory, with a root-mean-square error of about  $1.3^{\circ}\text{C}$  and a coefficient of determination  $R^2$  of 0.87 when used for stream temperature prediction in “thermally climate-driven” catchments. These catchments, which are by far the most abundant ones in Switzerland, correspond to those with a glacier cover lower than 50 % and whose stream is not impacted by groundwater infiltration from a deep aquifer. Model precision is the lowest in winter, due to the inability of the model to reproduce the fact that stream temperature asymptotically tends towards  $0^{\circ}\text{C}$  for negative air temperature values.

The precision of the model was also assessed by comparing it with a more standard regression model. The latter was observed to perform slightly better, with a RMSE about  $0.2^{\circ}\text{C}$  lower. However, its parameters could not be interpreted from a physical point of view, hereby hindering the restriction of their respective calibration ranges based on physical considerations. This led the regression model to simulate some aspects of the stream temperature dynamics wrongly. For example, some physiographic variables known to have a cooling effect on water

temperature were modelled as warming up the stream. The standard regression model was also observed to be much more sensitive than its physics-inspired counterpart with respect to the stream network resolution. When discarding all stream segments with a Strahler order equal to 1, the RMSE of the regression model increased from 1.12 to 1.26 °C, whereas the one of the physics-inspired model remained constant up to 0.01 °C.

Despite a few deficiencies, the physics-inspired statistical model can be used to analyse some aspects of the physics governing stream temperature. As an example, the relative importance of each one of the stream heat sources could be determined from the model. Climatic forcing was found to be the major driver of water temperature, as expected (e.g. Caissie, 2006). More interestingly, the lateral inflow of water was identified as a non-negligible secondary heat flux. This fact is confirmed by other studies (e.g. Bogan et al., 2004; Herb and Stefan, 2011), but nonetheless fails to be accounted for in many stream temperature models (e.g. Caissie et al., 2005; Bustillo et al., 2014). We therefore wish to emphasize the role of lateral water inflow in stream temperature, even in catchments—such as those used in this study—which are not impacted by groundwater infiltration originating from a deep aquifer.

Among the improvements that can be brought to the physics-inspired model, a more accurate parametrization of the discharge fraction originating from lateral water inflow  $\eta$  appears as a promising enhancement. In particular,  $\eta$  could be estimated from a geomorphological analysis of the catchments. This approach was not retained here due to the discrepancy between the stream networks predicted by the geomorphological analysis and the observed ones. In case it could be implemented, such a revision is expected to improve the predicted slope of the stream–air temperature curve. A geomorphological analysis could also positively influence the modelling of the source and lateral inflow temperatures. The parametrization of these two terms could be improved by including predictor variables accounting for e.g. the glacier cover fraction or the mean altitude of the area drained by each source (or stream reach). The model could also be substantially improved in case the characteristic stream length  $L_c$ , which controls the extent of the spatial area over which the operator  $\langle \cdot \rangle_{\mathcal{L}}$  acts, could be computed instead of calibrated. Indeed,  $L_c$  does not only present a seasonal variation, but also differs across the individual catchments, a fact which was neglected in the present work. Finally, one might expect the model precision to improve by using a more physically based parametrization for the net radiation heat flux—instead of the multi-linear model used here.

We expect the physics-inspired model to be easily transferable to other regions of the globe. The parametrization of the net radiation heat flux at the air–water interface might need some adaptation in order to correctly reflect the dominant physiographic controls on local stream climate. For example, topographic shading is certainly not a relevant predictor variable over flat regions. Similarly to the approach presented in this work, the most appropriate set of predictor variables for the net radiation heat flux over a particular region can be obtained through AICc ranking. Once set, the stream temperature model can be used to investigate e.g. the extent of the stream network which is thermally suitable for sensitive fish species at the regional scale (e.g. Isaak et al., 2010). This investigation can in turn serve as a basis for the

introduction of regulation policies or protection measures.



## 3 Deterministic stream temperature modeling in high alpine watersheds

*A slightly shortened version of this chapter has been submitted as an article to journal Geophysical Model Development (GMD) under the title “StreamFlow 1.0: An extension to the spatially distributed snow model Alpine3D for hydrological modeling and deterministic stream temperature prediction.” The authors are, in publication order: Aurélien Gallice, Mathias Bavay, Tristan Brauchli, Francesco Comola, Michael Lehning and Hendrik Huwald. Concerning the author contributions, A. Gallice re-wrote and enhanced the original model developed by F. Comola, performed the analysis presented in this chapter, produced the figures and wrote the manuscript; M. Bavay helped designing the structure of StreamFlow, wrote the CMake scripts to compile the code, set up the CTest environment and provided much appreciated guidance on MeteoIO usage and various aspects of C++ coding; T. Brauchli installed the two intermediate gauging stations in the Dischma catchment, performed the salt dilution gaugings and helped a lot in setting up the Alpine3D simulation; F. Comola gave much help regarding the structure and usage of the original version of StreamFlow and suggested some of the analysis presented in this work; H. Huwald and M. Lehning co-supervised the work; all co-authors helped write the manuscript.*

### 3.1 Introduction

Mountainous areas play a major role in hydrology by accumulating precipitation as snow and ice during the winter and redistributing it as melt water during spring and summer. Downstream areas hereby receive larger amounts of water during the hot season, when demand—especially in terms of agriculture—is highest. In fact, Viviroli et al. (2011) estimate that more than 40% of the world’s mountainous regions provide an important supply for low-land water use. Accordingly, more than one sixth of the world’s population is currently living in areas depending on snow melt for their water supply (Barnett et al., 2005). Apart from its relevance for downstream areas, mountain hydrology also strongly impacts hydropower production (e.g. Schaefli et al., 2007; Finger et al., 2012; Majone et al., 2016), determines the habitat suitability of numerous aquatic organisms (e.g. Short and Ward, 1980; Hari et al., 2006; Wilhelm et al., 2015; Padilla et al., 2015) and even plays a noticeable role in the global emission of carbon dioxide into the atmosphere (Butman and Raymond, 2011; Raymond et al., 2013).

Mountainous environments have recently been identified as being especially sensitive to climate change (Barnett et al., 2005; Stewart et al., 2005; Viviroli et al., 2011, e.g.). In particular, winter air temperature over the last 70 years has been observed to increase by more than twice the global mean in the European Alps (Beniston, 2012), and this trend is forecasted to remain unchanged in the next decades (Kormann et al., 2015b). Rising air temperature will be responsible for less precipitation falling as snow in winter and an earlier onset of snow melt in spring (Barnett et al., 2005; Bavay et al., 2009, 2013, e.g.). As a consequence, the spring freshet will occur earlier in the season and, assuming mean annual precipitation to remain constant, will also have a reduced magnitude (e.g. Stewart et al., 2005; Kormann et al., 2015b,a, to name just a few). Some studies predict an increase in winter precipitation, which could at least partially compensate for the decreased fraction of solid precipitation and sustain the spring freshet close to its actual level (Schaepli et al., 2007; Beniston, 2012; Finger et al., 2012; Fatichi et al., 2015). Autumn and winter stream discharge is expected to increase in magnitude and variability as a result of the higher fraction of precipitation falling as rain, which might result in greater flood risks in winter (Barnett et al., 2005; Bavay et al., 2009; Finger et al., 2012; Beniston, 2012). Summer discharge will likely be much reduced and the drought risks therefore more pronounced, at least in the watersheds with little or no glacier cover (Schaepli et al., 2007; Stewart et al., 2015). In glaciated catchments, increased summer ice melt might (over)compensate for the reduced snow melt on an annual average basis (Bavay et al., 2013; Kormann et al., 2015a). This compensation is however expected to last only until the glaciers have shrunk to the point where ice melt discharge starts to decrease as well, a phenomenon which has already been observed in some parts of the world (see e.g. studies mentioned in Kormann et al., 2015a). In summary, the hydrological regimes of many mountainous catchments are forecasted to shift from glacio-nival and nival signatures to nivo-pluvial or even pluvial regimes (Aschwanden and Weingartner, 1985; Beniston, 2012).

As a result of the changes in climate and hydrological regime, the thermal regime of the mountain streams will change as well in the coming decades (e.g. Morrison et al., 2002; Null et al., 2013; Ficklin et al., 2014; Stewart et al., 2015). Due to the strong correlation between stream and air temperatures (e.g. Mohseni et al., 1998; Caissie, 2006), the increase in air temperature is expected to result in globally higher stream temperatures over the year (e.g. Ferrari et al., 2007; Ficklin et al., 2012). The increase in mean annual precipitation predicted by some studies will only slightly mitigate this temperature rise through an increase of the mean annual discharge—and hence the heat capacity—of the streams (Ficklin et al., 2012, 2014). The reduction of the spring freshet will diminish the buffering effect of snowmelt on stream temperature, hereby leading to larger stream temperature increases in spring (Ficklin et al., 2014). Similarly, lower summer flows in little glaciated catchments are likely to result in increased mean summer stream temperature and more frequent extreme temperature events (Stewart et al., 2005; Null et al., 2013). All these predictions support the hypothesis that stream temperature will respond in a non-linear way to the air temperature rise.

The climate change induced modifications of the hydrological and thermal regimes of alpine streams are expected to strongly impact their ecology. The forthcoming air temperature rise

will lead to a modification of the riparian vegetation, which in turn will affect the stream ecosystem (Hauer et al., 1997). The higher stream temperatures will also have consequences on the cold water fish species encountered in mountain streams, whose fry emergence date (Elliott and Elliott, 2010), growth rate (Hari et al., 2006) and death rate (Wehrly et al., 2007) are all mostly dependent on stream temperature. Future increases in stream temperature are expected to result in a shift of the suitable habitat for such species to higher elevations, where dams and other physical barriers might limit their migration and imply a reduction of their habitat (Hauer et al., 1997; Hari et al., 2006). Padilla et al. (2015) report that the summer stream discharge variability is currently increasing, which is detrimental to the spawning rate of fish. However, they note that reduced spring discharge might partly compensate for the increase in stream temperature by facilitating the upstream migration of fish.

Hydropower production might also suffer from the effects of climate change on alpine hydrology (e.g. Schaepli et al., 2007; Beniston, 2012; Fatichi et al., 2015). This fact is all the more worrying in the current context of transition towards renewable energy sources, especially for small alpine countries such as Switzerland which heavily rely on hydropower for their electricity production (Schaepli, 2015). Several studies point at the future decrease of up to 36% in the energy production of the dams located at high altitudes (Schaepli et al., 2007; Finger et al., 2012; Fatichi et al., 2015), resulting from the shift of the hydrological regime from glacio-nival to pluvial-nival. Schaepli et al. (2007) also mentions that the spillway—an emergency van intended to avoid dam overflow—may have to be occasionally activated in the future, with all the dramatic consequences that it entails for downstream areas.

The modification of the stream ecology and the reduction of the hydropower production are only two examples of the consequences of climate change on mountain streams. In order to better evaluate and predict these consequences, numerous numerical models have been developed over the last decades. Most of them concentrate either on the prediction of discharge (e.g. Grillakis et al., 2010; Bürger et al., 2011; Schaepli et al., 2014; Ragetti et al., 2014) or water temperature (e.g. Caldwell et al., 2013; Tung et al., 2014; Hébert et al., 2015; Toffolon and Piccolroaz, 2015), but few are able to simulate the two at the same time (e.g. Loinaz et al., 2013; MacDonald et al., 2014; Comola et al., 2015). Regarding the models predicting only discharge, they can be classified—among other possibilities and in order of increasing spatial resolution—either as lumped, semi-distributed or fully distributed (e.g. Khakbaz et al., 2012). Lumped models are often based on empirical equations and only allow for the computation of stream discharge at the catchment outlet. Fully distributed models, on the other hand, typically solve the full mass and momentum conservation equations, but require extensive computational resources (e.g. Beven, 2012). As a trade-off between the two approaches, semi-distributed models have become quite popular over the last decades, since they can be applied over large areas while at the same time accounting for sub-catchment characteristics (Khakbaz et al., 2012; Beven, 2012). An equivalent sort of classification is commonly applied to stream temperature models, which are usually separated into statistical and mechanistic models (Caissie, 2006). Statistical models require less input data and are usually easier to use, but their lack of physical basis is often seen as a limit to the validity of their predictions in the context of

### Chapter 3. Deterministic stream temperature modeling in high alpine watersheds

Table 3.1: List of semi-distributed hydrological models which simulate both stream discharge and stream temperature and have been reviewed in the context of the present study.

Model name	Publication	Time resolution	Target geographic location
LARSIM-WT	Haag and Luce (2008)	hourly, daily	small to large river basins
MODEL-Y	Sullivan et al. (1990)	hourly	forested catchments
SHADE-HSPF	Chen et al. (1998)	hourly	forested catchments
VIC-RMB	van Vliet et al. (2012a)	daily	large river basins
CEQUEAU	St-Hilaire et al. (2000)	hourly, daily	forested catchments in Canada
UBC	Morrison et al. (2002)	hourly	large river basins
GISS GCM	Ferrari et al. (2007)	monthly	large river basins
SWAT	Ficklin et al. (2012)	daily, monthly	medium to large scale catchments
MIKE-SHE MIKE11	Loinaz et al. (2013)	hourly	medium-scale catchments
WEAP21-RTEMP	Null et al. (2013)	weekly	large river basins
DHSVM	Sun et al. (2015)	hourly	small forested or urban catchments
GENESYS	MacDonald et al. (2014)	hourly	mountainous catchments
PCR-GLOBWB	van Beek et al. (2012)	daily	large river basins

climate change studies (e.g. Piccolroaz et al., 2016). On the contrary, more credit is generally given to the long-term forecasts of the deterministic stream temperature models, although their accuracy is about the same—if not worse (Ficklin et al., 2014)—than the statistical models. It should be mentioned that an intermediate sort of model, referred to as hybrid, has recently been developed (Gallice et al., 2015; Toffolon and Piccolroaz, 2015) and shown by Piccolroaz et al. (2016) to be suitable for climate change studies.

As opposed to the separate simulation of discharge and stream temperature, the coupled modeling of the two offers new perspectives to investigate the effects of climate change on mountain hydrology (e.g. Ficklin et al., 2014). For example, the variations of temperature resulting from the fluctuations in discharge can be better resolved (e.g. van Vliet et al., 2012a; Null et al., 2013). The use of both discharge and temperature measurement data to calibrate the model has also been shown by Comola et al. (2015) to improve the quality of the simulation. Surprisingly, only a few coupled hydro-thermal models have been developed to date (see Table 3.1), probably as a result of the rather small size of the scientific community involved in stream temperature research. Out of the 13 semi-distributed coupled models listed in Table 3.1, only one was specifically developed for mountainous environments (MacDonald et al., 2014). The other ones were either tailored to large-scale applications (Morrison et al., 2002; Ferrari et al., 2007; van Vliet et al., 2012a; van Beek et al., 2012; Null et al., 2013) or aimed at being used over low-altitude catchments (e.g. Sullivan et al., 1990; Chen et al., 1998; Haag and Luce, 2008; Sun et al., 2015). In addition, all of these models simulate the snowpack energy-balance using a more or less simplified approach, most of them relying on the degree-day method (e.g. van Beek et al., 2012; Null et al., 2013; MacDonald et al., 2014).

The present study aims at presenting the improvements brought to the semi-distributed model recently developed by Comola et al. (2015) for coupled streamflow discharge and temperature simulations. This model, referred to as *StreamFlow* in the following, was specifically developed

for high Alpine environments as it builds upon the detailed snow model *Alpine3D* (Lehning et al., 2006). It was decided to entirely rewrite the code of Comola et al. so as to fully exploit the advantages offered by object-oriented programming in terms of flexibility and code structure. In particular, the new model is much more modular, allowing for various components of the hydrological cycle to be modeled using different approaches. Some of these approaches have been implemented which were not present in the original model of Comola et al., hereby offering a wider range of modeling possibilities to the end user. The mass- and energy-balance equations implemented in the model are detailed in Sect. 3.2, and the new code structure in Sect. 3.3. The model is applied to a case study in Sect. 3.4 in order to demonstrate some of its features and provide an assessment of its accuracy. Conclusions are found in Sect. 3.5.

## 3.2 Model description

*StreamFlow* is built as an independent extension to the spatially-distributed snow model *Alpine3D* (Lehning et al., 2006, 2008). The latter was developed to study multiple subjects such as the impact of climate change on snow cover (Bavay et al., 2009, 2013), the effect of wind and topography on snow deposition (Mott and Lehning, 2010; Mott et al., 2014) or the sublimation of drifting snow (Groot Zwaaftink et al., 2013). *Alpine3D* operates on a regular mesh grid, and essentially runs the one-dimensional *Snowpack* model over each grid cell independently. *Snowpack* computes the time evolution of the vertical snow profile, as well as the vertical profiles of soil moisture and soil temperature (Bartelt and Lehning, 2002; Lehning et al., 2002b,a). It accounts for the canopy layer (Gouttevin et al., 2015) and can simulate the vertical water transport using either the Richards equation or a simple bucket scheme (Wever et al., 2014, 2015).

*StreamFlow* is implemented as a semi-distributed model, i.e. based on the subdivision of the catchment into subwatersheds. This subdivision is typically performed using the well-known tool suite TauDEM (Tarboton, 1997), which extracts both the stream network and its corresponding set of subwatersheds from the digital elevation model (DEM). The stream network is automatically partitioned into so-called *stream reaches*, where each reach is uniquely associated with a subwatershed and corresponds to the portion of the stream network which specifically drains the subwatershed in question. It should be stressed out that subwatersheds are independent and distinct from each other, i.e. they do not spatially overlap and are considered not to interact from a hydrological point of view. Stream reaches, on the other hand, are connected to each other: the computation of discharge and temperature in a given reach requires the same variables to be computed in its upstream tributaries first.

As schematically represented in Fig. 3.1, *StreamFlow* pursues the simulation of the water flow from the point where *Alpine3D* stops to model it. Each subwatershed is approximated in *StreamFlow* as a linear reservoir. The total percolation rate computed by *Alpine3D* at the bottom of all the soil columns belonging to a given subwatershed is considered by *StreamFlow* as the inflow rate into the associated linear reservoir. The latter then computes the discharge

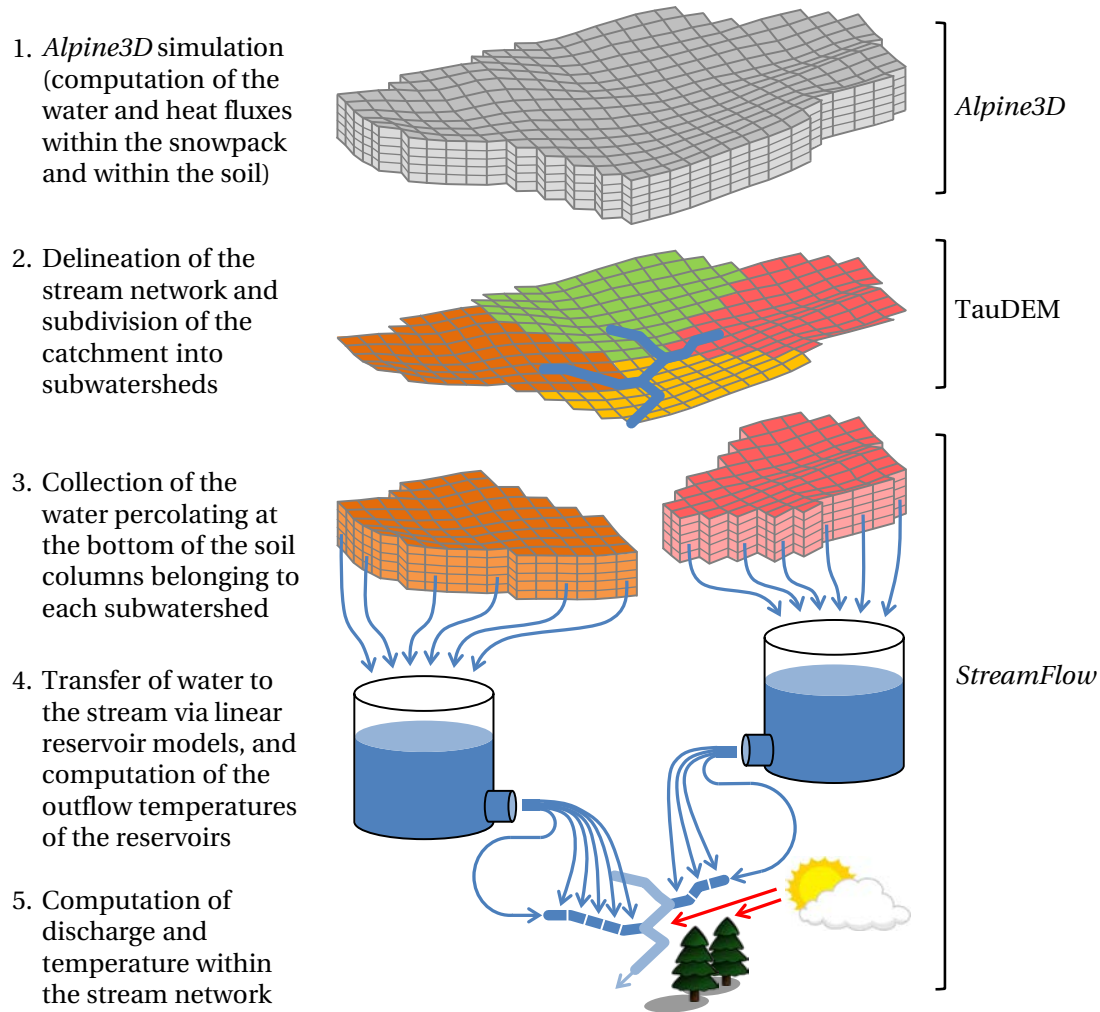


Figure 3.1: Schematic representation of the work flow in *StreamFlow*. Note that the first two steps are not performed in *StreamFlow* itself but in *Alpine3D* and with the help of *TauDEM*, respectively.

and temperature of the subsurface runoff flowing out of the subwatershed. Note that the term *subsurface runoff* will be used in the remaining of this paper as a generic word standing for both the fast and slow components of the subsurface runoff, which are sometimes referred to as interflow and baseflow in the literature. Subsurface runoff produced by each subwatershed is delivered as lateral inflow to its associated stream reach (see Fig. 3.1). In other words, the subwatersheds are used in *StreamFlow* to compute the amount of subsurface water and heat penetrating the stream network. As such, the model is only able to reproduce so-called *gaining streams*, as opposed to *losing streams* which would require a mechanism to transfer water from the stream network to the subwatersheds. As a final step, *StreamFlow* advects water and energy within the stream network down to the catchment outlet point. To this end, discharge and temperature are computed within each stream reach, taking notably the water and heat

inflows originating from the upstream reaches and from the subsurface runoff into account. The different processing steps of *StreamFlow* are described into more detail below.

### 3.2.1 Subwatershed modeling

In *StreamFlow*, the discharge  $Q_{\text{subw}}$  ( $\text{m}^3 \text{s}^{-1}$ ) of subsurface runoff is computed independently from its temperature  $T_{\text{subw}}$  (K). This allows for the different temperature modeling approaches to be combined with every discharge computation alternative.

#### Water transfer

Only the linear reservoir approach developed by Comola et al. (2015) has been implemented so far for the estimation of the subsurface runoff discharge, but the modular structure of *StreamFlow* supports the integration of more complex, physically-based algorithms. The approach of Comola et al. represents each subwatershed as two superposed linear reservoirs, the lower one being filled at a maximum inflow rate  $R_{\text{max}}$  ( $\text{m s}^{-1}$ ) and the upper one receiving the excess inflow water. The model behavior is controlled by three user-specified parameters: the mean characteristic residence times  $\bar{\tau}_{\text{res,u}}$  (s) and  $\bar{\tau}_{\text{res,l}}$  (s) in the upper and lower reservoirs, and  $R_{\text{max}}$ . The complete mathematical background underlying this approach is detailed in Comola et al. (2015); a summary of the main equations and an explanatory figure can be found in Appendix B. Depending on the approach used to spatially discretize the stream reaches, water flowing out of each subwatershed is either transferred to its associated reach as a whole or partitioned between the different cells composing the stream reach (see below).

#### Computation of the subwatershed outflow temperature

Three alternatives are available in *StreamFlow* for the estimation of subsurface runoff temperature. The first approach corresponds to the one developed by Comola et al. (2015), which requires subsurface runoff to be modeled as in Sect. 3.2.1 above and is therefore not compatible with potential future alternatives for subsurface runoff discharge modeling. It performs a simplified energy-balance of subsurface water at the subwatershed scale. The temperature of water stored in each one of the two superposed reservoirs is computed based on the temperature of infiltrating water, taking thermal exchange with the surrounding soil into account. This model requires the specification of a parameter,  $k_{\text{soil}}$  (s), which corresponds to the characteristic time of thermal diffusion between the water stored in the reservoirs and the soil. The complete description of this technique can be found in Comola et al. (2015) and is also summarized in Appendix B for convenience.

The second method implemented in *StreamFlow* for the computation of  $T_{\text{subw}}$  is adapted from the approach used in the Hydrological Simulation Program–Fortran (HSPF Bicknell et al., 1997). This technique essentially approximates the time evolution of  $T_{\text{subw}}$  by smoothing and

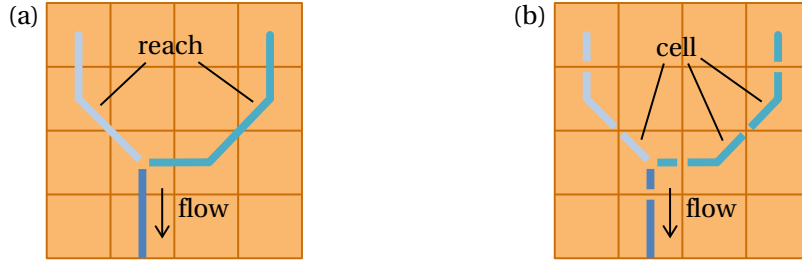


Figure 3.2: Available methods for spatially discretizing the stream reaches in *StreamFlow*: **(a)** the lumped approach, treating each stream reach as a lumped entity, and **(b)** the discretized approach, subdividing each reach into smaller entities called *cells*. Each stream reach is represented using a different shade of blue in the figure. The grid shown in brown corresponds to the DEM used by TauDEM to identify the subwatersheds and the stream network.

adding an offset to the time series of air temperature  $T_a$  (K),

$$\frac{dT_{\text{subw}}}{dt} = \frac{1}{\tau_{\text{HSPF}}} (T_a - T_{\text{subw}} + D_{\text{HSPF}}). \quad (3.1)$$

In the above equation,  $T_a$  is taken as the mean air temperature over the subwatershed as computed by *Alpine3D*, and the smoothing coefficient  $\tau_{\text{HSPF}}$  (s) and the temperature offset  $D_{\text{HSPF}}$  (K) can be freely specified by the user. This equation is solved in *StreamFlow* using a second order Crank-Nicholson scheme.

Finally, the third technique for estimating the temperature of subsurface flow relies on the assumption that infiltrated water is in thermal equilibrium with the surrounding soil matrix. As such,  $T_{\text{subw}}$  can be considered to have the same value as the local soil temperature  $T_{\text{soil}}$  averaged between the soil surface and a given depth  $z_d$  (m). In practice,  $T_{\text{subw}}$  is determined at any point along the stream network by identifying the cell of the *Alpine3D* mesh in which it is located, and then averaging the soil temperature values computed by *Alpine3D* in this cell down to depth  $z_d$ .

#### 3.2.2 Stream network modeling

As mentioned above, the computation of discharge and temperature within the stream network is based on the subdivision of the latter into reaches. Each reach is uniquely associated with its corresponding subwatershed and is automatically identified by TauDEM based on a geomorphological analysis of the DEM. The stream reaches can be modeled in *StreamFlow* using two different approaches (see Fig. 3.2):

- (a) A lumped approach, in which each reach is treated as a single entity whose mean water depth, outlet discharge and temperature are to be computed. This method was already implemented by Comola et al. (2015) in the first version of *StreamFlow*. In this approach,



each reach collects the subsurface runoff originating from its associated subwatershed as a whole—no spatial discretization is performed.

- (b) A discretized approach, which subdivides each reach into smaller spatial units referred to as *cells* in the following. The cells are delineated using the grid pattern of the DEM used by TauDEM to identify the subwatersheds and the stream network (see Fig. 3.2); as a consequence, all cells do not have the same length within a single reach. This discretization method provides higher spatial resolution than the lumped approach and supports more advanced techniques for water and temperature routing (e.g. the resolution of the shallow water equations). In this approach, the water flowing out of each subwatershed is transferred to the cells of its corresponding stream reach, proportionally to the specific drainage area of each cell.

The different methods available in *StreamFlow* for in-stream routing of water and energy are described below.

#### Water routing

Stream discharge can be computed using two different approaches, which can both be used with lumped or discretized reaches. A third approach, namely the shallow water equation solver for the discretized reaches, is currently being developed and should be available in the near future.

The first water routing technique is the same as the one already available in the original version of *StreamFlow*, namely the instantaneous advection of water down to the catchment outlet. This approach is based on the fact that, in small catchments, the amount of time required for a rain drop to reach the catchment outlet is mostly dominated by the time spent within the hillslopes (see e.g. Comola et al., 2015). Water depth  $h$  (m) is computed using a power function of discharge  $Q$  ( $\text{m}^3 \text{s}^{-1}$ ), i.e.  $h = \alpha_h Q^{\beta_h}$ , where the coefficients  $\alpha_h$  and  $\beta_h$  can be calibrated or specified a priori.

The second approach corresponds to the well-known Muskingum-Cunge technique, shown by Cunge (1969) to be a diffusive-wave approximation of the shallow water equations. *StreamFlow* implements the modified three-point variable parameter method developed by Ponce and Changanti (1994), which is first-order accurate in time and second-order in space. This method can be used with both lumped and discretized stream reaches. In discretized reaches, it estimates discharge  $Q_i^{n+1}$  ( $\text{m}^3 \text{s}^{-1}$ ) at the outlet of cell  $i$  at time  $t_{n+1} = t_n + \Delta t$  as (see e.g. Tang et al., 1999):

$$Q_i^{n+1} = c_1 Q_{i-1}^n + c_2 Q_{i-1}^{n+1} + c_3 Q_i^n, \quad (3.2)$$

where  $\Delta t$  (s) denotes the time step,  $Q_{i-1}^n$  the sum of the outlet discharge of cell  $i - 1$  and the lateral subsurface flow discharge into cell  $i$  at time  $t_n$ , and the coefficients  $\{c_k\}_{k=1,2,3}$  (–) are

computed as:

$$\begin{aligned} c_1 &= \frac{k_i x_i + 0.5 \Delta t}{k_i (1 - x_i) + 0.5 \Delta t}, \\ c_2 &= \frac{-k_i x_i + 0.5 \Delta t}{k_i (1 - x_i) + 0.5 \Delta t}, \\ c_3 &= \frac{k_i (1 - x_i) - 0.5 \Delta t}{k_i (1 - x_i) + 0.5 \Delta t}. \end{aligned}$$

Parameters  $k_i$  (s) and  $x_i$  (–) can be related to hydraulic properties of the stream cell,

$$k_i = \frac{l_i}{c_r}, \quad (3.3)$$

$$x_i = \frac{1}{2} \min \left( 1, 1 - \frac{Q_r}{c_r w S_0 l_i} \right), \quad (3.4)$$

with  $l_i$  (m) denoting the cell length,  $w$  (m) the stream width,  $S_0$  (–) the local bed slope in cell  $i$ ,  $c_r$  ( $\text{ms}^{-1}$ ) a representative wave celerity and  $Q_r$  ( $\text{m}^3 \text{s}^{-1}$ ) a representative discharge. Manning's formula is used to derive  $c_r$  from  $Q_r$  under the assumption of a rectangular channel cross-section,

$$c_r = \frac{5}{3} \left( \frac{S_0}{n_m^2} \right)^{3/10} \left( \frac{Q_r}{w} \right)^{2/5}, \quad (3.5)$$

where  $n_m$  ( $\text{s m}^{-1/3}$ ) is the Manning coefficient, whose value is generally accepted to be within the approximate range 0.03–0.10 for small natural streams (e.g. Phillips and Tadayon, 2006).  $Q_r$  is computed as:

$$Q_r = \frac{Q_{i-1}^n + Q_{i-1}^{n+1} + Q_i^n}{3}. \quad (3.6)$$

Manning's formula is also used to determine the water depth  $h_i^{n+1}$  (m) in cell  $i$  at time  $t_{n+1}$  based on  $Q_i^{n+1}$ :

$$h_i^{n+1} = \left( \frac{n_m Q_i^{n+1}}{w S_0} \right)^{3/5}. \quad (3.7)$$

In order to avoid numerical instabilities, the time step  $\Delta t$  is chosen according to the recommendations of Tang et al. (1999),

$$\max_i (2k_i x_i) \leq \Delta t \leq \min_i (2k_i (1 - x_i)). \quad (3.8)$$

Equation (3.8) must be verified for all cells belonging to the entire stream network.

When using lumped stream reaches, Eqs. (3.2)–(3.8) have to be adapted as follows:  $l_i$  is to be replaced with the reach length,  $S_0$  with the average bed slope over the reach, and  $Q_{i-1}^n$  with the sum of the outlet discharge(s) of the upstream reach(es) and the lateral subsurface flow

discharge into the stream reach at time  $t_n$ . In addition,  $Q_i^n$  and  $h_i^n$  have to be interpreted as the outlet discharge and mean water depth in the reach at time  $t_n$ .

Both water routing techniques assume the stream width  $w$  to be spatially constant within each reach. Several methods are available for the computation of  $w$ , such as for instance a linear function of the total area drained by the stream reach. The possibility is also offered to set  $w$  as a power-law function of the reach outlet discharge, hereby making  $w$  time-dependent. Each of these methods requires the specification of two parameters, which should be set prior to the *StreamFlow* simulation.

#### Stream energy-balance computation

The computation of in-stream temperature assumes a constant cross-sectional profile in each stream reach separately; it is based on the one-dimensional mass and energy balance equations solved over each stream reach (adapted from Gallice et al., 2015),

$$\frac{\partial A}{\partial t} + \frac{\partial Q}{\partial x} = q_{\text{subw}}, \quad (3.9)$$

$$\frac{\partial(A T_w)}{\partial t} + \frac{\partial(Q T_w)}{\partial x} = \frac{w \phi}{\rho_w c_{p,w}} + q_{\text{subw}} T_{\text{subw}} + Q \frac{g}{c_{p,w}} S_0, \quad (3.10)$$

where  $t$  (s) denotes time and  $x$  (m) the streamwise distance;  $A$  ( $\text{m}^2$ ),  $Q$  ( $\text{m}^3 \text{s}^{-1}$ ),  $T_w$  (K) and  $w$  (m) stand for the cross-sectional area, discharge, temperature and width of the stream reach;  $\phi$  ( $\text{W m}^2$ ) corresponds to the sum of the net heat fluxes at the air–water and water–bed interfaces;  $\rho_w$  ( $\text{kg m}^{-3}$ ) and  $c_{p,w}$  ( $\text{J kg}^{-1} \text{K}^{-1}$ ) denote the mass density and specific heat capacity of water;  $q_{\text{subw}}$  ( $\text{m}^3 \text{s}^{-1} \text{m}^{-1}$ ) is the lateral subsurface water inflow per unit streamwise distance; and  $g$  ( $\text{m s}^{-2}$ ) stands for the gravitational acceleration at the Earth's surface. Both  $T_{\text{subw}}$ , the temperature of subsurface water inflow, and  $S_0$ , the local bed slope, have been defined previously. Equations (3.9) and (3.10) are both written in conservative form. Assuming a smooth variation of  $A$ ,  $Q$  and  $T_w$  along the stream reach, the partial derivatives on the left-hand side of Eq. (3.10) can be developed using the product rule. By inserting Eq. (3.9) and re-arranging the terms, one obtains the following expression:

$$\frac{\partial T_w}{\partial x} + v \frac{\partial T_w}{\partial x} = \frac{\phi}{\rho_w c_{p,w} h} + \frac{q_{\text{subw}}}{h w} (T_{\text{subw}} - T_w) + \frac{g Q}{c_{p,w} h w} S_0, \quad (3.11)$$

where  $v = Q/A$  ( $\text{m s}^{-1}$ ) corresponds to the flow velocity and  $h = A/w$  (m) to the stream water depth.

In Eqs. (3.9)–(3.11), the values of  $A$ ,  $Q$ ,  $v$ ,  $h$  and  $w$  are provided by the water routing module of *Streamflow* (see Sect. 3.2.2), while  $T_{\text{subw}}$  is obtained from the subsurface runoff temperature module (see Sect. 3.2.1). The value of  $q_{\text{subw}}$  is derived from the subsurface runoff discharge  $Q_{\text{subw}}$  (see Sect. 3.2.1) depending on the stream reach type. In lumped reaches, it is simply computed as  $Q_{\text{subw}}$  divided by the reach length, whereas it is calculated in each discretized

### Chapter 3. Deterministic stream temperature modeling in high alpine watersheds

reach cell as the fraction of  $Q_{\text{subw}}$  proportional to the cell specific drainage area, divided by the cell length.

The net heat flux  $\phi$  is computed as in Westhoff et al. (2007) with the following modifications:

1. Incoming short and long wave radiation are directly obtained from meteorological measurements. They are spatially interpolated by *Streamflow* over the stream network using library *MeteoIO* (Bavay and Egger, 2014), taking topographic shading into account. Riparian forest shading is currently not represented in the model, hereby restricting the application of *StreamFlow* to high-altitude catchments. This limitation might be relaxed in the near future through the implementation of an appropriate shade model, taking e.g. advantage of the improvements brought by Gouttevin et al. (2015) to the canopy module of *Snowpack*.
2. The heat flux at the water–bed interface  $\phi_b$  ( $\text{Wm}^{-2}$ ) is computed at any given point along the stream according to Haag and Luce (2008):

$$\phi_b = k_{\text{bed}}(T_{\text{bed}} - T_w), \quad (3.12)$$

where  $k_{\text{bed}}$  ( $\text{Wm}^{-2}\text{K}^{-1}$ ) denotes the bed heat transfer coefficient, which corresponds to the bed heat conductivity multiplied by the distance over which the heat transfer occurs. The value of  $k_{\text{bed}}$  can be freely specified by the user, but is fixed here to  $52.0 \text{ Wm}^{-2}\text{K}^{-1}$  after Moore et al. (2005b) and MacDonald et al. (2014). Stream bed temperature  $T_{\text{bed}}$  (K) is assumed to be equal to soil temperature as modeled by *Alpine3D* at the point of interest, averaged over depth  $z_d$ . This depth is the same one as used by the subsurface runoff temperature module (see Sect. 3.2.1) and should be specified prior to running the *Alpine3D* simulation.

3. The latent heat flux  $\phi_l$  ( $\text{Wm}^{-2}$ ) is approximated using a simplified Penman equation (e.g. Hannah et al., 2004; Haag and Luce, 2008; Magnusson et al., 2012),

$$\phi_l = -\frac{\rho_a c_{p,a}}{\gamma} (a_{vw} v_{\text{wind}} + b_{vw}) (e_s(T_w) - e(T_a)), \quad (3.13)$$

where  $T_a$  (K),  $\rho_a$  ( $\text{kgm}^{-3}$ ) and  $c_{p,a}$  ( $\text{Jkg}^{-1}\text{K}^{-1}$ ) denote the temperature, mass density and specific heat capacity of air,  $v_{\text{wind}}$  ( $\text{ms}^{-1}$ ) the wind velocity,  $\gamma$  ( $\text{PaK}^{-1}$ ) the psychrometric constant,  $e_s(T_w)$  (Pa) the saturated vapor pressure measured at stream temperature, and  $e(T_a)$  (Pa) the actual vapor pressure measured at air temperature. The values of parameters  $a_{vw}$  (–) and  $b_{vw}$  ( $\text{ms}^{-1}$ ) are chosen after Webb and Zhang (1997), namely  $a_{vw} = 2.20 \times 10^{-3}$  and  $b_{vw} = 2.08 \times 10^{-3} \text{ ms}^{-1}$ , although they can be changed by the user.

4. The sensible heat flux  $\phi_h$  ( $\text{Wm}^{-2}$ ) is computed based on an approach similar to the one

used in Comola et al. (2015), namely as

$$\phi_h = -\rho_a c_{p,a} (a_{vw} v_{wind} + b_{vw}) (T_w - T_a). \quad (3.14)$$

This expression for  $\phi_h$  is preferred over the one used in Westhoff et al. (2007), since the latter contains a term  $e_s(T_w) - e(T_a)$  in the denominator which we observed to be responsible for numerical instabilities when  $T_w$  approaches  $T_a$  (not shown).

In the case of lumped stream reaches, *StreamFlow* uses the first order upwind finite difference approximation of Eqs. (3.9)–(3.10) to estimate stream temperature  $T_{w,j}$  in each reach  $j$  (see e.g. Westhoff et al., 2007):

$$A_j \frac{dT_{w,j}}{dt} = \frac{Q_{in,j}}{L_j} (T_{in,j} - T_{w,j}) + q_{subw,j} (T_{subw,j} - T_w) + \frac{w_j \phi_j}{\rho_w c_{p,w}} + L_j Q_j \frac{g}{c_{p,w}} \overline{S_0}, \quad (3.15)$$

where  $A_j$  ( $m^2$ ),  $Q_j$  ( $m^3 s^{-1}$ ),  $\overline{S_0}$  ( $-$ ),  $L_j$  (m) and  $w_j$  (m) denote the cross-sectional area, outlet discharge, mean bed slope, length and width of reach  $j$ , and  $\phi_j$  ( $W m^{-2}$ ) corresponds to the net heat flux into reach  $j$ .  $Q_{in,j}$  and  $T_{in,j}$  stand for the discharge and temperature of water draining into the reach inlet.  $Q_{in,j}$  is simply computed as the sum of the outlet discharges of the upstream reaches, whereas  $T_{in,j}$  is approximated as the discharge weighted mean of the outlet temperatures of the upstream reaches.  $T_{subw,j}$  and  $q_{subw,j}$  denote the temperature and discharge per unit streamwise distance of the subsurface water inflow into reach  $j$ . Equation (3.15) is discretized in time using an implicit Euler scheme, whose solution is obtained thanks to the simplified Brent's root finding method proposed by Stage (2013).

In discretized stream reaches, Eq. (3.11) is solved using a splitting scheme (e.g. LeVeque, 2002). The idea is to decompose the equation into two simpler ones, where the solution of the first equation serves as initial condition for the second one. Similarly to Loinaz et al. (2013), we chose here to separate heat advection from the accounting of the heat sources, since standard approaches are available for the numerical resolution of advection in the absence of sources. The resulting splitting scheme is the following (adapted from Loinaz et al., 2013):

$$\frac{\partial T_w}{\partial t} + v \frac{\partial T_w}{\partial x} = 0, \quad (3.16)$$

$$\frac{dT_w}{dt} = \frac{\phi}{\rho_w c_{p,w} h} + \frac{q_{subw}}{h w} (T_{subw} - T_w) + \frac{g Q}{c_{p,w} h w} S_0. \quad (3.17)$$

Equation (3.16) is discretized over each stream reach using an explicit upwind finite volume scheme with second-order precision in space and first-order precision in time (Berger et al., 2005):

$$T_{w,i}^{n+1} = T_{w,i}^n - \frac{v_i^n \Delta t}{l_i} (T_{w,i+1/2}^L - T_{w,i-1/2}^L). \quad (3.18)$$

In the above equation,  $T_{w,i}^n$  (K) and  $v_i^n$  ( $ms^{-1}$ ) denote the stream temperature and flow ve-

locity in reach cell  $i$  at time  $t_n$ ,  $\Delta t$  corresponds to the time step and  $l_i$  is the length of cell  $i$ .  $T_{w,i+1/2}^L$  (K) refers to the so-called *left state* at the right boundary of cell  $i$ , which is computed as:

$$T_{w,i+1/2}^L = T_{w,i}^n + \frac{1}{2}\psi_i(T_{w,i}^n - T_{w,i-1}^n), \quad (3.19)$$

where the factor  $\psi_i$  (–), known as a *slope limiter*, is introduced so as to limit numerical dispersion. Many slope limiters have been derived for regular space discretizations (LeVeque, 2002), but very few are available for irregular meshes (Berger et al., 2005; Zeng, 2013). *StreamFlow* implements the slope limiter developed by Zeng (2013),

$$\psi_i = \frac{B(r + r^k)}{1 + Ar^k}, \quad (3.20)$$

with

$$\begin{aligned} r &= \frac{T_{w,i+1} - T_{w,i}}{T_{w,i} - T_{w,i-1}}, \\ A &= \frac{l_{i-1} + l_i}{l_i + l_{i+1}}, \\ B &= \frac{2l_i}{l_i + l_{i+1}}, \\ k &= \left\lceil \frac{B}{2 \min(1, A) - B} \right\rceil. \end{aligned}$$

The solution to Eq. (3.18) is used as initial condition for Eq. (3.17), which is discretized in time according to an implicit Euler scheme and solved using the root-finding method developed by Stage (2013). A validation of the splitting scheme can be found in Appendix C, where it is compared with analytical solutions to the heat balance equation in two simple test cases.

### 3.3 Model implementation

In order to allow for the calibration of its parameters, *StreamFlow* was developed as a stand-alone program rather than being seamlessly integrated into *Alpine3D*. This permits a higher flexibility, since *Alpine3D*—whose typical computation time is of the order of 24 hours when simulating a 1 year period on a standard personal computer—does hereby not need to be newly run each time a new parameter set is tested in *StreamFlow*.

For the sake of consistency, *StreamFlow* is, similarly to *Alpine3D*, implemented in C++ and compiled using CMake. The choice was made to use version C++11 of the C++ language, since it offers new practical features such as anonymous functions or ranged-based for loops as compared to the C++99 standard (Lippman et al., 2012)—regardless of the fact that C++11 is meant to supersede C++99 on the long term. The same coding strategy as detailed in Bavay and Egger (2014) is used here, namely:

- Advantage is taken of the object-oriented nature of C++ to clearly structure the code and make it as modular as possible, so as to facilitate understandability and ease future developments.
- The dependence towards third-party software is avoided as much as possible in order to limit installation issues. The only external utility required by *StreamFlow* is the library *MeteoIO* (Bavay and Egger, 2014), which is used to read input files and interpolate meteorological data in space and time.
- Significant effort is put in documenting the code, both for end-users and future developers. On-line documentation provides indications regarding the installation procedure and the steps to follow in order to launch a simulation (see <http://models.slf.ch/p/streamflow/doc/>). In addition, technical documentation is directly integrated into the source code using the doxygen tool (van Heesch, 2008).
- Particular attention is paid at keeping the coding style consistent. This task is facilitated by the small size of the development team—mostly one person—and the young age of the project—the creation of *StreamFlow* dates from 2015. The coding style is essentially the same as in *MeteoIO*, with additional conventions regarding the naming of class attributes.<sup>1</sup>
- When compiling the code, all possible gcc warnings are activated and requested to be passed successfully. The code currently compiles on Windows, Linux and OS X.
- The program is designed so as to be as flexible as possible. In particular, its behavior can be adapted without recompiling the code by modifying the configuration file, which regroups all adjustable parameters. Additionally, the use of library *MeteoIO* for preprocessing allows input data to be provided in a large variety of formats.
- Daily automated tests were set into place using CTest. This ensures that potential errors introduced by code modifications are rapidly identified and corrected, therefore increasing code stability.

The following sections provide some details about the code implementation and the program work flow.

#### 3.3.1 Program main architecture

The program is structured around a main class, *HydrologicalModel*, which is in charge of computing the transport of water and energy within the hillslopes and along the stream network (see Fig. 3.3a). This class regroups an object of type *Watershed*—representing the catchment—and another one of type *StreamNetwork*—symbolizing the stream network.

---

<sup>1</sup>See <http://models.slf.ch/p/streamflow/page/CodingStyle/>

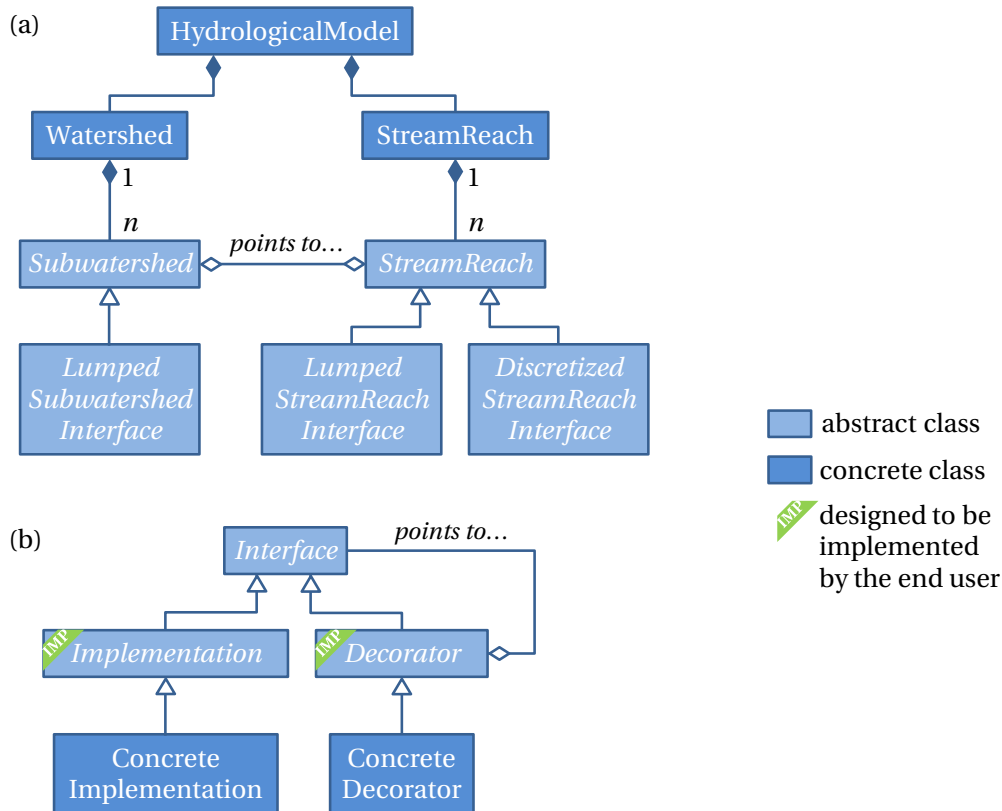


Figure 3.3: Structure of *StreamFlow*'s source code. **(a)** Simplified diagram of *StreamFlow*'s high level classes; **(b)** Diagram of the Decorator pattern used to implement abstract classes *LumpedSubwatershedInterface*, *LumpedStreamReachInterface* and *DiscretizedStreamReachInterface*.

Class *Watershed* is nothing but a container storing a collection of *Subwatershed* objects, each one of them representing one of the subcatchments identified by TauDEM. As depicted in Fig. 3.3a, class *Subwatershed* is subclassed into *LumpedSubwatershedInterface*, which defines the interface to be implemented by lumped subwatersheds—i.e. subwatersheds being treated as single points (see Sect. 3.2.1). Future code developments could include the definition of a second interface inherited from *Subwatershed*, representing the subwatersheds as spatially-distributed entities. Each concrete subclass of *LumpedSubwatershedInterface* is intended to implement a different approach for calculating the discharge and/or temperature of subsurface runoff (see below).

Every *Subwatershed* object holds a pointer to its corresponding stream reach, which is represented in the code by class *StreamReach*. The latter is subdivided into two abstract subclasses: *LumpedStreamReachInterface* representing lumped stream reaches, and *DiscretizedStreamReachInterface* symbolizing discretized stream reaches. Each one of these subclasses is further subclassed into concrete implementations, each implementation corresponding to a specific method for computing stream discharge and/or temperature (see below). All the *StreamReach*



objects belonging to the stream network are regrouped into the container class *StreamNetwork*.

Classes *LumpedSubwatershedInterface*, *LumpedStreamReachInterface* and *DiscretizedStreamReachInterface* are intentionally abstract in order to allow for the implementation of the Decorator pattern. This standard design pattern, illustrated in Fig. 3.3b, is aimed at dynamically extending the functionality of a class (Gamma et al., 1994). It is used here to separate the discharge computation from the temperature calculation, which allows each temperature modeling approach to be combined with every discharge computation method. In its commonly accepted definition, the Decorator pattern requires the declaration of a wrapper class—called *ConcreteDecorator* in Fig. 3.3b—which implements the same interface as the objects to be decorated—called *ConcreteImplementation* in the figure. The presence of abstract class *Decorator* in the pattern (see Fig. 3.3b) allows for multiple decorators to be stacked on top of each other, a feature which might be of interest for future developments of *StreamFlow* in case e.g. pollutant transport was to be implemented in the model as an additional decorator. Abstract class *Implementation* is not part of the traditional Decorator pattern, but was introduced in *StreamFlow* in order to implement functionalities which are common to all of its subclasses, hereby reducing duplicate code. In the Decorator pattern, each call to a member function of the wrapper is usually forwarded to the decorated object, with additional operations occurring before and/or after the forwarded function call. As mentioned above, this pattern is used in *StreamFlow* to separate the computation of discharge from the one of temperature. For example, the concrete subclass of *LumpedSubwatershedInterface*, which implements the linear reservoir model described in Sect. 3.2.1, is only concerned with the modeling of subsurface runoff discharge. The three possible methods detailed in Sect. 3.2.1 for computing subsurface runoff temperature are implemented each in separate decorators of this class. Similarly, some subclasses of *LumpedStreamReachInterface* and *DiscretizedStreamReachInterface* are in charge of computing stream discharge only; the estimation of stream temperature occurs in the decorators. The interfaces of both decorated and decorator classes—namely classes *Implementation* and *Decorator* in Fig 3.3b—have been designed in *StreamFlow* so as to be easily extended by a casual developer, therefore facilitating the implementation of future discharge or temperature computation methods.

#### 3.3.2 Input reading

For *StreamFlow* to run properly, *Alpine3D* has to be configured so as to output the grids of the water percolation rate at the bottom of the soil columns. In case stream temperature is to be computed, *StreamFlow* additionally expects grids of soil temperature from *Alpine3D* (see Sect. 3.2.1), on top of the same meteorological measurements as those required by *Alpine3D* as input. These measurements will be interpolated by *MeteoIO* over the stream reaches, taking topographic shading into account in the case of incoming short wave radiation.

Similarly to *MeteoIO*, *StreamFlow* processes its input files in a centralized manner, hereby facilitating the understanding and reuse of the code by casual developers. All required files

are parsed by a single class, *InputReader*, which supports various input formats thanks to the integrated use of *MeteoIO* utilities (see Bavay and Egger, 2014). It delegates the actual parsing of the input files to low-end classes, devised to be easily modified or enriched by end users.

### 3.3.3 Output writing

As a result of its semi-distributed nature, *StreamFlow* is able to output the discharge and temperature of subsurface runoff produced by each subwatershed, as well as the water depth, discharge and temperature in each stream reach. Output files are currently produced in the SMET format,<sup>2</sup> for which various utilities—such as parsing and visualizing functions in Matlab and Python—are available in *MeteoIO*. The possibility is offered to the user to generate output files only for certain subwatersheds and/or stream reaches.

As for the parsing of the input files, the writing of the output data is handled by a high-level class, *OutputWriter*, which delegates the actual generation of the output files to low-level classes. As mentioned in the previous section, this architecture both facilitates future developments and eases the understanding of the global code structure.

### 3.3.4 Calibration module

*StreamFlow* comes with an optimization module used to calibrate the model parameters. It aims to identify the parameter set minimizing the so-called *objective function*. The latter can be freely specified by the user based on the following standard error measures:

- The root mean square error (RMSE)
- The Nash-Sutcliffe efficiency (NSE Nash and Sutcliffe, 1970), also known as the coefficient of determination  $R^2$
- The mean absolute error (MAE), corresponding to the average over all time steps of the model error absolute values
- The bias, defined as the mean value of the model errors over all time steps.

Each one of the above four measures can be evaluated either for water depth, discharge or temperature, bringing to a total of 12 the number of different error measures at disposal. *StreamFlow* also supports the case where measurement data is available at more than one point along the stream network. The objective function can be defined as any weighted sum of some (or all) of the available error measures, hereby making the model calibration entirely flexible. Monte Carlo simulations are currently used for calibrating the model, but other well-known optimization algorithms such as DREAM (Vrugt and Ter Braak, 2011) or GLUE (Beven and Binley, 1992) could be easily integrated into the code.

---

<sup>2</sup>See [https://models.slf.ch/docserver/meteoio/SMET\\_specifications.pdf](https://models.slf.ch/docserver/meteoio/SMET_specifications.pdf)

For the sake of modularity and flexibility, the list of model parameters is not managed centrally in the source code. Instead, each parametrizable class is responsible of defining its own associated parameters. This operation is performed through inheritance of a dedicated abstract class, *ParametrizableObject*, which essentially possesses two member functions *getParameters* and *setParameters* for obtaining and modifying the class parameters, respectively. The calibration module can then reconstruct the complete list of model parameters by simply calling method *getParameters* on each object inheriting from *ParametrizableObject*. Based on this list, it can compute new parameter values to be tested, which are transferred back to the individual objects through a call to their method *setParameters*.

In addition to its name, value and units, each model parameter in *StreamFlow* is associated with a range of physically acceptable values and a flag specifying whether it should be calibrated or not. The physically acceptable range is used by the calibration module to restrict the search domain for the best parameter value. The properties of each parameter can be freely set by the user in the program configuration file. In particular, the calibration flag can be individually set to true or false for every parameter, hereby making it possible to calibrate only a given subset of parameters.

## 3.4 Case study

In view of assessing its accuracy and demonstrating some of its capabilities, *StreamFlow* is tested over a high altitude catchment in Switzerland. Section 3.4.1 presents the test catchment and the measurement data used to validate the model. The model setup is described in Sect. 3.4.2 and the simulation results are detailed in Sect. 3.4.3.

### 3.4.1 Study site and measurement data

*StreamFlow* is tested over the Dischma catchment, located in the eastern Swiss Alps (see insert in Fig. 3.4). The gauging station operated by the Swiss Federal Office for the Environment (FOEN) at the location named Davos Kriegesmatte—referred to as *Outlet* in Fig. 3.4—is chosen as the catchment outlet. At this point, the watershed has an area of 43.3 km<sup>2</sup> and is mostly covered with pasture (36 %), rock outcrops (24 %) and bare soil (16 %), with only 2 % of glacier cover (Schaeffli et al., 2014). Very little riparian vegetation is present along the stream, which ensures that the current absence of riparian shade model in *StreamFlow* does not have a large influence on the quality of the stream temperature simulation. The watershed elevation ranges from about 1700 m to more than 3100 m above sea level. Its hydrological regime was classified as glacio-nival by Aschwanden and Weingartner (1985), i.e. the stream discharge is low in winter and peaks in June–July due to snow and ice melt, therefore corresponding to a typical watershed over which *StreamFlow* is meant to be used. More information on the Dischma catchment can be found in e.g. Zappa et al. (2003) and Schaeffli et al. (2014).

Water depth, discharge and temperature are continuously monitored by the FOEN at the

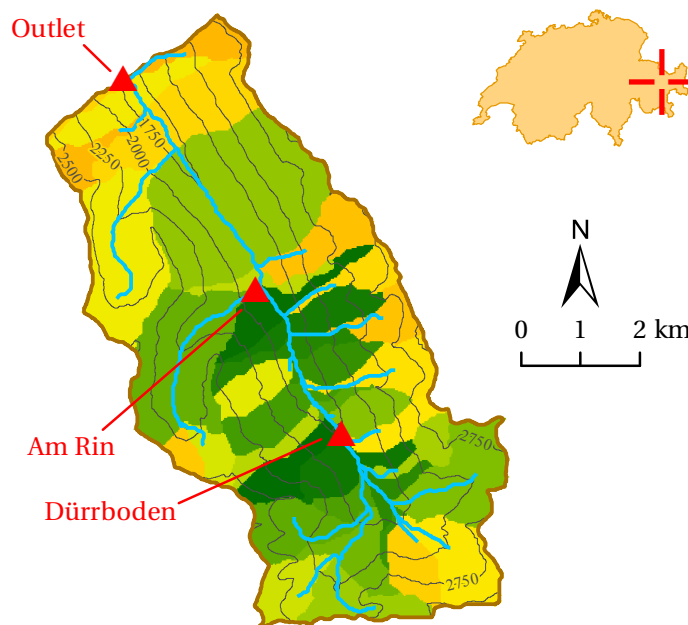


Figure 3.4: Map of the Dischma catchment displaying the subwatersheds (colored areas) and stream network (light blue line) derived from the DEM using TauDEM. The locations of the stream gauges are indicated as red triangles.

catchment outlet. In complement to the quality control performed by the FOEN, hourly mean data is also corrected here using the procedure described in Gallice et al. (2015), namely a combination of visual inspection and automatized outlier identification. In addition to the FOEN station, two temporary gauging stations were installed starting on 16 January 2015 at the locations named Am Rin and Dürrboden, indicated as red triangles in Fig. 3.4. The gauging station at Am Rin was positioned in a small stream coming from a side valley, just above its confluence with the main stream. The station at Dürrboden was deployed in the upper part of the main stream, just below the confluence with the rivulet coming from the glacier. Both stations continuously measured water depth and stream temperature at a rate of one hour. Discharge was manually estimated using the salt dilution technique on a few days during winter and spring, which enabled the derivation of a rating curve to convert the continuous water depth measurements into discharge values (e.g. Weijs et al., 2013). The data from the gauging stations at Am Rin and Dürrboden is corrected using the same protocol as the data provided by the FOEN.

The meteorological data used to run the *Alpine3D* simulation and compute the stream temperature in *StreamFlow* is obtained from two different sources:

- (a) The Swiss Federal Office of Meteorology and Climatology, MeteoSwiss, which operates a country-wide network of automatic weather stations. Two of these are in the vicinity of the Dischma catchment: the Davos and Weissfluhjoch stations, whose respective

locations are about 5 and 8.5 km on the North-West of the catchment outlet. They are both equipped with heated rain gauges, the one at Davos being unshielded and the one at Weissfluhjoch shielded. These stations provide measurements of air temperature, relative humidity, incoming long and short wave radiation, precipitation, wind direction and snow height every hour.

- (b) The Intercantonal Measurement and Information System (IMIS), a network of automated weather stations mostly used for avalanche forecasting in Switzerland (Lehning et al., 1999). Four of these stations are used in the present study, whose distances to the catchment outlet are 0.9, 4.7, 5.9 and 9.5 km. They continuously measure air temperature, relative humidity, outgoing short wave radiation, wind speed and snow depth at a rate of one hour.

All meteorological time series are visually inspected to detect sensor failure. Data flagged as erroneous is removed from the time series.

#### 3.4.2 Model setup

As mentioned previously, *StreamFlow* requires *Alpine3D* to be executed first. In the present case, *Alpine3D* is run over a grid with 100 m resolution and with an internal time step of 15 minutes. The simulated time period extends over three hydrological years, namely from 1<sup>st</sup> October 2012 to 1<sup>st</sup> October 2015. All meteorological input data are spatially interpolated using the inverse-distance weighting approach with lapse rate, except for solar radiation and precipitation. Solar radiation is computed based on the measurements at Weissfluhjoch station alone, taking atmospheric attenuation into account for each grid cell separately. Precipitation is interpolated using the data measured at the Davos station only. It is corrected for undercatch using the approach advocated by the World Meteorological Organization (WMO) for Hellmann gauges (Goodison et al., 1998), before being distributed over each grid cell based on a lapse rate proportional to the measured precipitation intensity at Davos. Another procedure using the data from Weissfluhjoch station in addition to the one from Davos was also tested for interpolating precipitation. However, it was rejected since it largely overestimated the total amount of precipitation falling over the catchment, due to the existence of a strong North-South precipitation gradient in the area, making the measurements at Weissfluhjoch station—located further North—less representative of the situation in the Dischma catchment than those at Davos station—located closer to the catchment (Voegeli et al., 2016).

As an additional preliminary step to the *StreamFlow* simulation, the stream network and its corresponding set of subwatersheds are, as described in Sect. 3.2, extracted from a 25 m resolution DEM<sup>3</sup> provided by the Swiss Federal Office of Topography, SwissTopo. Application of the automatic Peuker–Douglas extraction method provided by TauDEM<sup>4</sup> results in a subdivision of the catchment into 39 subwatersheds, ranging in size from 0.2 ha to 6.4 km<sup>2</sup> (see Fig. 3.4). It

<sup>3</sup>See <http://www.swisstopo.admin.ch/internet/swisstopo/en/home/products/height/dhm25.html>

<sup>4</sup>See <http://hydrology.usu.edu/taudem/taudem5/help53/PeukerDouglas.html>

### Chapter 3. Deterministic stream temperature modeling in high alpine watersheds

Table 3.2: Parameters used by *StreamFlow* to simulated water depth, discharge and temperature using various approaches. The parameters are described into more detail in the main text (Sect. 3.2 and Appendix B). First column of the table mentions the part of the model in which the parameter is used. The absence of a calibration range (marked as n/a) indicates a fixed parameter.

Model part	Parameter	Units	Defined in	Calibrated or chosen value	Calibration range	Rationale for the chosen value or calibration range
Subwatershed outflow discharge (Sect. 3.2.1)	$R_{\max}$	(mm day <sup>-1</sup> )	main text	6.93	[0, 50]	Comola et al. (2015)
	$\bar{\tau}_{\text{res},u}$	(day)	Eq. (B.5)	22.5	[0, 60]	Comola et al. (2015)
	$\bar{\tau}_{\text{res},l}$	(day)	Eq. (B.6)	567.1	[0, 600]	Comola et al. (2015)
Subwatershed outflow temperature (Sect. 3.2.1)	$k_{\text{soil}}$	(day)	Eqs. (B.7)–(B.8)	49.6	[0, 50]	Comola et al. (2015)
	$\tau_{\text{HSPF}}$	(day)	Eq. (3.1)	58.2	[0.1, 100]	
	$D_{\text{HSPF}}$	(°C)	Eq. (3.1)	0.99	[-3, 1]	
	$z_d$	(m)	main text	2.40	n/a	
Channel water discharge (Sect. 3.2.2)	$a_w$	(m <sup>-1</sup> )	main text	$1.52 \times 10^{-7}$	n/a	aerial photographs
	$b_w$	(m)	main text	0.39	n/a	aerial photographs
	$\alpha_h$	(m <sup>1-3</sup> $\beta_h$ s <sup><math>\beta_h</math></sup> )	main text	0.57	n/a	discharge gauging curve at watershed outlet
	$\beta_h$	(-)	main text	0.32	n/a	same as for $\alpha_h$
	$n_m$	(-)	Eqs. (3.5) and (3.7)	0.04, 0.07, 0.10	n/a	Phillips and Tadayon (2006)
Channel water temperature (Sect. 3.2.2)	$a_{vw}$	(-)	Eq. (3.13)	$2.20 \times 10^{-3}$	n/a	Webb and Zhang (1997)
	$b_{vw}$	(m s <sup>-1</sup> )	Eq. (3.13)	$2.08 \times 10^{-3}$	n/a	Webb and Zhang (1997)
	$k_{\text{bed}}$	(W m <sup>-2</sup> K <sup>-1</sup> )	Eq. (3.12)	52.0	n/a	Moore et al. (2005b) and MacDonald et al. (2014)

should be mentioned that the difference in resolution between the DEM provided as input to *Alpine3D* (100 × 100 m) and the one used to extract the stream network (25 × 25 m) is seamlessly handled by *StreamFlow*. This allows, as in the present case, for *Alpine3D* to be run over a coarser grid than *StreamFlow*, hereby saving computational power and resources.

*StreamFlow* is configured so as to compute the width  $w$  of each stream reach as:  $w = a_w A_{\text{reach,tot}} + b_w$ , where  $A_{\text{reach,tot}}$  (m<sup>2</sup>) denotes the total area drained by the reach—including its upstream reaches. Parameters  $a_w$  (m<sup>-1</sup>) and  $b_w$  (m) are determined approximately based on the width of the main stream estimated at sample locations using aerial photographs of the Dischma catchment. In addition, the values of parameters  $\alpha_h$  and  $\beta_h$ , which are required by the model to estimate water depth when simulating discharge based on the instantaneous advection technique (see Sect. 3.2.2), are derived from the discharge gauging curve provided by the FOEN at the catchment outlet. All model parameters used for the *StreamFlow* simulations presented in the next section are summarized in Table 3.2, along with their respective calibration ranges when appropriate. For the purpose of reducing the impact of the initial conditions on the modeled stream variables, a warm-up period of one year is considered. In other words, the model is run over a random year before each simulation, and its state at the end of the warm-up period is used as an initial condition for the actual simulation. The model is calibrated over hydrological year 2013 using Monte-Carlo simulations, and validated over hydrological years 2014 and 2015. Calibration is performed in two steps:

1. All parameters associated with water routing, whether within the hillslopes or along the

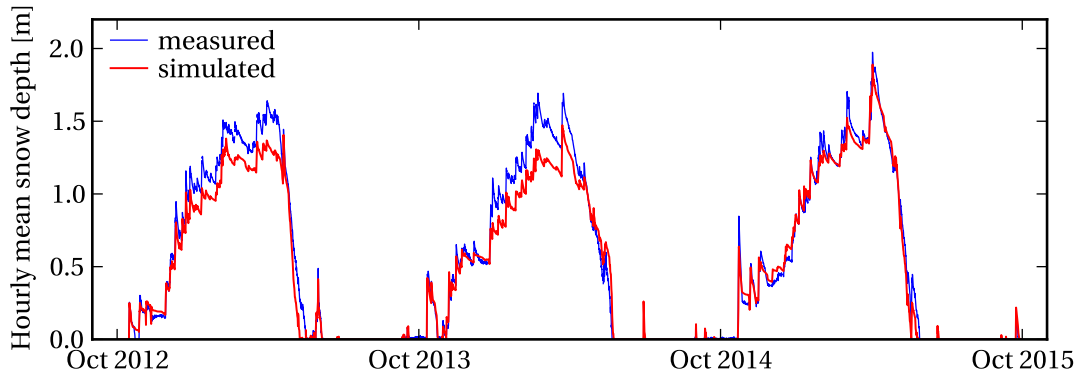


Figure 3.5: Comparison between the measured (blue line) and simulated (red line) snow depth at the Stillberg meteorological station over the period 2013–2015. The simulated curve corresponds to the mean snow depth as computed by *Alpine3D* over the  $100 \times 100$  m grid cell containing the Stillberg station.

stream network, are calibrated by maximizing the Nash-Sutcliffe efficiency of simulated discharge at the catchment outlet. Only the parameters associated with subsurface runoff modeling are actually calibrated in this step (namely  $R_{\max}$ ,  $\bar{\tau}_{\text{res,u}}$  and  $\bar{\tau}_{\text{res,l}}$ ), since the only parameter related to water routing within the stream channels (i.e. Manning's coefficient) is fixed to some predefined values (see Sect. 3.4.3 and Table 3.2).

2. The parameters calibrated in step 1 are kept fixed to their respective best values, while the parameters related to stream temperature modeling are calibrated by maximizing the NSE of simulated temperature at the catchment outlet. This step is repeated for each method used to compute the temperature of subsurface runoff (see Sect. 3.2.1). The parameters associated with the water heat balance in the stream network are fixed to specific values based on physical considerations (see Table 3.2).

In order to better assess the accuracy of *StreamFlow*, the approach advocated by Schaepli and Gupta (2007) is followed here. The error measures associated with *StreamFlow* are compared to those of a simplistic benchmark model, so as to verify whether *StreamFlow* allows for more robust predictions than those that could be made based on a basic procedure. Two benchmark models are actually considered here, one for discharge and one for temperature. Both are constructed by averaging, for each hour of each day of the year, the values of discharge and temperature measured at the catchment outlet on those particular hour and day over a period of 10 years (2005–2014). Stated otherwise, the two models correspond to the measured yearly curves of mean hourly discharge and temperature at the catchment outlet, averaged over ten years.

Table 3.3: Comparison of the total volume of water  $V_{in,simu}$  simulated by *Alpine3D* to percolate at the bottom of the watershed soil columns over each year, and the measured total volume of water  $V_{out,meas}$  flowing out of the catchment each year via the river.

Hydrological year	$V_{in,simu}$ (m <sup>3</sup> )	$V_{out,meas}$ (m <sup>3</sup> )	Relative difference (%)
2013	$5.28 \times 10^7$	$5.64 \times 10^7$	-6.3
2014	$5.88 \times 10^7$	$5.57 \times 10^7$	5.7
2015	$5.57 \times 10^7$	$5.18 \times 10^7$	7.6

#### 3.4.3 Model evaluation

##### Results of the *Alpine3D* simulation

The *Alpine3D* simulation is observed to rather accurately capture the time evolution of the snow pack. As an example, Fig. 3.5 depicts the simulated snow depth in comparison with the measured one at the Stillberg meteorological station, which is located at an altitude of 2085 m above sea level on the Western slope of the catchment. It can be noticed that the onset of snow accumulation and the timing of the melting period are satisfyingly reproduced, in addition to the fact that the snow depth appears to be overall well simulated. A more quantitative assessment of the accuracy of the *Alpine3D* simulation is obtained by considering the global volume of water transiting through the watershed each year. Thus, the measured cumulated volume of water  $V_{out,meas}$  flowing through the catchment outlet each year is compared to the simulated cumulated volume of water  $V_{in,simu}$  percolating at the bottom of all the soil columns belonging to the watershed over the same year. As can be observed in Table 3.3, the relative difference between  $V_{out,meas}$  and  $V_{out,simu}$  remains within the range  $\pm 8\%$  for all three hydrological years.

##### *StreamFlow* simulations of discharge and water depth

As mentioned in the previous section, *StreamFlow* parameters related to discharge computation are calibrated against measured discharge at the catchment outlet. To this end, 10000 Monte-Carlo simulations are run, with *StreamFlow* configured so as to use a time step of 1 hour and advect water in the stream channels based on the instantaneous routing scheme (see Sect. 3.2.2). Figure 3.6 presents a comparison of the simulated and measured hourly mean discharges over the three considered hydrological years. The uncertainty range of the simulated curve is defined by all parameter sets associated with a NSE larger than 0.85 during the calibration period, which amounts to a total of 300 curves. As observed in panel (a), the simulation corresponding to the highest NSE value matches globally well with the observations, except for a few discharge peaks which are not well captured in 2013 and 2015. The simulation uncertainty range appears to be relatively narrow on an annual scale. When looking at a finer scale, it can be observed that the daily fluctuations of discharge are relatively well captured by the model, as for example shown in panel (b) for the period 29 May to 8 June



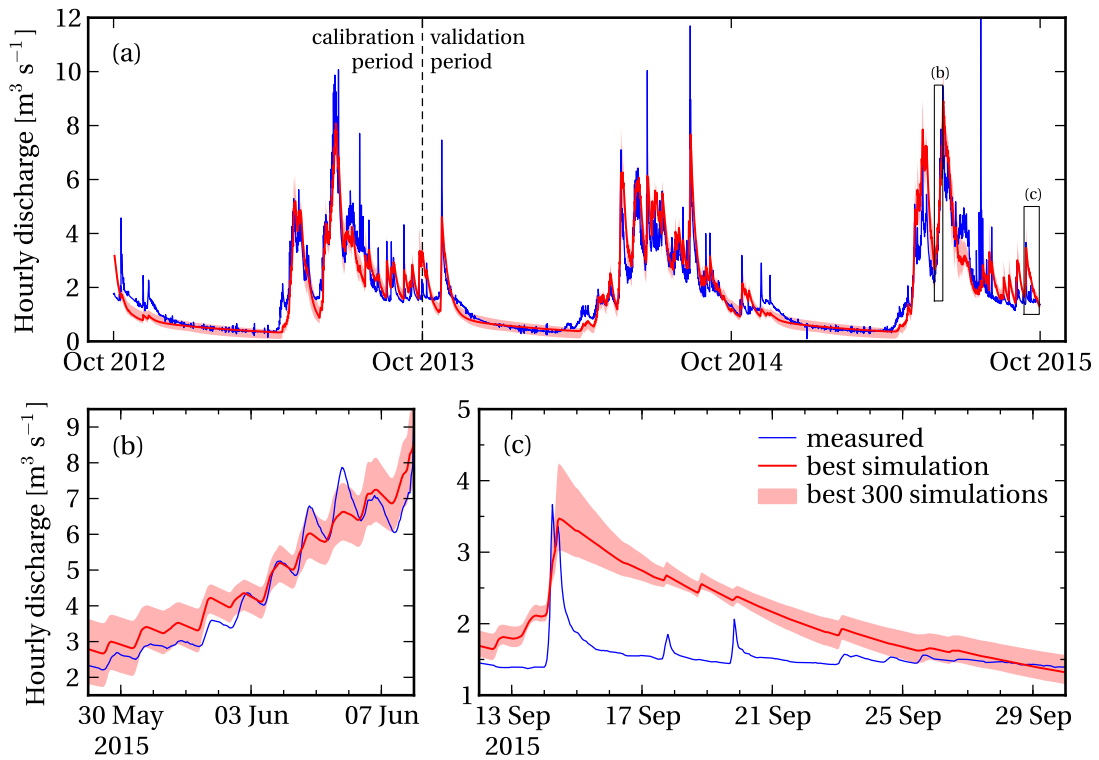


Figure 3.6: Comparison between the measured (blue line) and simulated (red line) hourly mean discharge at the watershed outlet. Panel (a) pictures the entire simulated period, and panels (b) and (c) correspond to zooms on two selected time periods (their extents are indicated as black rectangles in panel (a)). The simulated curve was obtained with *StreamFlow* configured so as to advect water in the stream channels using the instantaneous routing approach. The uncertainty range corresponds to the 300 best runs of the model out of the 10 000 Monte-Carlo simulations.

2015. On the other hand, the absence of a fast runoff component in *StreamFlow* prevents the model to correctly capture short-lived discharge peaks. As displayed in panel (c), the modeled recession in these cases is much too slow compared to the observed one.

Table 3.4 presents quantitative error measures of discharge modeled over the validation period at the three gauging points located in the Dischma catchment (see Fig. 3.4), for the same *StreamFlow* configuration as in Fig. 3.6. The accuracy of the benchmark model at the catchment outlet is also indicated in the table for comparison. It should be mentioned that the benchmark model could not be evaluated at the two intermediate stations since the measurement time series at these points extend over less than a year (see Sect. 3.4.1). As observed in the table, the discharge NSE value associated with the best *StreamFlow* simulation is larger than 0.80 at all three points, as opposed to the NSE value of the benchmark model not exceeding 0.74. On the other hand, the values of NSE-log—defined as NSE computed with the logarithm of the discharge values—are quite comparable between both models. This is not particularly surprising in view of the strong seasonality of the baseflow component of

### Chapter 3. Deterministic stream temperature modeling in high alpine watersheds

Table 3.4: Accuracy of the hourly mean discharge simulations performed by *StreamFlow* using the instantaneous water routing technique. The performance of the discharge benchmark model is indicated in the last row for comparison. The third column contains the period over which the error measures are computed. NSE-log corresponds to the Nash-Sutcliffe efficiency computed with the logarithm of the discharge values.

Model	Location	Time period	RMSE ( $\text{m}^3 \text{s}^{-1}$ )	NSE (-)	NSE-log (-)	Bias ( $\text{m}^3 \text{s}^{-1}$ )
<i>StreamFlow</i>	Outlet	entire validation period	0.60	0.82	0.90	0.14
	Dürrboden	17 Jan. to 25 Sept. 2015	0.30	0.81	0.91	0.11
	Am Rin	17 Jan. to 17 Jul. 2015	0.10	0.82	0.76	0.02
Benchmark	Outlet	entire validation period	0.73	0.74	0.88	-0.04

discharge, particularly during the winter season. The NSE-log value at point Am Rin is rather low, but should be considered with caution since the discharge gauging curve at this point is rather uncertain (not shown). The bias of *StreamFlow* is observed to be positive at all three gauging points, which certainly results from the slight overestimation of the rate of water percolating at the bottom of the soil columns in the *Alpine3D* simulation (see above). Overall, the performance of *StreamFlow* regarding discharge computation based on the instantaneous water routing scheme can be considered as satisfying. Its accuracy is comparable to the one of other existing hydrological models applied over high Alpine catchments (e.g. MacDonald et al., 2014; Schaefli et al., 2014).

Regarding the calibration parameters, it appears that the values of  $R_{\max}$  and  $\bar{\tau}_{\text{res},u}$  are rather well identified (see Fig. 3.7). Indeed, their respective distributions based on the best 300 parameter sets are contained within a rather narrow interval, clearly separated from the bounds of the respective calibration ranges. Within this interval however, the two parameters are strongly correlated with one another, as pictured in panel (c) of Fig. 3.7. This points at the equifinality of the parameter sets (Bárdossy, 2007), since an increase in  $\bar{\tau}_{\text{res},u}$  conjugated with a decrease in  $R_{\max}$  maintains the model accuracy almost constant. As opposed to  $\bar{\tau}_{\text{res},u}$  and  $R_{\max}$ , parameter  $\bar{\tau}_{\text{res},l}$  is associated with a broad distribution, sticking to the upper boundary of the calibration interval (see panel (a) of Fig. 3.7). As such, *StreamFlow* appears to be relatively insensitive to the value of  $\bar{\tau}_{\text{res},l}$ , as further emphasized by the low correlation between  $\bar{\tau}_{\text{res},l}$  and the other two parameters (Bárdossy, 2007).

In order to evaluate the influence of the channel water routing scheme on the modeled discharge, *StreamFlow* was run with the following configurations in complement to the instantaneous routing technique evaluated above: (a) the Muskingum-Cunge approach with lumped stream reaches and Manning's coefficient  $n_m$  set to 0.04, (b) same as (a) but with  $n_m = 0.10$ , and (c)–(d) same as (a)–(b) but with discretized stream reaches. The chosen values for Manning's coefficient correspond to the lower and upper boundaries of the uncertainty interval estimated in the Dischma catchment based on the work of Phillips and Tadayan (2006). The results indicate that the modeled hourly mean discharge curves in all cases (a) to (d) almost

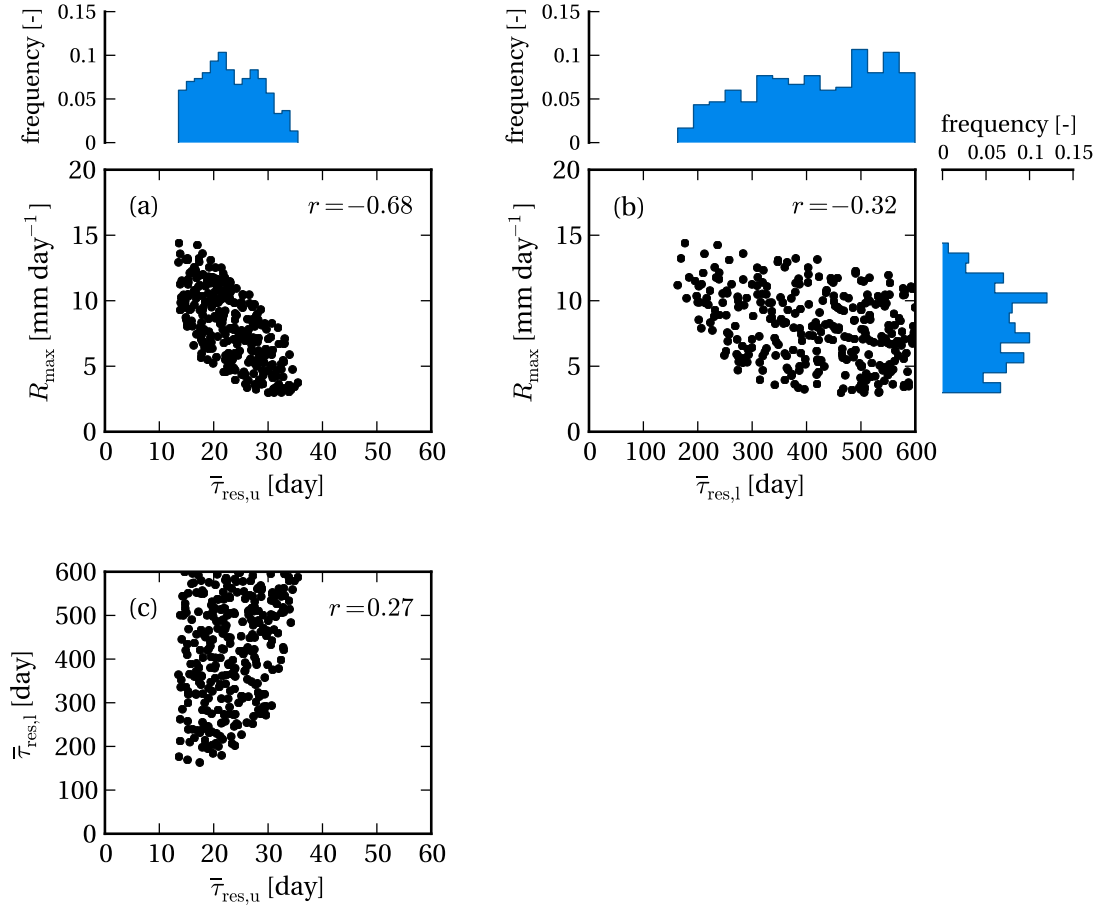


Figure 3.7: The 300 best sets of parameters associated with water transport (see Table 3.2 for more information on the parameters). Each panel contains the values of two parameters displayed as a function of each other: **(a)**  $R_{\max}$  versus  $\bar{\tau}_{\text{res},l}$ , **(b)**  $\bar{\tau}_{\text{res},u}$  versus  $\bar{\tau}_{\text{res},l}$  and **(c)**  $R_{\max}$  versus  $\bar{\tau}_{\text{res},u}$ . Each x or y axis spans the entire calibration range of its associated parameter. The parameter distributions are indicated in blue on the sides of the corresponding panels; for example, the distribution of the 300 best  $R_{\max}$  values is shown on the right-hand side of panel **(a)**. Person's correlation coefficient  $r$  between each pair of parameters is indicated in the upper right-hand corner of the associated graph.

identically correspond to the one depicted in Fig. 3.6, up to a maximum RMSE of  $0.03 \text{ m}^3 \text{ s}^{-1}$  between all curves over the entire simulated period (not shown). Similarly, the error measures reported in Table 3.4 are also valid in cases (a) to (d). The routing technique therefore appears to have only a very limited impact on the simulated discharge in the Dischma catchment, which is easily explained by the small size of the watershed (Schaepli et al., 2014). Indeed, the average streamwise distance between the stream cells and the catchment outlet is about 6.6 km, which—assuming a flow velocity of  $1 \text{ m s}^{-1}$ —corresponds to a mean travel time of about 2 hours down to the catchment outlet. This also explains the observed low sensitivity of *StreamFlow* to the value of Manning's coefficient in the present case. As expected, the above results suggest that, in small to medium-sized catchments, the use of spatially discretized

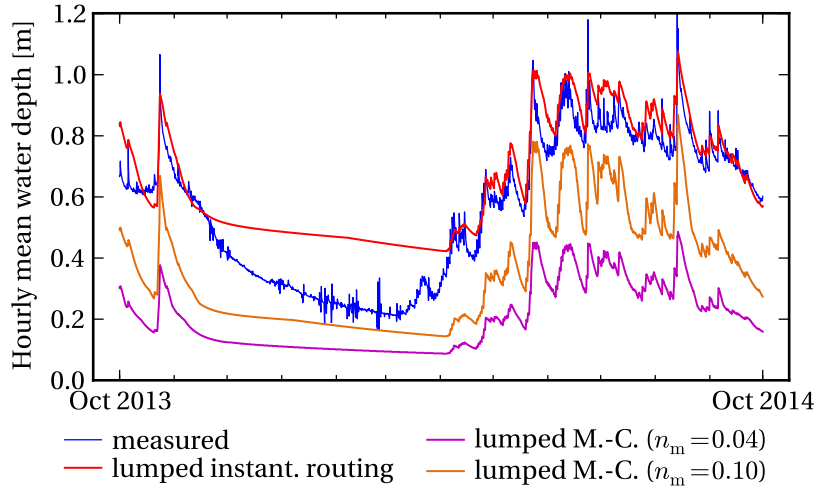


Figure 3.8: Water depth simulated by *StreamFlow* in hydrological year 2014 using various channel water routing techniques. The measured water depth is indicated in blue and shown here only as an indication (see text). Regarding the curves associated with the Muskingum-Cunge routing technique, only those obtained using lumped stream reaches are shown (orange and violet curves). Those corresponding to discretized stream reaches almost overlap with their lumped counterparts, with the difference between each pair of curves amounting to a RMSE of 0.5 mm for  $n_m = 0.04$  and 3.9 mm for  $n_m = 0.10$  over the entire period 2013–2015.

stream reaches to simulate discharge is not associated with any marked improvement with respect to the lumped approach.

Albeit discharge is simulated unequivocally by all water routing techniques, water depth and flow velocity are not. As pictured in Fig. 3.8 for hydrological year 2014, differences between the simulated water depth curves are quite large, with for example a RMSE of 44.5 cm between the curve associated with the instantaneous routing technique and the one corresponding to the Muskingum-Cunge approach with  $n_m = 0.04$ . The instantaneous water routing technique predicts here a higher water depth as compared to the Muskingum-Cunge approach, reflecting the values of the gauging curve coefficients  $\alpha_h$  and  $\beta_h$  (see Sect. 3.2.2 and Table 3.2). In addition, the predictions based on the Muskingum-Cunge technique depend on the value of Manning's coefficient, as expected from Eq. (3.7): the higher  $n_m$ , the higher the simulated water depth. However, as for the case of discharge, the water depth estimations do not appear to benefit from the use of discretized stream reaches as opposed to lumped ones, since both corresponding curves almost overlap for a fixed  $n_m$  (see legend of Fig. 3.8). It should be mentioned that comparison with the measured water depth is hazardous since the modeled river width at the outlet gauging station was not verified to correspond to the observed one. The measured curve is therefore only shown here as an indication. The fact that it diverges from the curve associated with the instantaneous advection approach during winter is due to the fact that the discharge gauging curve of FOEN is linear for small water depth values, and adopts the form of a power function as in *StreamFlow* only for larger values of  $h$ . Given that

simulated discharge is almost the same for all water routing techniques, the differences in simulated water depth result in large differences in the simulated flow velocity as well (not shown).

### ***StreamFlow* simulations of stream temperature**

Turning now to the stream temperature simulations, we first determine an appropriate value for the soil temperature averaging depth  $z_d$  (see Sect. 3.2.1 and Eq. (3.12)). Five different possibilities are considered here: 0.15, 0.30, 0.60, 1.20 and 2.40 m. Using *StreamFlow* configured so as to approximate the temperature of subsurface runoff as the depth-averaged soil temperature (Sect. 3.2.1), we find that the choice  $z_d = 2.40$  m leads to the best results in terms of temperature-based NSE (not shown). This rather large value may be due to the relatively low resolution of the vertical soil temperature profile computed by *Alpine3D*, which was configured here to use a coarse vertical discretization of the soil columns in order to spare computational power. The value  $z_d = 2.40$  m is nevertheless used in the remaining of this study, since emphasis is on demonstrating the model capabilities rather than performing particularly accurate simulations.

Figure 3.9 displays stream temperature as simulated by *StreamFlow* over the hydrological years 2013–2015, with channel water being advected based on the instantaneous routing scheme and subwatershed outflow temperature being approximated as the depth-averaged soil temperature (same configuration as above). Several observations can be formulated from the inspection of the figure:

- As evident from panel (a), stream temperature is generally underestimated by the model on a daily time scale, particularly during the snow melt season in spring and throughout the entire winter. This may be due to the simulated soil temperature being too low, since its value averaged down to 2.40 m typically remains around 0°C until mid-June (not shown). Soil temperature is then modeled by *Alpine3D* to rapidly increase past the snowmelt season, which might explain the better agreement between the simulated and measured stream temperature curves during summer. In winter, measured stream temperature is observed to present rises up to more than 2°C, which are not reproduced by *StreamFlow*. These temperature surges actually reflect the evolution of air temperature (not shown). The fact that *StreamFlow* fails at reproducing them mostly results from simulated stream temperature being constrained to remain above 0°C. This constraint, combined with the underestimation of modeled stream temperature by a few degrees, results in the simulated temperature curve appearing as mostly constant in winter and explains the inability of *StreamFlow* to reproduce the temperature surges. Given that soil temperature increases with depth, the simulation might be improved by averaging soil temperature over a deeper depth when computing the temperature of lateral water inflows. This would correct the underestimation of temperature both in winter and in spring, but might result in a temperature overestimation in summer. Such an approach

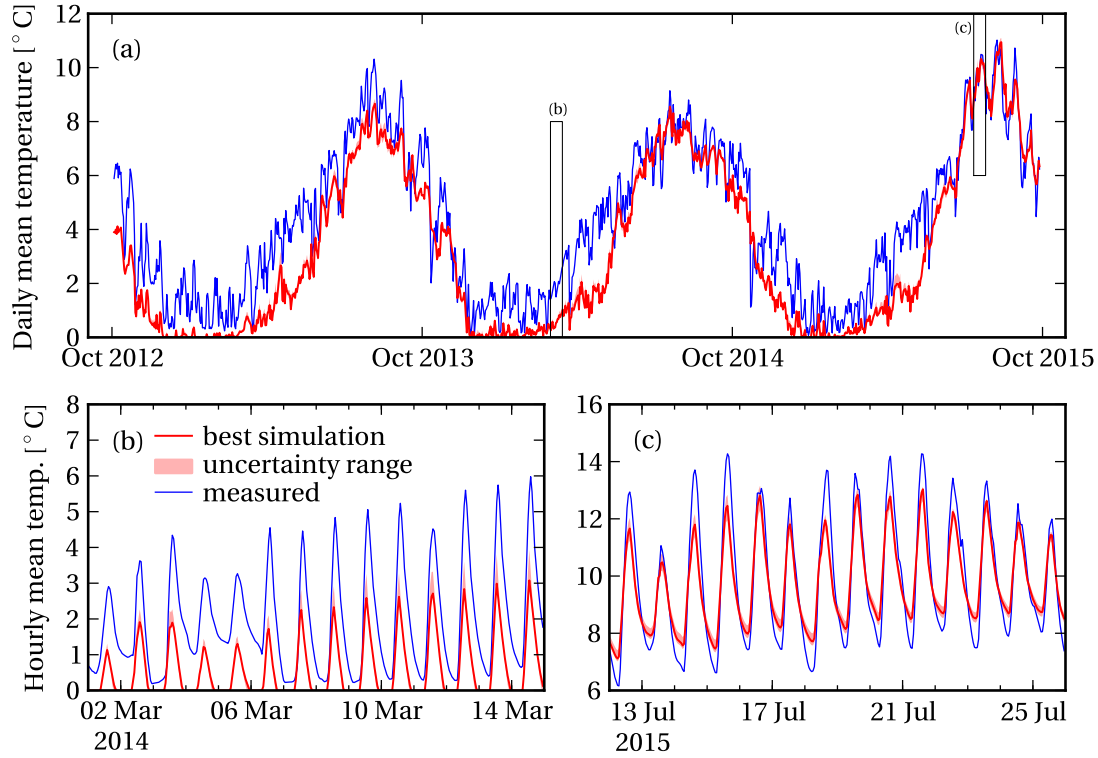


Figure 3.9: Comparison between the simulated (red line) and measured (blue line) stream temperature at the catchment outlet. Panel (a) pictures the entire simulated period (hydrological years 2013 to 2015), with temperature aggregated into daily mean values for visibility. Panels (b) and (c) display the hourly mean temperature over two selected periods of 14 days (their respective extents are indicated as black rectangles in panel (a)). The simulated curve was obtained with *StreamFlow* based on the instantaneous water routing scheme, with the temperature of subsurface runoff being approximated as the soil temperature averaged over a depth of 2.40 m. The uncertainty range (displayed in light red) is obtained by evaluating *StreamFlow* for each one of the 300 best sets of parameters  $R_{\max}$ ,  $\bar{\tau}_{\text{res,u}}$  and  $\bar{\tau}_{\text{res,u}}$  identified during calibration step 1 (see Sect. 3.4.2).

would nevertheless need to be confirmed by detailed geological surveys of the Dischma catchment, in order to verify that the average soil depth over the watershed is larger than the value considered here for  $z_d$ , namely 2.4 m.

- Panels (b) and (c) present a zoom on two selected periods during winter and summer, respectively. *StreamFlow* is observed to be capable of simulating the diurnal cycle of stream temperature, albeit its magnitude is in general too low. This underestimation of the diurnal cycle may originate from an overestimation of water depth or, equivalently, from an underestimation of the stream width. This hypothesis can unfortunately hardly be tested, since water depth and stream width are difficult to quantify in small mountainous streams with irregular, boulder-covered beds. We verified whether the latent and sensible heat fluxes are not underestimated by *StreamFlow*. To this end, we increased

the values of coefficients  $a_{vw}$  and  $b_{vw}$  by 50% (see Eq. (3.13) and Table 3.2), however this did not result in a marked improvement of the simulated diurnal cycle (not shown). The effect of the heat exchange with the stream bed was also tested by reducing the value of  $k_{bed}$  by 50% (see Eq. 3.12 and Table 3.2), but this had almost no impact on the simulated temperature curve either (not shown). It should be noted that the simulated discharge is not thought to be at the origin of the underestimation of the temperature diurnal cycle, owing to the fact that the daily fluctuations of discharge are quite well captured by the model (see Fig. 3.6)—except for a few short-lived discharge surges. The underestimated amplitude of the temperature diurnal cycle therefore appears to mostly originate from the approach selected for the modeling of subsurface runoff temperature, as discussed into more detail below.

- From the inspection of all three panels in Fig. 3.9, it can be stated that modeled temperature is not particularly affected by the uncertainty in the values of hydrological parameters  $R_{max}$ ,  $\bar{\tau}_{res,u}$  and  $\bar{\tau}_{res,l}$ . As a matter of fact, the uncertainty range of the simulated temperature curve remains globally narrow, except around midday where it reaches a value up to 1 °C on some days (see panel (b)). This limited sensitivity of modeled temperature with respect to simulated discharge (and water depth) further hints at the probable role of subsurface runoff temperature on the underestimation of the temperature diurnal cycle.

The values of the error measures associated with Fig. 3.9 are summarized in Table 3.5. The NSE value of the hourly mean temperature curve (0.78) is much lower than the one of the benchmark model (0.87), which denotes a strong improvement potential. This has to be put into perspective with the fact that the Dischma river is rather small and heavily turbulent, and therefore more challenging to model as compared to larger, low altitude rivers. In addition, the NSE value is comparable to the one reported by MacDonald et al. (2014) over a mountainous watershed of similar size and altitudinal range as the Dischma catchment. The RMSE equals 1.45 °C, which is not very far from the RMSE of the benchmark model (1.14 °C). On the other hand, the bias is rather large and negative (−0.88 °C), as already noted from the observation of Fig 3.9 above. Regarding the model performance at the two intermediate gauging points, the values of the error measures at Dürrboden are found to be essentially the same as at the outlet point, except for the positive bias (see Table 3.5). Concerning Am Rin, the apparent better values for RMSE, NSE and bias have to be weighted against the short time period over which they are evaluated (17 January 2015 to 17 July 2015). The fact that the model accuracy is about the same at Dürrboden and at the outlet point is a further hint that the temperature error mostly originates from the approach used to compute lateral inflow temperature. As a matter of fact, we would have expected a better agreement between the observed and measured stream temperature when moving upstream along the river network in case the source and lateral inflow temperatures had been correctly estimated by the model. As the model error is rather constant along the stream network, we conclude that the approach used to compute the temperature of subsurface runoff could be improved (see below).

### Chapter 3. Deterministic stream temperature modeling in high alpine watersheds

Table 3.5: Accuracy of the hourly mean stream temperature predictions of *StreamFlow* (with  $z_d = 2.40\text{m}$ ), based on various approaches for advecting water in the stream channels and computing the temperature of subsurface runoff. The accuracy of the temperature benchmark model at the catchment outlet is indicated in the last row for comparison. All error measures are computed over the entire validation period (1<sup>st</sup> October 2013 to 1<sup>st</sup> October 2015), except at points Am Rin and Dürrboden for which the considered time period is the same as in Table 3.4.

Model	Channel water routing scheme <sup>a</sup>	Subwatershed outflow temperature scheme <sup>b</sup>	Location	RMSE (°C)	NSE (–)	Bias (°C)
<i>StreamFlow</i>	Instant. advection (lumped)	Soil temperature	Outlet	1.45	0.78	–0.88
			Dürrboden	1.45	0.78	0.75
			Am Rin	1.11	0.89	–0.05
	Instant. advection (discr.) M.-C. ( $n_m = 0.07$ , lumped) M.-C. ( $n_m = 0.07$ , discr.)	Soil temperature	Outlet	1.40	0.80	–0.85
				1.49	0.77	–0.85
				1.46	0.78	–0.80
	Instant. advection (lumped)	Energy-balance HSPF	Outlet	2.06	0.56	–1.63
				1.69	0.70	0.54
Benchmark	—	—	Outlet	1.14	0.87	–0.03

<sup>a</sup> “M.C.” denotes the Muskingum-Cunge routing scheme, and the indications “lumped” and “discr.” between brackets refer to the spatial discretization of the stream reaches (see Sect. 3.2.2)

<sup>b</sup> The schemes described in Sect. 3.2.1 for the computation of subsurface runoff temperature are denoted as follows here: “soil temperature” for the scheme assuming subsurface runoff to be in thermal equilibrium with surrounding soil, “energy-balance” for the original scheme implemented in *StreamFlow*, and “HSPF” for the scheme inspired from the Hydrological Simulation Program–Fortran.

As already discussed above, the simulated stream temperature is not particularly sensitive to the modeled discharge. This fact is confirmed by the values of the error measures reported in Table 3.5 for four temperature simulations, each one based on a different water routing scheme—namely the instantaneous advection technique or the Muskingum-Cunge approach, combined with either a lumped or discretized modeling of the stream reaches. In the simulations based on the Muskingum-Cunge approach, Manning’s coefficient is fixed to 0.07, which corresponds to the middle of the above-defined range of plausible values in the case of the Dischma. It appears that all four simulations are associated with a similar accuracy in terms of stream temperature modeling, as indicated by the narrow range of NSE (0.77–0.80) and RMSE (1.40–1.49°C) values. Contrary to the discharge simulations, the discretized representation of the stream reaches enables here a slight improvement of the results as compared to the lumped approach, mainly due to a better resolution of the diurnal cycle (not shown).

In a recent study, Leach and Moore (2015) reviewed the approaches implemented in some of the most popular stream temperature models for approximating the temperature of subsurface runoff. Based on a comparison with data collected in a small Canadian watershed, they concluded that none of them performed well, except for the method implemented in the HSPF model approaching the observations relatively closely. More interestingly, the authors pointed at large discrepancies between the predictions of the various models. As a further step, we propose here to investigate the effect of modeled subsurface runoff temperature on



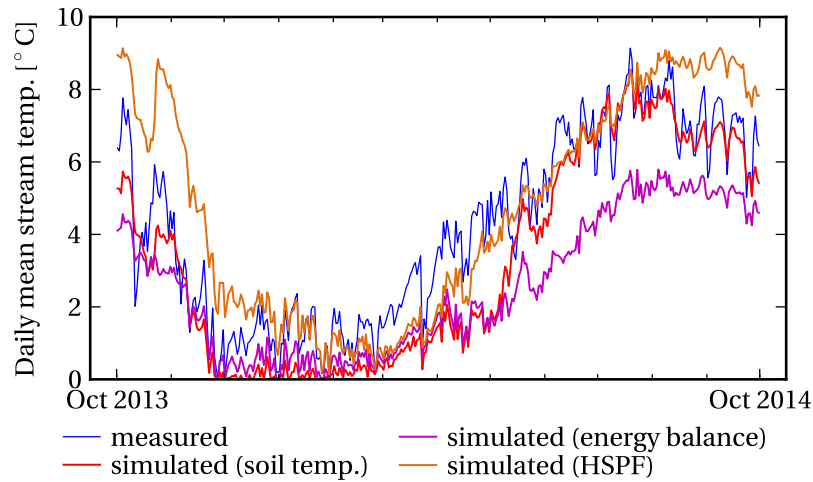


Figure 3.10: Comparison between various predictions of stream temperature at the catchment outlet, where the temperature of subsurface runoff is computed based on the following methods: the original scheme implemented in *StreamFlow* (“energy-balance”), the technique of the Hydrological Simulation Program–Fortran (“HSPF”), or as soil temperature averaged over a depth of 2.40 m (“soil temp.”). All curves are aggregated into daily mean values for visibility.

the simulated stream temperature at the catchment outlet. To this end, three *StreamFlow* simulations are run with the same configuration as above—namely lumped reaches and the instantaneous routing scheme—except that the temperature of subsurface runoff is computed each time based on a different method out of the three available ones (see Sect. 3.2.1). It should be mentioned that, in virtue of the modular structure of *StreamFlow*, changing from one method to the next simply requires one line to be modified in the configuration file. The simulation results are displayed in Fig. 3.10, and the corresponding error measures can be found in Table 3.5. It can be observed that the approach used to compute the temperature of subsurface runoff has a strong influence on the accuracy of the modeled stream temperature. The method originally implemented in *StreamFlow* appears to perform worse (NSE of 0.56, RMSE of 2.06 °C), followed by the HSPF approach (NSE of 0.70, RMSE of 1.69 °C). The method based on the depth-averaged soil temperature is associated with the best performance measures (see above). Overall, the three methods seem to determine the temperature of in-stream water to a large extent, leading to variations of more than 4 °C between the different curves (see Fig. 3.10).

As deduced above for the remarkable performances of the benchmark model in terms of stream temperature simulation, the actual implementation of *StreamFlow* could be improved upon. Given the observed strong influence of subsurface runoff temperature on modeled stream temperature, we recommend here that future developments of *StreamFlow* concentrate on a more accurate method for computing the temperature of lateral inflow. Following the approach presented in Leach and Moore (2015), such a method could first be developed for a given catchment of interest. In particular, in-depth geological surveys would need to be con-

ducted in order to gain more understanding on the dominant hillslope hydrothermal processes in the selected catchment. These processes could then be translated into a simple process-based model, which could be finally integrated into *StreamFlow* as an additional option for computing the temperature of subsurface runoff. Ideally, additional field investigations would need to be conducted in other catchments in order to make the process-based model more generic, i.e. applicable over various geographical and topographical environments.

### 3.5 Conclusions

Combined modeling of hydrological and thermodynamic processes offers promising perspectives for the prediction of stream temperature at the catchment scale. The present study describes a new coupled hydro-thermal model, named *StreamFlow*, which is currently intended to be used in high Alpine environments. Designed as an independent extension to the spatially-distributed snow model *Alpine3D*, it has been written entirely anew compared to its initial version. The resulting code has a clear and modular structure which takes advantage of some of the latest available object-oriented features. Several of the hydrological processes represented in the model can be simulated using various alternatives. For example, the advection of water in the stream channels can be computed using either the Muskingum-Cunge technique or an instantaneous routing approach. This modularity enables the model to be adapted to the specific needs of each user, but also provides a rapid means to estimate the uncertainty of the simulation results by comparing the predictions of the various modeling alternatives.

Based on an evaluation over a high Alpine catchment, the model accuracy is shown to be satisfying, with Nash-Sutcliffe efficiencies for the hourly mean discharge and hourly mean temperature being equal to 0.82 and 0.78, respectively. Comparison with a simple benchmark model indicates that *StreamFlow* correctly accounts for the dominant hydrological processes in terms of discharge simulation, whereas its modeling of stream temperature could be improved. The various water routing techniques available in *StreamFlow* do not appear to have a marked effect on the quality of the simulations. On the other hand, it was observed that the approach used to compute the temperature of subsurface runoff strongly impacts the simulated stream temperature at the catchment outlet. This effect has not been reported in any previous study and points at the need for more intensive field investigations of subsurface runoff temperature.

In addition to the development of a more accurate method for computing subsurface runoff temperature (as discussed in the previous section), several improvements can be brought to the actual state of the model. The representation of riparian shading would allow *StreamFlow* to be applied in lower-altitude, vegetated watersheds. However, similarly to the case of subsurface runoff temperature, the shading by riparian vegetation is a complex phenomenon which is difficult to simulate and requires further research (Moore et al., 2005b). The modeling of the ice and snow sheet forming over the stream in winter could also be included in

*StreamFlow*, using for example an approach similar to the one introduced by van Beek et al. (2012). Finally, additional modeling alternatives could be implemented for various components of *StreamFlow*, such as the full St-Venant equations for the routing of water in the stream channels.

In the near future, we plan to use *StreamFlow* in order to evaluate the effects of climate change on the hydrological functioning of high alpine watersheds. In particular, advantage will be taken of the coupled hydro-thermal nature of the model in order to investigate the impact of the future discharge modifications on stream temperature. This study will be especially relevant for summer time, when drought events are forecasted to become more frequent in the future. In a second time, *StreamFlow* might be used to quantitatively assess the impacts of anthropogenic thermal discharges into mountain streams. The consequences of artificial water derivations—such as those used to transfer water into dams—on the thermal regime of Alpine streams could also be investigated using the model. Such studies could serve as a basis for the establishment of environmental protection and/or restoration measures, aiming for example at preserving fish and macrovertebrate populations.



## 4 Discussion

The statistical and deterministic models have been described independently in Chaps. 2 and 3, respectively. This chapter aims at discussing various points common to both models, as well as comparing their respective domains of application.

### 4.1 Complementarity of the modeling approaches

The two developed models can be seen as being complementary, in the sense that the statistical (physics-based) model is aimed at providing *spatial* predictions of stream temperature, whereas the deterministic model is more related to (long-term) *temporal* predictions. Indeed, although it resolves the annual cycle of stream temperature, the statistical model is primarily intended to provide temperature estimates in ungauged locations. In this respect, it may be treated as a *spatial interpolation tool*, since multiple measurement sites are used to calibrate its parameters, which are in turn used to make predictions in nearby catchments. The deterministic model, on the other hand, is not expected—despite its physically-based nature—to be directly transferable from one catchment to the next without modification of its parameters. As a counter part, its long-term predictions are generally considered to be more reliable (e.g. van Beek et al., 2012; MacDonald et al., 2014). It may therefore be referred to as a *temporal interpolation tool*, since temperature data in a given time period can be used by the model to estimate temperature in another distant time period through proper calibration.

Taking advantage of their complementarity, the two models could actually be combined to perform long-term predictions of stream temperature over large spatial areas. The approach would be similar to the one followed by Hrachowitz et al. (2010), namely: (a) perform long-term predictions of stream temperature in selected catchments using the deterministic model, and (b) spatially interpolate these predictions with the help of the statistical model. As a strong limitation, it should be mentioned that anthropogenic impacts are not taken into account by any of the two models, hereby limiting the validity of the temperature predictions to (semi)natural streams.

Alternatively, the two models might complement each other when studying thermally sensitive areas. The statistical model could be used to rapidly identify, in a large spatial area, the locations where stream temperature reaches critical levels. The deterministic model could then be applied over these locations to study into more detail the causes of the critical temperature values or the solutions that could be considered to mitigate them.

From a model development perspective, the two models are complementary in the sense that the deterministic one benefited from the conclusions drawn using the statistical model. In particular, the following observations made in Chap. 2 were used during the implementation of *StreamFlow* in Chap. 3:

- The characteristic length  $L_c$  of the upstream area controlling stream temperature at a given point was found in Chap. 2 to be of the order of 4 to 8 km. As such, the entirety of the watershed is expected to contribute to the value of the outlet stream temperature in small catchments, which motivated our choice to take the entire stream network into account in *StreamFlow* rather than a simple reach portion.
- In the formulation of the statistical model, discharge is observed to have a strong impact on stream temperature, since it partly controls the weighting of the different contributions to the stream temperature value at a given point and appears in the expression of  $L_c$ . This supported the decision to implement *StreamFlow* as a coupled hydro-thermal model, so as to account for the effect of hydrology on stream temperature.
- Evaluation of the statistical model over selected catchments showed that subsurface runoff had a non-negligible effect on stream temperature. As a consequence, it was decided to investigate this effect into more detail through the implementation of three different possibilities to compute the temperature of subsurface runoff in *StreamFlow*.

In addition, it was shown in Chap. 2 that the statistical model successfully reproduces the annual cycle of stream temperature in a variety of catchments. This hints at the fact that catchments may have a similar thermal behavior, hereby providing more generality to the conclusions of Chap. 3 which were obtained over a single catchment.

### 4.2 Extent of the spatial domain of application

As mentioned in the previous chapters, both models developed in the present thesis are primarily intended to be used in small to medium-sized catchments, i.e. catchments ranging in size from a few  $\text{km}^2$  to 200–300  $\text{km}^2$ . In the case of the statistical model, this restriction originally arose from the wish to have a well-defined hydrological regime in each one of the studied catchments. As stated by Aschwenden and Weingartner (1985), this condition is verified in Switzerland only for watersheds smaller than 500  $\text{km}^2$ . It was expected that catchments with different hydrological regimes might display different thermal behaviors. As shown in Chap. 2 however, the statistical model could indifferently reproduce the annual

temperature curve of streams with various hydrological regimes, except for the glacial ones. Given certain adjustments, the model could therefore be applied over larger catchments. In particular, the model assumes the characteristic length  $L_c$  to be constant across catchments, which might no longer be true if the range of catchment sizes is too large. As explained in Chap. 2,  $L_c$  is expected to be roughly proportional to water depth. In very large catchments, this depth is so much larger than in the medium-sized catchments that the model may fail. As a workaround, different sets of model parameters could be considered, each one associated with a different range of catchment sizes. In the model version corresponding to the largest catchments, the first two terms of the analytical solution—i.e. those associated with the source temperature and lateral inflow temperature contributions, respectively—might be dropped as their corresponding weights are close to zero (see discussion in Sect. 2.3.1 and Eqs. (2.13) and (2.14)).

Regarding the deterministic model, the restriction to medium-sized catchments resulted both from computational resource limitations and from the absence of a riparian shade module which would have enabled the model to be applied in low-land areas. The computational resource problem can be solved by taking advantage of the possibility offered by *StreamFlow* to use a different mesh grid than the one of the *Alpine3D* simulation. As such, given that the largest fraction of the simulation time is consumed by *Alpine3D*, the latter could be run over a coarse mesh grid. This is expected to affect relatively little the *StreamFlow* simulation, as long as the DEM used to delineate the stream network and the subwatersheds remains relatively fine. The absence of a vegetation module, on the other hand, might require more efforts to be remedied. Many different approaches to account for riparian shading have been reported in the literature, ranging from a calibrated constant factor applied to incoming solar radiation (e.g. Westhoff et al., 2007; Haag and Luce, 2008) to sophisticated models accounting for the full riparian vegetation geometry (e.g. Boyd and Kasper, 2003; Moore et al., 2014), passing through simple attenuation coefficients computed based on the vegetation height, size or type (e.g. DeWalle, 2010; MacDonald et al., 2014). Selection of one approach over the other ones should be dictated by the available data. It should be noted that the modularity of *StreamFlow* allows several techniques to be implemented, which can then be independently selected by the user depending on the data at his disposal.

### 4.3 Temporal resolution

The two models do not have the same temporal resolution: while the deterministic model can provide temperature estimates up to every second, the statistical model is not expected to deliver reliable temperature values for time steps smaller than a week. The coarse temporal resolution of the statistical model mostly results from the steady-state assumption which was considered when analytically solving the heat-balance equation. This assumption cannot be considered to hold for time steps smaller than a day, hereby constraining the model time step. In addition, the linear functions of air temperature used to estimate the source temperature  $T_s$  and lateral inflow temperature  $T_\ell$  are no longer valid at small time steps (see Eqs. (2.19)

and (2.20)). As a matter of fact,  $T_s$  and  $T_\ell$  are generally thought to evolve in time roughly similarly to soil temperature, whose time variation is similar to the one of air temperature at large time scales but much less fluctuating at small time scales. As a workaround, the value of air temperature used in the expressions of  $T_s$  and  $T_\ell$  could be averaged over a moving time window when considering small time steps in order to better mimic the soil temperature variations.

Concerning the deterministic model, it should be noted that its temporal resolution is entirely dependent on the one of the input data. Even though the model internally runs with a time step of a few seconds to a few minutes—so as to be compliant with the CFL conditions—the intrinsic output resolution cannot possibly be higher than the input one. It is therefore essential that the sampling rate of the input data matches the user needs in terms of output resolution.

### 4.4 Utility of the models for biologists and stakeholders

The two models developed herein might be of interest for stream biologists, particularly those working on fish. Indeed, as mentioned in Chap. 1, water temperature controls many biological aspects of fish, from the functioning of its enzymes to its resistance to diseases or even its feeding behavior (e.g. McCullough et al., 2009). Many of these aspects have recently been written under the form of equations, as a result of ecology gradually moving from a descriptive science to a quantitative, experimental-based science. For example, empirical models have been developed for various salmonid species to predict their respective growth rates (e.g. Elliott et al., 1995; Sullivan et al., 2000), their resistance to several diseases (e.g. Nelitz et al., 2007), or even the date at which fry emerges from the nest (e.g. Elliott and Hurley, 1998). It is noteworthy to mention that most of these behavioral models use daily mean stream temperature as their sole—or at least principal—variable, which emphasizes once more the predominant role of temperature on the physiology of fish. The deterministic stream temperature model presented in Chap. 3 may therefore prove useful, when used in association with the fish behavioral models, to predict the effect of climate change on various aspects of the life cycle of salmonids. As an example, the daily mean temperature predictions of *StreamFlow* could be used together with the model of Elliott and Hurley (1998) in order to investigate whether the incubation period of brown trout will shorten or lengthen as a function of catchment altitude in the future. This would in turn give insights into the geographical areas most susceptible to serve as nesting grounds for trout. A full understanding of the climate change effects on fish using this technique is nevertheless illusory, since not only temperature but also pollution, ultra-violet increase and oxygen concentration (among other variables) should be taken into account (Graham and Harrod, 2009).

Sullivan et al. (2000) and Nelitz et al. (2007) have shown that weekly averages of stream temperature correlate well with several aspects of fish biology, such as the length of the growth period or the resistance to diseases. As a consequence, not only *StreamFlow* but also the



#### 4.4. Utility of the models for biologists and stakeholders

---

statistical model presented in Chap. 2 may prove useful for stream biologists, as long as it is configured to provide weekly mean temperature estimates instead of monthly mean values. As opposed to *StreamFlow* however, this model would not be used in climate change studies but rather as a means to overcome the lack of stream temperature measurements so as to investigate selected aspects of fish biology in ungauged catchments.

The effects of stream temperature on fish biology are so diverse and complex that their translation into simple temperature criteria for fish protection is not an easy task. A certain temperature range might be suitable for a particular species but undesirable for another one (see e.g. Sullivan et al., 2000; Graham and Harrod, 2009). It may also be suitable for a certain life stage, such as for the adults, but not for other life stages, such as alevins or parrs (see e.g. Elliott and Elliott, 2010). Depending on the life stages, fish might even show temperature preferences as a function of the season. The fact that the fish responses are gradual to the level and period of exposition to harmful temperatures is a further complication which makes the definition of fixed temperature criteria even more difficult (Sullivan et al., 2000). Three different approaches have been followed to date by scientists and water management agencies to define such criteria:

1. The historical approach was based on the review of scientific literature by experts. Both too cold or too warm temperatures may be harmful for fish (e.g. Sullivan et al., 2000; Elliott and Elliott, 2010), but experts have generally concentrated on warm temperatures in anticipation of the expected temperature rise due to climate change. Their recommendations were usually expressed as a maximum temperature not to be exceeded over a certain period of time (typically a week). A safety margin was generally included in their decision in order to account for unknown processes or measurement errors. However, as noted by Sullivan et al. (2000), this method lacks reproducibility and is subjective with respect to the choice of studies on which the experts base their judgement.
2. As an alternative, some authors have proposed to derive stream temperature criteria from field measurements. Their idea was to take advantage of concomitant observations of fish presence and stream temperature in order to empirically define temperature ranges suitable for a particular fish species. For example, Hari et al. (2006) obtained the optimal temperature range for brown trout as a function of the day of the year by combining the annual temperature cycles of all stream reaches in which brown trouts were observed in Switzerland over 25 years. The same approach was followed by Eaton et al. (1995) for 30 fish species in the United States. The advantage of this method, from a scientific point of view, is that it provides different optimal values over the course of the year instead of a single maximum threshold. On the other hand, this turns into a disadvantage from a management point of view, since the application of time-varying criteria is much more difficult to enforce and monitor.
3. A third approach has recently been investigated by authors like Sullivan et al. (2000) and Nelitz et al. (2007), namely the derivation of a single temperature threshold value based

on the fish physiological models described above. The method consists in choosing a particular aspect of fish biology which is thought to best account for fish health, define the range of healthy values for that aspect, and finally convert this healthy range into a temperature threshold not to be exceeded. For instance, Sullivan et al. (2000) chose to concentrate on the growth rate of fish, since large fishes have been observed to be more resilient to diseases and have better chances of overwintering. They decided to fix the maximum allowable difference between the observed fish weight at the end of summer and the weight it could have reached under optimal temperature conditions to 10 %. Based on a growth model similar to the one of Elliott et al. (1995), they computed the theoretical weight difference at the end of summer for an idealized fish in 19 different rivers using daily mean temperature records. They then correlated these weight differences with an aggregate measure of the daily mean temperature data, namely the maximum weekly mean temperature over summer. This correlation was used to translate the 10 % weight deficit criterion into a simple temperature threshold in terms of the aggregate measure. A similar procedure was proposed by Nelitz et al. (2007) using additional aspects of fish biology on top of the growth rate, namely the resistance of fish to two diseases and the survival rate of eggs. This approach is considered by Sullivan et al. (2000) to be promising, since it is based on sound science and allows for reproducibility.

All of the three methods described above for specifying stream temperature criteria require the identification of target species to be protected. Salmonids have usually been chosen in northern countries as a consequence of their high economic value and strong sensitivity to warm temperatures. Other species—not necessarily fishes—have been considered in some regions of the world, such as for instance macroinvertebrates in South Africa (Dallas and Rivers-Moore, 2012). It should be emphasized that most of the current stream temperature criteria are expressed in terms of a maximum weekly mean temperature threshold (Eaton et al., 1995; Sullivan et al., 2000; Nelitz et al., 2007; Dallas and Rivers-Moore, 2012). Given that the two models derived in the present thesis are able to provide weekly estimates of stream temperature, both of them could be used by water management agencies to identify sensitive stream reaches and/or predict their apparition in the future. Being spatially explicit and having a fine time resolution, the deterministic model could also be used in the regulation of anthropogenic heat discharges into streams. As a matter of fact, many states impose water temperature increase to remain below a certain threshold downstream of thermal emissions.<sup>1</sup> Such an application of the model would however require the daily stream temperature cycle to be better approximated by *StreamFlow*, since the daily maximum temperature is currently underestimated and the daily minimum temperature overestimated (see Chap. 3).

In order to facilitate its use by third parties, the statistical model described in Chap. 2 could first be turned into an operational tool. To this end, the existing Python scripts which were developed in the framework of the present thesis could be merged into a single program.

---

<sup>1</sup>See e.g. <https://www.admin.ch/opc/fr/classified-compilation/19983281/index.html> for legislative text about the protection of surface water in Switzerland.

Documentation, which is currently only present as comments in the scripts, could also be greatly enhanced. Finally, the implementation of a graphical user interface—although time and effort consuming—may also prove a valuable addition, especially if the model ends up being used by persons with little or no programming background. *StreamFlow*, on the other hand, is thought to be already sufficiently documented and well-written to be distributed to external users. As it happens, the model is actually currently being used by an Italian start-up in order to perform hydrological simulations. Although more targeted towards experts, *StreamFlow* might also benefit from the addition of a graphical user interface in the long term in order to gain in attractiveness.

### 4.5 Role of subsurface runoff temperature

One of the key findings of the present thesis is that subsurface runoff appears to exert a strong impact on stream temperature in mountainous catchments. This finding is all the more important as subsurface runoff has generally received less attention than other components of the stream energy-balance, such as the surface energy exchange (Caissie, 2006). Accordingly, many deterministic stream temperature models developed to date have either neglected this term or been applied over stream reaches where lateral inflow was not present (e.g. Brown, 1969; Sinokrot and Stefan, 1993; Caissie et al., 2007; Roth et al., 2010; Null et al., 2013).

Both models developed in the framework of the present thesis tend to underline the prominent role played by subsurface runoff on the shape of the annual temperature curve. Indeed, it was shown in Chap. 2 that lateral water inflows significantly contribute to the monthly mean stream temperature values observed in the selected catchments, especially in summer and autumn. Similarly, the evaluation of *StreamFlow* in Chap. 3 revealed that the general shape of the simulated annual stream temperature curve was very sensitive to the approach chosen for computing the temperature of subsurface runoff. This effect might also be present at smaller time scales; in particular, subsurface runoff might impact the diurnal cycle of stream temperature. As such, the incorrect simulation of the subsurface runoff temperature dynamics at the sub-daily time scale might be one of the reasons explaining the poor simulation of the daily temperature extrema by *StreamFlow*. As mentioned in Chap. 3, future developments of *StreamFlow* should seek at improving the simulation of the lateral energy inflows into the stream, possibly based—as detailed below—on an approach similar to the one introduced by Leach and Moore (2015).

The present investigations of the role of subsurface runoff on stream temperature have been limited to small to medium-sized catchments. It would be interesting to extend this analysis to larger, low-land catchments. We suspect that the role of lateral inflows would tend to decrease with catchment size. As a matter of fact, assuming lateral inflow to be relatively independent of catchment size, the ratio of lateral to in-stream discharge is expected to decrease with increasing river size. This reasoning is supported by the expressions which were obtained in Chap. 2 for the various weights appearing in the analytical solution to the heat

## Chapter 4. Discussion

---

balance equation: it was noted that the weights associated with the source and lateral inflow temperatures decreased with increasing catchment size.

Among the experimental work needed to validate the models developed herein, the further investigation of subsurface runoff temperature appears as one of the clear priorities. To this end, experiments inspired from the one led by Leach and Moore (2015) should be conducted in order to gain a better understanding of the sub-daily and seasonal dynamics of subsurface runoff temperature, as well as of the controls on these dynamics. The Dischma catchment, with its already long record of hydrological and snow studies and its dense instrumentation, appears as a suitable choice for such experiments. In particular, piezometers equipped with thermometers and water level gauges could be installed in the vicinity of the stream. Influence of spatial scale on the subsurface temperature response could be evaluated by placing some of these thermometers around sources, others along small tributaries and finally some along the main channel. Detailed geological surveys of the catchment would also need to be performed in order to identify the different soil layers and potential preferential flow paths. All these investigations would ideally lead to the development of a conceptual model similar to the one of Leach and Moore (2015), but better suited for high-altitude mountainous catchments in Switzerland. This model could in turn be incorporated in *StreamFlow*, hereby improving the accuracy and forecast capabilities of the model.

## 5 Conclusions

Stream temperature controls many aspects of the riverine ecosystem, from the habitat suitability of many aquatic species to the concentration of various chemical species. As most studies have been conducted in low-land rivers to date, the comprehension of temperature dynamics in mountainous streams is still incomplete. In an attempt at improving this comprehension, two new models for the prediction of stream temperature in Alpine catchments were introduced in the present thesis.

The first model was conceived with the intention of estimating stream temperature in ungauged catchments. Through its development, demonstration was made that a new hybrid approach could be adopted as a trade-off between the statistical and deterministic approaches. The idea consists in simplifying the stream energy-balance equation up to the point where it can be solved analytically, so as to obtain an expression which can be used to compute stream temperature. The key point is to select a proper set of simplifying assumptions, not too reductive but at the same time allowing for an analytical solution to be found. A very similar approach was recently followed by another group of researchers (Piccolroaz et al., 2016), with whom a collaboration was established. Using slightly more restrictive assumptions, they obtained a simpler expression for estimating stream temperature, which does not require the averaging of physiographic variables over the stream network. As a counter part, their solution is somewhat less physically-based than the one reported here. For instance, it cannot be used to estimate the relative contributions of the different heat sources on the temperature measured at a given point. The hybrid modeling approach therefore appears to be a promising technique, since its physical contents can be adapted as a function of the user requirements. Researchers on stream temperature might be more interested in the complex model developed here, while water management stakeholders might profit more from the simpler model of Piccolroaz et al. (2016). The hybrid approach is of course not restricted to these two models: further studies on the subject might lead to the development of new prediction tools, just awaiting to be discovered.

The second model reported in the present work is intended to be used in climate change and land use change studies. It relies on a deterministic approach to simulate the hydrological

processes at the subwatershed scale, in addition to the flows of water and energy along the stream network. It is one of the only physically-based stream temperature models available to date which can be applied over an entire catchment. This property allows it to be run solely with meteorological and land use input data, contrary to most other models which also require discharge and water depth measurements. In addition, the present model accounts for the snow pack in a detailed manner since it is designed as an extension to the physically-based snow model *Alpine3D*. As a consequence, it is particularly suited for the simulation of discharge and stream temperature in high alpine watersheds. Some of its aspects need to be improved in order for it to be applied over lower-altitude catchments, notably the inclusion of shading due to the riparian vegetation. Future work on this model will mostly consist in its application over selected catchments in order to evaluate various climate-change scenarios. It is also planned to develop a module to represent artificial water reservoirs and water intakes (or rejections).

A common observation was made through the application of both models in Alpine catchments: the inflow of water from the surrounding hillslopes appears to have a strong influence on stream temperature. This fact has been neglected in many of the stream temperature models developed so far, possibly due to the fact that they mostly concentrated on short stream portions. In the present case, the modeling of stream temperature over entire catchments enabled the role of subsurface runoff to become more evident. As such, the hybrid model estimated subsurface heat inflow to represent a noticeable part of the seasonal stream heat balance in summer and autumn. In addition, the deterministic model pointed at the control exerted by subsurface runoff temperature on the annual cycle of stream temperature. Of course, these observations need to be confirmed with experimental measurements. Advantage is taken of the present discussion to emphasize once more the need for field campaigns focusing on the temperature of subsurface flow.

More generally, the future of stream temperature research probably lies in the development of new measurement techniques and the intensification of the field campaigns. The incredible increase of computational power over the last decades has allowed for the development of very detailed physically-based models. As an example, the latter are currently able to simulate pore flow at the scale of an entire catchment. However, most of their predictions cannot be validated due to the lack of appropriate experimental data. Even in the cases where measurements are available, the question arises as to whether the models actually simulate the same variable as what is actually measured. Some researchers believe in technical progress to come up with new instruments providing the required data, but others are more in favor of adapting our models to the data at hand—e.g. avoiding to account into detail for the processes which cannot be validated. These questions are for the moment completely open and may still require many years to be answered. In the mean time they are responsible for intense scientific debates, which is probably the way research has always moved forward...

# A Analytical solution to the energy-balance equation

This section details the procedure for deriving the analytical solution to Eqs. (2.5)–(2.6) introduced in Chapter 2.

The solution is first obtained for the case of a simple stream reach of length  $L$  (see Fig. A.1a). Let the downstream distance be denoted as  $x$ , with  $x_0$  and  $x_1$  referring to the positions of the reach origin and end points, respectively. The discharge  $Q(x_1)$  and stream temperature  $T(x_1)$  can be easily computed by integrating Eqs. (2.5)–(2.6) between  $x_0$  and  $x_1$ ,

$$Q(x_1) = Q(x_0) + q_\ell L, \quad (\text{A.1})$$

$$T(x_1) = \frac{Q(x_0)}{Q(x_1)} e^{-d(x_0)/L_c} T(x_0) + \frac{1}{Q(x_1)} \int_{x_0}^{x_1} e^{-d(x)/L_c} \psi(x) dx, \quad (\text{A.2})$$

where

$$\psi(x) = q_\ell T_\ell(x) + Q(x) \left( \frac{\gamma \phi_r(x) + T_a(x)}{L_c} - \frac{g}{c_p} \frac{dz}{dx} \right). \quad (\text{A.3})$$

In Eq. (A.2),  $d(x) = x_1 - x$  denotes the distance between any point  $x$  and the downstream end point  $x_1$  (see Figure A.1a).

The above equations require the values of discharge and temperature at the upstream end of the reach to be known. By applying them iteratively to all the reaches of a network, starting from the most downstream one, the expressions for discharge  $Q_{\text{out}}$  and water temperature  $T_{\text{out}}$  at the network outlet can be expressed as a function of the discharges and temperatures of the sources. At the confluences, the discharges  $Q_{u,1}$  and  $Q_{u,2}$  and the temperatures  $T_{u,1}$  and  $T_{u,2}$  of the two upstream reaches can be related to the discharge  $Q_d$  and temperature  $T_d$  of the downstream reach using the mass and energy-balance equations (Westhoff et al., 2007),

$$Q_d = Q_{u,1} + Q_{u,2}, \quad (\text{A.4})$$

$$T_d = \frac{Q_{u,1}}{Q_d} T_{u,1} + \frac{Q_{u,2}}{Q_d} T_{u,2}. \quad (\text{A.5})$$

## Appendix A. Analytical solution to the energy-balance equation

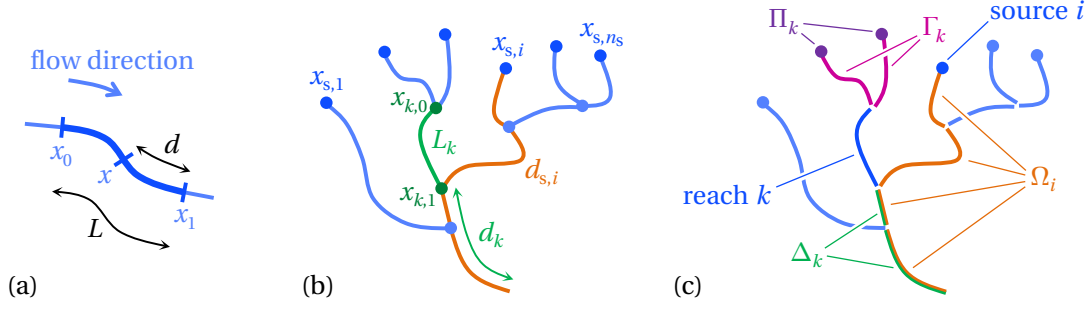


Figure A.1: Schematic representations of **(a)** a stream reach and **(b–c)** a stream network, illustrating the notation used to derive the analytical solution to the stream energy balance equation.

Based on Eqs. (A.1)–(A.5), the derivation of the expressions for  $Q_{\text{out}}$  and  $T_{\text{out}}$  is straightforward and leads to the following relations:

$$Q_{\text{out}} = \sum_{i=1}^{n_s} Q_{s,i} + q_\ell L_{\text{tot}}, \quad (\text{A.6})$$

$$T_{\text{out}} = \sum_{i=1}^{n_s} \frac{Q_{s,i}}{Q_{\text{out}}} e^{-d_{s,i}/L_c} T_{s,i} + \frac{1}{Q_{\text{out}}} \int_{\mathcal{L}} e^{-d(x)/L_c} \psi(x) dx. \quad (\text{A.7})$$

In the above equations,  $n_s$  refers to the number of sources in the network,  $L_{\text{tot}}$  denotes the total length of the stream network,  $d_{s,i}$  corresponds to the downstream distance of source point  $x_{s,i}$  to the network outlet,  $d(x)$  refers to the distance between any point  $x$  along the network and the network outlet,  $\mathcal{L}$  corresponds to the geometrical union of all reaches in the stream network, and  $T_{s,i}$  and  $Q_{s,i}$  denote the stream temperature and discharge at source point  $x_{s,i}$ , respectively. The reader is referred to Fig. A.1b for a graphical illustration of some of the variables. The integral over  $\mathcal{L}$  is a shorthand notation for the sum of the respective integrals over all the reaches in the network.

Equations (A.6)–(A.7) can be written in a more convenient form using space-averaging operators. Replacing  $\psi$  with its expression defined in Eq. (A.3), the integral on the right-hand side of Eq. (A.7) can be written as

$$\int_{\mathcal{L}} e^{-d(x)/L_c} \psi(x) dx = A_1 q_\ell \langle T_\ell \rangle_{\mathcal{L}} + \frac{A_2}{L_c} \langle \gamma \phi_r + T_a - L_c \frac{g}{c_p} \frac{dz}{dx} \rangle_{\mathcal{Q}}, \quad (\text{A.8})$$

where the two averaging operators  $\langle \cdot \rangle_{\mathcal{L}}$  and  $\langle \cdot \rangle_{\mathcal{Q}}$  are defined as

$$\langle f \rangle_{\mathcal{L}} = \frac{1}{A_1} \int_{\mathcal{L}} e^{-d(x)/L_c} f(x) dx \text{ and} \quad (\text{A.9})$$

$$\langle f \rangle_{\mathcal{Q}} = \frac{1}{A_2} \int_{\mathcal{L}} e^{-d(x)/L_c} Q(x) f(x) dx, \quad (\text{A.10})$$

for any integrable function  $f$  defined on  $\mathcal{L}$ , with the normalizing factors  $A_1$  and  $A_2$  being



defined as

$$\begin{aligned}
A_1 &= \int_{\mathcal{L}} e^{-d(x)/L_c} dx, \\
&= \sum_{k=1}^{n_r} \int_{x_{k,0}}^{x_{k,1}} e^{-d(x)/L_c} dx \\
&= \sum_{k=1}^{n_r} L_k e^{-d_k/L_c} (1 - e^{-L_k/L_c})
\end{aligned} \tag{A.11}$$

and

$$\begin{aligned}
A_2 &= \int_{\mathcal{L}} e^{-d(x)/L_c} Q(x) dx \\
&= \sum_{k=1}^{n_r} \int_{x_{k,0}}^{x_{k,1}} e^{-d(x)/L_c} Q_k(x) dx.
\end{aligned} \tag{A.12}$$

In the above equations,  $n_r$  denotes the number of reaches in the network;  $x_{k,0}$ ,  $x_{k,1}$  and  $L_k$  refer to the upstream point, downstream point and length of reach  $k$ , respectively;  $d_k$  refers to the distance along the stream network between  $x_{k,1}$  and the network outlet; and  $Q_k(x)$  denotes the discharge along reach  $k$  (see Fig. A.1b). Based on Eq. (A.1),  $Q_k$  may be expressed as

$$\begin{aligned}
Q_k(x) &= Q(x_{k,0}) + q_\ell(x - x_{k,0}) \\
&= \sum_{j \in \Pi_k} Q_{s,j} + q_\ell \sum_{r \in \Gamma_k} L_r + q_\ell(x - x_{k,0}),
\end{aligned} \tag{A.13}$$

where  $\Pi_k$  and  $\Gamma_k$  denote the set of source points and reaches draining into reach  $k$ , respectively, as illustrated in Fig. A.1c. Inserting the above equation into Eq. (A.12) and re-arranging the terms,  $A_2$  may be written as

$$\begin{aligned}
A_2 &= \sum_{i=1}^{n_s} Q_{s,i} \sum_{j \in \Omega_i} \int_{x_{j,0}}^{x_{j,1}} e^{-d(x)/L_c} dx \\
&\quad + q_\ell \sum_{k=1}^{n_r} L_k \sum_{r \in \Delta_k} \int_{x_{r,0}}^{x_{r,1}} e^{-d(x)/L_c} dx \\
&\quad + q_\ell \sum_{k=1}^{n_r} \int_{x_{k,0}}^{x_{k,1}} e^{-d(x)/L_c} x dx,
\end{aligned} \tag{A.14}$$

where  $\Omega_i$  refers to the set of reaches linking the  $i$ th source point to the network outlet, and  $\Delta_k$  denotes the set of reaches linking reach  $k$  to the network outlet, not including reach  $k$  itself (see Fig. A.1c). Assuming that all source points have the same discharge  $Q_s$ , and replacing the integrals along the reaches with their respective values, Eq. (A.14) can be written more simply

## Appendix A. Analytical solution to the energy-balance equation

---

as

$$\begin{aligned} A_2 &= L_c Q_s \sum_{i=1}^{n_s} (1 - e^{-d_{s,i}/L_c}) + q_\ell L_c \sum_{k=1}^{n_r} \{L_k - L_c e^{-d_k/L_c} (1 - e^{-L_k/L_c})\} \\ &= L_c (Q_{\text{tot}} - q_\ell L_{\text{tot}}) (1 - \delta_s) + q_\ell L_c L_{\text{tot}} (1 - \delta_\ell), \end{aligned} \quad (\text{A.15})$$

where Eq. (A.6) has been used in the second step to replace  $n_s Q_s$  with  $Q_{\text{tot}} - q_\ell L_{\text{tot}}$ , and the factors  $\delta_s$  and  $\delta_\ell$  are defined as

$$\delta_s = \frac{1}{n_s} \sum_{i=1}^{n_s} e^{-d_{s,i}/L_c} \text{ and} \quad (\text{A.16})$$

$$\delta_\ell = \frac{L_c}{L_{\text{tot}}} \sum_{k=1}^{n_r} e^{-d_k/L_c} (1 - e^{-L_k/L_c}) = \frac{A_1}{L_{\text{tot}}}. \quad (\text{A.17})$$

Combining Eqs. (A.7), (A.8), (A.11) and (A.15), the expression for stream temperature at the network outlet can eventually be written in a more convenient form,

$$\begin{aligned} T_{\text{out}} &= (1 - \eta) \delta_s \overline{T_s} + \eta \delta_\ell \langle T_\ell \rangle_{\mathcal{L}} \\ &\quad + [1 - (1 - \eta) \delta_s - \eta \delta_\ell] \langle \gamma \phi_r + T_a - L_c \frac{g}{c_p} \frac{dz}{dx} \rangle_{\mathcal{L}}, \end{aligned} \quad (\text{A.18})$$

where the averaging operator  $\langle \cdot \rangle_{\mathcal{L}}$  has been approximated by  $\langle \cdot \rangle_{\mathcal{L}}$ , and  $\overline{T_s}$  corresponds to the distance-weighted source temperature, averaged over all sources and weighted by a factor decreasing exponentially with the respective distance of each source to the network outlet,

$$\overline{T_s} = \frac{1}{n_s \delta_s} \sum_{i=1}^{n_s} e^{-d_{s,i}/L_c} T_{s,i}. \quad (\text{A.19})$$

The factor  $\eta$  appearing in Eq. (A.18) denotes the ratio between the discharge originating from lateral inflow and the total discharge at the network outlet,

$$\eta = \frac{q_\ell L_{\text{tot}}}{Q_{\text{tot}}}. \quad (\text{A.20})$$

## B Original formulation of *StreamFlow*'s subwatershed bucket model

This section briefly describes the approaches originally implemented in the first version of the code for computing the discharge and temperature of the subsurface flow generated by each subwatershed.

### B.1 Subwatershed outflow discharge computation

As illustrated in Fig. B.1a, the original model of Comola et al. approximates each subwatershed as the vertical superposition of two linear reservoirs, where the upper one simulates the fast response to rainfall events and the lower one the slow response. Water percolating at the bottom of the subwatershed soil columns fills the lower reservoir up to a maximum flow rate  $R_{\max}$  ( $\text{m s}^{-1}$ ), the excess water draining into the upper reservoir. This translates into the following equations for the water levels  $S_{\text{res,u}}$  (m) and  $S_{\text{res,l}}$  (m) in the upper and lower reservoirs, respectively:

$$\frac{dS_{\text{res,u}}}{dt} = I_{\text{res,u}} - \frac{Q_{\text{res,u}}}{A_{\text{subw}}}, \quad (\text{B.1})$$

$$\frac{dS_{\text{res,l}}}{dt} = I_{\text{res,l}} - \frac{Q_{\text{res,l}}}{A_{\text{subw}}}, \quad (\text{B.2})$$

where the water inflow rates  $I_{\text{res,u}}$  ( $\text{m s}^{-1}$ ) and  $I_{\text{res,l}}$  ( $\text{m s}^{-1}$ ) into the upper and lower reservoirs are expressed as  $I_{\text{res,u}} = I - I_{\text{res,l}}$  and  $I_{\text{res,l}} = \min(I, R_{\max})$ , with  $I$  ( $\text{m s}^{-1}$ ) denoting the total flow rate of water percolating at the bottom of the subwatershed soil columns and  $A_{\text{subw}}$  ( $\text{m}^2$ ) the subwatershed surface area.  $Q_{\text{res,u}}$  ( $\text{m}^3 \text{s}^{-1}$ ) and  $Q_{\text{res,l}}$  ( $\text{m}^3 \text{s}^{-1}$ ) correspond to the discharge at the outlet of the upper and lower reservoirs, which are linearly related to the reservoir water levels,

$$Q_{\text{res,u}} = A_{\text{subw}} \frac{S_{\text{res,u}}}{\tau_{\text{res,u}}}, \quad (\text{B.3})$$

$$Q_{\text{res,l}} = A_{\text{subw}} \frac{S_{\text{res,l}}}{\tau_{\text{res,l}}}. \quad (\text{B.4})$$

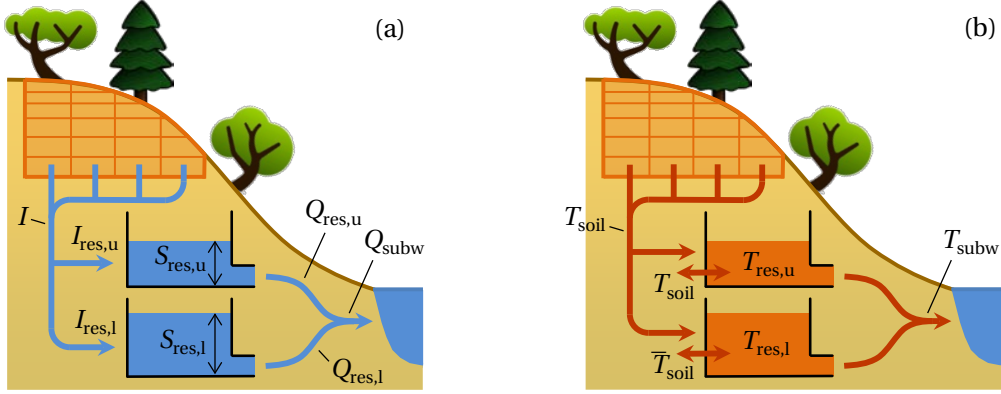


Figure B.1: Illustrations of the models devised by Comola et al. (2015) for the computation of **(a)** subsurface runoff discharge, and **(b)** subsurface runoff temperature. The symbols are defined in the text.

The characteristic residence times  $\tau_{\text{res},u}$  (s) and  $\tau_{\text{res},l}$  (s) are expressed as power functions of the subwatershed area:

$$\tau_{\text{res},u} = \bar{\tau}_{\text{res},u} \left( \frac{A_{\text{subw}}}{A_{\text{tot}}} \right)^{\frac{1}{3}}, \quad (\text{B.5})$$

$$\tau_{\text{res},l} = \bar{\tau}_{\text{res},l} \left( \frac{A_{\text{subw}}}{A_{\text{tot}}} \right)^{\frac{1}{3}}, \quad (\text{B.6})$$

where  $\bar{\tau}_{\text{res},u}$  (s) and  $\bar{\tau}_{\text{res},l}$  (s) are two user-specified parameters and  $A_{\text{tot}}$  ( $\text{m}^2$ ) denotes the area of the entire parent watershed. The total discharge  $Q_{\text{subw}}$  ( $\text{m}^3 \text{s}^{-1}$ ) flowing from the subwatershed into the stream is then computed as  $Q_{\text{subw}} = Q_{\text{res},u} + Q_{\text{res},l}$ . The subwatershed behavior can be adjusted by modifying the values of parameters  $R_{\text{max}}$ ,  $\bar{\tau}_{\text{res},u}$  and  $\bar{\tau}_{\text{res},l}$ .

## B.2 Subwatershed outflow temperature computation

The method developed by Comola et al. (2015) for the computation of the subwatershed outflow temperature  $T_{\text{subw}}$  (K) is depicted in Fig. B.1b. Temperatures  $T_{\text{res},u}$  (K) and  $T_{\text{res},l}$  (K) of water stored in the upper and lower reservoirs are computed as:

$$\frac{dT_{\text{res},u}}{dt} = \frac{I_{\text{res},u}}{S_{\text{res},u}} (T_{\text{soil}} - T_{\text{res},u}) + \frac{T_{\text{soil}} - T_{\text{res},u}}{k_{\text{soil}}}, \quad (\text{B.7})$$

$$\frac{dT_{\text{res},l}}{dt} = \frac{I_{\text{res},l}}{S_{\text{res},l}} (T_{\text{soil}} - T_{\text{res},l}) + \frac{\bar{T}_{\text{soil}} - T_{\text{res},l}}{k_{\text{soil}}}, \quad (\text{B.8})$$

where  $k_{\text{soil}}$  (s) is a calibration parameter corresponding to the characteristic time of thermal diffusion and  $T_{\text{soil}}$  (K) refers to soil temperature at the bottom of the subwatershed soil columns as modeled by *Alpine3D*.  $\bar{T}_{\text{soil}}$  denotes the annual average of  $T_{\text{soil}}$ , which is used as a

## B.2. Subwatershed outflow temperature computation

---

proxy for the temperature of deep soil. The first term in the right hand-side of the above two expressions accounts for the heat flux associated with the inflow of water into the reservoirs. The second term corresponds to the diffusive heat exchange between water and the surrounding soil particles. These expressions were derived by assuming that the temperature of water percolating at the bottom of the soil columns is equal to the local soil temperature. They are solved using a second-order Crank Nicholson scheme, and their solution is used to compute  $T_{\text{subw}}$  (K) as:

$$T_{\text{subw}} = \frac{Q_{\text{res,u}} T_{\text{res,u}} + Q_{\text{res,l}} T_{\text{res,l}}}{Q_{\text{res,u}} + Q_{\text{res,l}}}. \quad (\text{B.9})$$



## C Validation of the scheme used to solve the heat balance equation

The splitting scheme described in Sect. 3.2.2 for numerically solving Eq. (3.11) is validated here by comparing its predictions against analytical solutions. The derivation of the analytical solutions is presented first, followed by the assessment the numerical scheme precision.

### C.1 Analytical solutions to the heat balance equation

Eq. (3.11) can be written in a more compact form:

$$\frac{\partial T_w}{\partial x} + \nu \frac{\partial T_w}{\partial x} = \frac{1}{\tau} T_w + \sigma, \quad (\text{C.1})$$

with

$$\tau = -\frac{hw}{q_{\text{subw}}},$$

$$\sigma = \frac{\phi}{\rho_w c_{p,w} h} + \frac{q_{\text{subw}}}{hw} T_{\text{subw}} + \frac{gQ}{c_{p,w} hw} S_0.$$

Similarly to (e.g. Lowney, 2000), Eq. (C.1) above is simplified by assuming  $\tau$  to be constant and  $\sigma$  to be a function of time only. The length of the spatial domain over which the equation is to be solved is denoted as  $L$ . It is assumed that  $\nu > 0$  for all  $x \in [0, L]$ , so that a boundary condition must be specified at  $x = 0$ . A Dirichlet boundary condition is considered here,

$$T_w(0, t) = T_{\text{in}}(t) \quad \text{for all } t \geq 0, \quad (\text{C.2})$$

where  $T_{\text{in}}(t)$  is a prescribed function of time. Since the spatial domain is finite, the analytical solution to Eq. (C.1), subject to boundary condition Eq. (C.2), will consist of a transient phase followed by a permanent regime. During the transient phase, the initial temperature distribution  $T_{w,\text{ini}}(x, t)$  is advected towards the right end of the spatial domain, while the boundary condition  $T_{\text{in}}$  dictates the value of temperature entering the domain through its left end. After the last remnant of the initial temperature distribution has exited the spatial

## Appendix C. Validation of the scheme used to solve the heat balance equation

---

domain, the solution reaches its permanent regime, which is the same regardless of the initial distribution. Only the permanent regime is of interest here, so that no initial condition needs to be specified.

The analytical solution to Eqs. (C.1)–(C.2), under the conditions  $\tau = \text{cst}$  and  $\sigma = \sigma(t)$ , is obtained by the method of characteristics (e.g. LeVeque, 2002). The two independent variables  $x$  and  $t$  are parametrized as a function of a path variable  $s$ . Using the definition  $\theta(s) = T(x(s), t(s))$ , we observe that

$$\frac{d\theta}{ds} = \frac{\partial T_w}{\partial t} \frac{dt}{ds} + \frac{\partial T_w}{\partial x} \frac{dx}{ds},$$

so that Eq. (3.11) can be re-written as

$$\frac{d\theta}{ds} = \frac{1}{\tau} \theta + \sigma, \quad (\text{C.3})$$

if the parametrizations of  $x$  and  $t$  are chosen such that:

$$\frac{dt}{ds} = 1, \quad (\text{C.4})$$

$$\frac{dx}{ds} = \nu. \quad (\text{C.5})$$

Equation (C.3) is an ordinary differential equation in which  $\sigma$  should be understood as a function of  $s$ , i.e.  $\sigma(s) = \sigma(t(s))$ . Its solution can be easily found and is given by:

$$\theta(s) = \int_{s_0}^s \left( \sigma(s') + \frac{\theta(s_0)}{\tau} \right) \exp\left(\frac{s-s'}{\tau}\right) ds' + \theta(s_0), \quad (\text{C.6})$$

where  $s_0$  denotes the lower integration bound, which needs to be specified. Equation (C.4) is trivially solved through integration between  $s_0$  and  $s$ ,

$$t(s) = s + s_0 - t_0,$$

where  $t_0 = t(s_0)$ . The above expression for  $t$  implies that  $s$  is equivalent to time (i.e.  $s \equiv t$ ), so that  $x$  can be interpreted as the position of a particle moving with instantaneous velocity  $\nu$  as per Eq. (C.5). In the permanent regime, each “particle” enters the spatial domain through its left-hand side boundary. As a consequence,  $s_0$ —or, equivalently,  $t_0$ —needs to be chosen such that  $x(s_0) = 0$  in the present case. This further implies that:

$$\theta(s_0) = T_w(x(s_0), t(s_0)) = T_w(0, t_0) = T_{\text{in}}(t_0), \quad (\text{C.7})$$

where Eq. C.2 has been used in the last step. Inserting the above expression in Eq. (C.6) and replacing  $\theta(s)$  with  $T_w(x, t)$  and  $s$  with  $t$ , one finally obtains:

$$T_w(x, t) = \int_{t_0}^t \left( \sigma(t') + \frac{T_{\text{in}}(t_0)}{\tau} \right) \exp\left(\frac{t-t'}{\tau}\right) ds' + T_{\text{in}}(t_0). \quad (\text{C.8})$$



## C.1. Analytical solutions to the heat balance equation

---

Closed-form expressions of the above equation can be found by choosing simple formulations for  $\sigma$  and  $v$ . Two cases are considered here:

**Test case 1:** Constant velocity and sinusoidal expression for  $\sigma$ ,

$$v(x, t) = \text{cst}, \quad \text{for all } x \in [0, L], t \geq 0, \quad (\text{C.9})$$

$$\sigma(t) = a_\sigma \sin(\omega t) + b_\sigma, \quad \text{for all } t \geq 0, \quad (\text{C.10})$$

with  $\omega$  ( $\text{s}^{-1}$ ),  $a_\sigma$  ( $\text{Ks}^{-1}$ ) and  $b_\sigma$  ( $\text{Ks}^{-1}$ ) constant. This test aims at assessing the ability of the splitting scheme to correctly account for time varying heat sources.

**Test case 2:** velocity varying linearly in space and no  $\sigma$ -term,

$$v(x, t) = a_v x + b_v, \quad \text{for all } x \in [0, L], t \geq 0, \quad (\text{C.11})$$

$$\sigma(t) = 0, \quad \text{for all } t \geq 0, \quad (\text{C.12})$$

where  $a_v$  ( $\text{s}^{-1}$ ) and  $b_v$  ( $\text{ms}^{-1}$ ) are constant and chosen such that  $v > 0$  for all  $x \in [0, L]$ . This test intends to validate the robustness of the splitting scheme in the case of non-uniform flow velocity profiles.

In both cases, the expression of  $T_{\text{in}}$  is chosen similarly to the one of (e.g. Lowney, 2000), who aimed at reproducing natural diurnal variations of stream temperature,

$$T_{\text{in}}(t) = a_{\text{in}} \sin(\omega t) + b_{\text{in}}, \quad (\text{C.13})$$

where  $a_{\text{in}}$  (K) and  $b_{\text{in}}$  (K) are constant, and  $\omega$  is the same as in Eq. (C.10).

### C.1.1 Analytical solution of test case 1

In test case 1, the solution to Eq. (C.5) under the constraint  $x(s_0) = 0$  is straightforward due to  $v$  being constant,

$$x(s) = v(s - s_0).$$

Replacing  $s$  with  $t$  and solving for  $t_0$ , one obtains:

$$t_0 = t - \frac{x}{v}.$$

After inserting this expression in Eq. C.8, replacing  $\sigma$  with its sinusoidal formulation and performing the integration, one gets the closed-form expression of the solution to Eq. (3.11) in

## Appendix C. Validation of the scheme used to solve the heat balance equation

Table C.1: Values chosen for the parameters associated with test cases 1 and 2 in order to validate the numerical splitting scheme.

Name	Units	Value
$\tau$	(s)	$2 \times 10^6$
$\omega$	(s <sup>-1</sup> )	$2\pi/3600$
$a_\sigma$	(Ks <sup>-1</sup> )	$5 \times 10^{-3}$
$b_\sigma$	(Ks <sup>-1</sup> )	$2 \times 10^{-4}$
$a_\nu$	(s <sup>-1</sup> )	$1/12800$
$b_\nu$	(ms <sup>-1</sup> )	0.5
$a_{\text{in}}$	(K)	1.5
$b_{\text{in}}$	(K)	283.15

the permanent regime (i.e. for  $t > L/\nu$ ),

$$\begin{aligned}
 T_w(x, t) = & T_{\text{in}} \left( t - \frac{x}{\nu} \right) \exp \left( \frac{x}{\tau \nu} \right) + b_\sigma \tau \left[ \exp \left( \frac{x}{\tau \nu} \right) - 1 \right] \\
 & - \frac{a_\sigma \tau}{1 + (\tau \omega)^2} (\sin(\omega t) + \tau \omega \cos(\omega t)) \\
 & + \frac{a_\sigma \tau}{1 + (\tau \omega)^2} \left( \sin \left[ \omega \left( t - \frac{x}{\nu} \right) \right] + \tau \omega \cos \left[ \omega \left( t - \frac{x}{\nu} \right) \right] \right) \exp \left( \frac{x}{\tau \nu} \right),
 \end{aligned} \tag{C.14}$$

with  $T_{\text{in}}$  as defined in Eq. (C.13). It should be mentioned that the above expression is actually valid for any formulation of  $T_{\text{in}}$ , not just Eq. (C.13).

### C.1.2 Analytical solution of test case 2

In case  $\nu$  is expressed as in Eq. (C.11), the solution to Eq. (C.5) satisfying  $x(s_0) = 0$  becomes:

$$x(s) = \frac{b_\nu}{a_\nu} (\exp[a_\nu(s - s_0)] - 1).$$

The expression for  $t_0$  is obtained by replacing  $s$  with  $t$  in the above equation:

$$t_0 = t - \frac{1}{a_\nu} \ln \left( \frac{a_\nu}{b_\nu} x + 1 \right).$$

The analytical solution of test case 2 is obtained by inserting the above expression for  $t_0$  in Eq. (C.8), imposing  $\sigma = 0$  and performing the integration:

$$T_w(x, t) = T_{\text{in}} \left( t - \frac{1}{a_\nu} \ln \left( \frac{a_\nu}{b_\nu} x + 1 \right) \right) \left( \frac{a_\nu}{b_\nu} x + 1 \right)^{1/(a_\nu \tau)}. \tag{C.15}$$

The above solution describes the permanent regime, i.e. it is valid for all  $t \geq \ln(a_\nu L/b_\nu + 1)/a_\nu$ . As opposed to the solution of test case 1, which has already been reported by Lowney (2000), the present one has—to the best of our knowledge—not been presented in any publication to

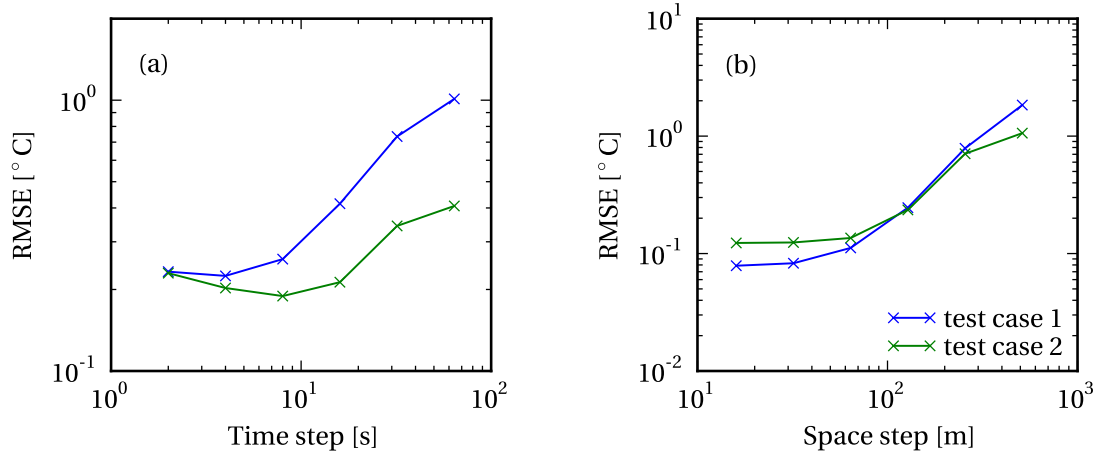


Figure C.1: Root mean square error (RMSE) of the splitting scheme used to solve the heat balance equation in test cases 1 (blue) and 2 (green). The RMSE is computed by comparing the simulated and analytical temperature profiles at the end of the simulation (8 hours). **(a)** Splitting scheme RMSE for various time steps with a fixed spatial discretization length of 128 m; and **(b)** Splitting scheme RMSE for various spatial discretization lengths with a fixed time step of 1 s.

date.

## C.2 Validation of the numerical splitting scheme

The splitting scheme is validated over a spatial domain of  $L = 12.8$  km, for a simulated time period of 8 hours. Table C.1 contains the values of the parameters considered in test cases 1 and 2.

Figure C.1 pictures the root mean square error (RMSE) of the splitting scheme compared to the analytical solutions of both test cases, for various time steps and spatial discretization lengths. Based on the RMSE values associated with test case 1, it can be suggested that the scheme is of order 1 in time and order 2 in space, as expected from its formulation (see Sect. 3.2.2). This is however less visible in test case 2, probably as a result of the RMSE varying over a smaller range of time steps and spatial discretizations lengths as in the first case. In all cases however, the scheme RMSE remains within acceptable bounds. As can be observed in Fig. C.2, the numerical scheme is also able to satisfactorily reproduce the strong fluctuations of the temperature profile in both test cases, except for the minima and maxima which are truncated.

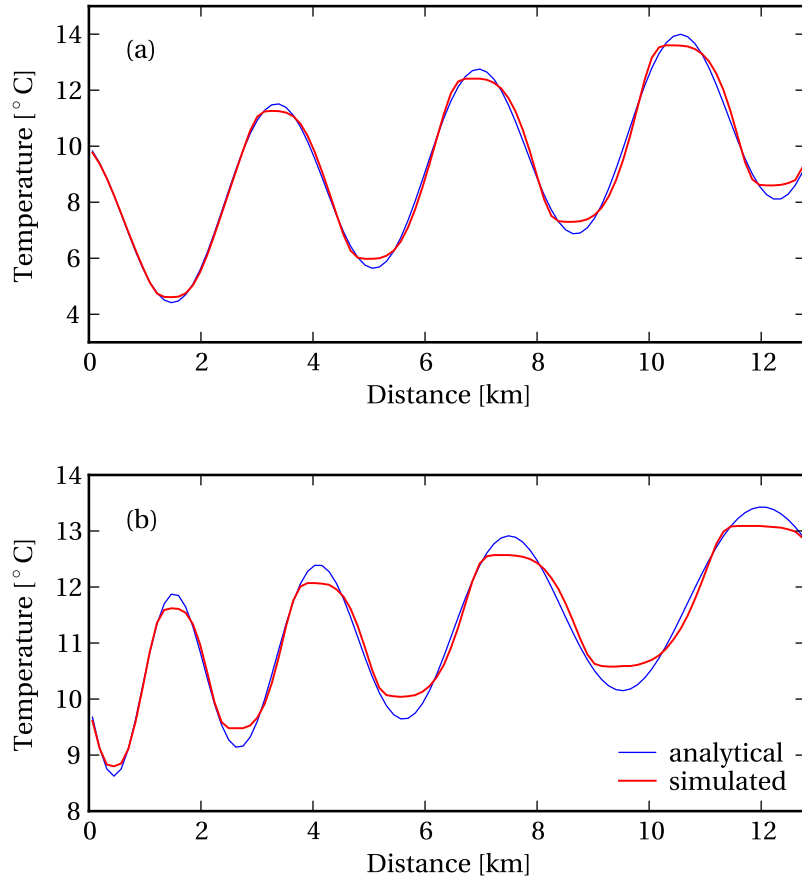


Figure C.2: Stream temperature profile at the end of the simulation (8 hours) in **(a)** test case 1, and **(b)** test case 2. The analytical temperature profiles are displayed in blue, and those simulated by the splitting scheme in red.



## Bibliography

- J. Armstrong, P. Kemp, G. Kennedy, M. Ladle, and N. Milner. Habitat requirements of Atlantic salmon and brown trout in rivers and streams. *Fisheries Research*, 62(2):143–170, 2003. ISSN 0165-7836. doi: [http://dx.doi.org/10.1016/S0165-7836\(02\)00160-1](http://dx.doi.org/10.1016/S0165-7836(02)00160-1). URL <http://www.sciencedirect.com/science/article/pii/S0165783602001601>.
- D. B. Arscott, K. Tockner, and J. Ward. Thermal heterogeneity along a braided floodplain river (Tagliamento River, northeastern Italy). *Canadian Journal of Fisheries and Aquatic Sciences*, 58(12):2359–2373, 2001.
- H. Aschwanden and R. Weingartner. Die Abflussregimes der Schweiz. Publikation Gewässerkunde Nr. 65, Geographisches Institut der Universität Bern, 1985.
- A. Bárdossy. Calibration of hydrological model parameters for ungauged catchments. *Hydrology and Earth System Sciences*, 11(2):703–710, 2007. doi: 10.5194/hess-11-703-2007. URL <http://www.hydrol-earth-syst-sci.net/11/703/2007/>.
- T. Barnett, J. Adam, and D. Lettenmaier. Potential impacts of a warming climate on water availability in snow-dominated regions. *Nature*, 438(7066):303–309, 2005. doi: 10.1038/nature04141.
- P. Bartelt and M. Lehning. A physical SNOWPACK model for the Swiss avalanche warning. Part I: numerical model. *Cold Regions Science and Technology*, 35(3):123–145, 2002. ISSN 0165-232X. doi: [http://dx.doi.org/10.1016/S0165-232X\(02\)00074-5](http://dx.doi.org/10.1016/S0165-232X(02)00074-5). URL <http://www.sciencedirect.com/science/article/pii/S0165232X02000745>.
- M. Bavay and T. Egger. Meteoi2 2.4.2: a preprocessing library for meteorological data. *Geoscientific Model Development*, 7(6):3135–3151, 2014. doi: 10.5194/gmd-7-3135-2014. URL <http://www.geosci-model-dev.net/7/3135/2014/>.
- M. Bavay, M. Lehning, T. Jonas, and H. Löwe. Simulations of future snow cover and discharge in Alpine headwater catchments. *Hydrological Processes*, 23(1):95–108, 2009. ISSN 1099-1085. doi: 10.1002/hyp.7195. URL <http://dx.doi.org/10.1002/hyp.7195>.
- M. Bavay, T. Grünwald, and M. Lehning. Response of snow cover and runoff to climate change in high Alpine catchments of Eastern Switzerland. *Advances in Water Resources*, 55:

## Bibliography

---

- 4–16, 2013. ISSN 0309-1708. doi: <http://dx.doi.org/10.1016/j.advwatres.2012.12.009>. URL <http://www.sciencedirect.com/science/article/pii/S0309170812003193>.
- M. Beniston. Impacts of climatic change on water and associated economic activities in the Swiss Alps. *Journal of Hydrology*, 412–413:291–296, 2012. ISSN 0022-1694. doi: <http://dx.doi.org/10.1016/j.jhydrol.2010.06.046>. URL <http://www.sciencedirect.com/science/article/pii/S0022169410004993>. Hydrology Conference 2010.
- L. Benyahya, D. Caissie, A. St-Hilaire, T. B. Ouarda, and B. Bobée. A review of statistical water temperature models. *Canadian Water Resources Journal*, 32(3):179–192, 2007. doi: 10.4296/cwrj3203179. URL <http://dx.doi.org/10.4296/cwrj3203179>.
- M. Berger, M. J. Aftosmis, and S. M. Murman. Analysis of slope limiters on irregular grids. In *43rd AIAA Aerospace Sciences Meeting*, Reno, NV, U.S.A., May 2005. NAS Technical Report NAS-05-007.
- K. Beven and A. Binley. The future of distributed models: Model calibration and uncertainty prediction. *Hydrological Processes*, 6(3):279–298, 1992. ISSN 1099-1085. doi: 10.1002/hyp.3360060305. URL <http://dx.doi.org/10.1002/hyp.3360060305>.
- K. J. Beven. *Rainfall-Runoff Modelling: The Primer, 2nd Edition*. Wiley-Blackwell, 2012. ISBN 978-0-470-71459-1.
- B. R. Bicknell, J. C. Imhoff, J. L. Kittle, A. S. Donigian, and R. C. Johanson. *Hydrological Simulation Program—FORTRAN User's Manual for Version 11*. U.S. Environmental Protection Agency, National Exposure Research Laboratory, Athens, GA, U.S., August 1997.
- B. Biswal and M. Marani. Geomorphological origin of recession curves. *Geophysical Research Letters*, 37(24), 2010. ISSN 1944-8007. doi: 10.1029/2010GL045415. URL <http://dx.doi.org/10.1029/2010GL045415>.
- T. Bogan, O. Mohseni, and H. G. Stefan. Stream temperature-equilibrium temperature relationship. *Water Resources Research*, 39(9), 2003. ISSN 1944-7973. doi: 10.1029/2003WR002034. URL <http://dx.doi.org/10.1029/2003WR002034>.
- T. Bogan, H. G. Stefan, and O. Mohseni. Imprints of secondary heat sources on the stream temperature/equilibrium temperature relationship. *Water Resources Research*, 40(12), 2004. ISSN 1944-7973. doi: 10.1029/2003WR002733. URL <http://dx.doi.org/10.1029/2003WR002733>.
- M. Boyd and B. Kasper. *Analytical methods for dynamic open channel heat and mass transfer: Methodology for Heat Source Model version 7.0*, 2003. URL <http://www.deq.state.or.us/wq/TMDLs/tools.htm>.
- G. W. Brown. Predicting temperatures of small streams. *Water Resources Research*, 5(1):68–75, 1969. ISSN 1944-7973. doi: 10.1029/WR005i001p00068. URL <http://dx.doi.org/10.1029/WR005i001p00068>.

- G. Bürger, J. Schulla, and A. T. Werner. Estimates of future flow, including extremes, of the Columbia River headwaters. *Water Resources Research*, 47(W10520), 2011. ISSN 1944-7973. doi: 10.1029/2010WR009716. URL <http://dx.doi.org/10.1029/2010WR009716>.
- K. P. Burnham and D. R. Anderson. *Model selection and multimodel inference: a practical information-theoretic approach*. Springer, New York, 2002.
- V. Bustillo, F. Moatar, A. Ducharne, D. Thiéry, and A. Poirel. A multimodel comparison for assessing water temperatures under changing climate conditions via the equilibrium temperature concept: case study of the Middle Loire River, France. *Hydrological Processes*, 28(3):1507–1524, 2014. ISSN 1099-1085. doi: 10.1002/hyp.9683. URL <http://dx.doi.org/10.1002/hyp.9683>.
- D. Butman and P. Raymond. Significant efflux of carbon dioxide from streams and rivers in the United States. *Nature Geoscience*, 4(12):839–842, 2011. doi: 10.1038/ngeo1294.
- D. Caissie. The thermal regime of rivers: a review. *Freshwater Biology*, 51(8):1389–1406, 2006. ISSN 1365-2427. doi: 10.1111/j.1365-2427.2006.01597.x. URL <http://dx.doi.org/10.1111/j.1365-2427.2006.01597.x>.
- D. Caissie, N. El-Jabi, and M. G. Satish. Modelling of maximum daily water temperatures in a small stream using air temperatures. *Journal of Hydrology*, 251(1–2):14–28, 2001. ISSN 0022-1694. doi: 10.1016/S0022-1694(01)00427-9. URL <http://www.sciencedirect.com/science/article/pii/S0022169401004279>.
- D. Caissie, M. G. Satish, and N. El-Jabi. Predicting river water temperatures using the equilibrium temperature concept with application on Miramichi River catchments (New Brunswick, Canada). *Hydrological Processes*, 19(11):2137–2159, 2005. ISSN 1099-1085. doi: 10.1002/hyp.5684. URL <http://dx.doi.org/10.1002/hyp.5684>.
- D. Caissie, M. G. Satish, and N. El-Jabi. Predicting water temperatures using a deterministic model: Application on Miramichi River catchments (New Brunswick, Canada). *Journal of Hydrology*, 336(3–4):303–315, 2007. ISSN 0022-1694. doi: <http://dx.doi.org/10.1016/j.jhydrol.2007.01.008>.
- R. J. Caldwell, S. Gangopadhyay, J. Bountry, Y. Lai, and M. M. Elsner. Statistical modeling of daily and subdaily stream temperatures: Application to the Methow River Basin, Washington. *Water Resources Research*, 49(7):4346–4361, 2013. ISSN 1944-7973. doi: 10.1002/wrcr.20353. URL <http://dx.doi.org/10.1002/wrcr.20353>.
- H. Chang and M. Pсарis. Local landscape predictors of maximum stream temperature and thermal sensitivity in the Columbia River Basin, USA. *Science of The Total Environment*, 461–462:587–600, 2013. ISSN 0048-9697. doi: 10.1016/j.scitotenv.2013.05.033. URL <http://www.sciencedirect.com/science/article/pii/S0048969713005767>.

## Bibliography

---

- Y. Chen, R. Carsel, S. McCutcheon, and W. Nutter. Stream temperature simulation of forested riparian areas: I. Watershed-scale model development. *Journal of Environmental Engineering*, 124(4):304–315, 1998. doi: 10.1061/(ASCE)0733-9372(1998)124:4(304). URL [http://dx.doi.org/10.1061/\(ASCE\)0733-9372\(1998\)124:4\(304\)](http://dx.doi.org/10.1061/(ASCE)0733-9372(1998)124:4(304)).
- F. Comola, B. Schaeffli, A. Rinaldo, and M. Lehning. Thermodynamics in the hydrologic response: Travel time formulation and application to Alpine catchments. *Water Resources Research*, 51(3):1671–1687, 2015. ISSN 1944-7973. doi: 10.1002/2014WR016228. URL <http://dx.doi.org/10.1002/2014WR016228>.
- J. A. Cunge. On the subject of a flood propagation computation method (Muskingum method). *Journal of Hydraulic Research*, 7(2):205–230, 1969. doi: 10.1080/00221686909500264. URL <http://dx.doi.org/10.1080/00221686909500264>.
- A. Daigle, A. St-Hilaire, D. Peters, and D. Baird. Multivariate modelling of water temperature in the Okanagan watershed. *Canadian Water Resources Journal*, 35(3):237–258, 2010. doi: 10.4296/cwrj3503237. URL <http://dx.doi.org/10.4296/cwrj3503237>.
- H. F. Dallas and N. A. Rivers-Moore. Critical thermal maxima of aquatic macroinvertebrates: towards identifying bioindicators of thermal alteration. *Hydrobiologia*, 679(1):61–76, 2012. ISSN 1573-5117. doi: 10.1007/s10750-011-0856-4.
- S. F. Daly. Anchor ice flooding in Jackson, WY. In *World Water and Environmental Resources Congress 2005: Impacts of Global Climate Change*, pages 1–9. American Society of Civil Engineers, 2005. doi: 10.1061/40792(173)240.
- P. Déom. La mulette perlière. *La Hulotte*, 101, 2014. ISSN 0337-2154. URL <http://www.lahulotte.fr/>.
- D. R. DeWalle. Modeling stream shade: Riparian buffer height and density as important as buffer width1. *JAWRA Journal of the American Water Resources Association*, 46(2):323–333, 2010. ISSN 1752-1688. doi: 10.1111/j.1752-1688.2010.00423.x. URL <http://dx.doi.org/10.1111/j.1752-1688.2010.00423.x>.
- J. T. DeWeber and T. Wagner. A regional neural network ensemble for predicting mean daily river water temperature. *Journal of Hydrology*, 517:187–200, 2014. ISSN 0022-1694. doi: 10.1016/j.jhydrol.2014.05.035. URL <http://www.sciencedirect.com/science/article/pii/S0022169414003990>.
- A. Ducharne. Importance of stream temperature to climate change impact on water quality. *Hydrology and Earth System Sciences*, 12:13, 2008 2008. ISSN 1027-5606. URL <http://www.hydrol-earth-syst-sci.net/12/797/2008/>.
- A. Ducharne. Reducing scale dependence in TOPMODEL using a dimensionless topographic index. *Hydrology and Earth System Sciences*, 13(12):2399–2412, 2009. doi: 10.5194/hess-13-2399-2009. URL <http://www.hydrol-earth-syst-sci.net/13/2399/2009/>.



- A. Durmayaz and O. S. Sogut. Influence of cooling water temperature on the efficiency of a pressurized-water reactor nuclear-power plant. *International Journal of Energy Research*, 30 (10):799–810, 2006. ISSN 1099-114X. doi: 10.1002/er.1186. URL <http://dx.doi.org/10.1002/er.1186>.
- J. G. Eaton, J. H. McCormick, B. E. Goodno, D. G. O'Brien, H. G. Stefany, M. Hondzo, and R. M. Scheller. A field information-based system for estimating fish temperature tolerances. *Fisheries*, 20(4):10–18, 1995.
- K. Eckhardt. How to construct recursive digital filters for baseflow separation. *Hydrological Processes*, 19(2):507–515, 2005. ISSN 1099-1085. doi: 10.1002/hyp.5675. URL <http://dx.doi.org/10.1002/hyp.5675>.
- J. E. Edinger, D. W. Duttweiler, and J. C. Geyer. The response of water temperatures to meteorological conditions. *Water Resources Research*, 4(5):1137–1143, 1968. ISSN 1944-7973. doi: 10.1029/WR004i005p01137. URL <http://dx.doi.org/10.1029/WR004i005p01137>.
- J. M. Elliott and J. A. Elliott. Temperature requirements of Atlantic salmon *Salmo salar*, brown trout *Salmo trutta* and Arctic charr *Salvelinus alpinus*: predicting the effects of climate change. *Journal of Fish Biology*, 77(8):1793–1817, 2010. ISSN 1095-8649. doi: 10.1111/j.1095-8649.2010.02762.x. URL <http://dx.doi.org/10.1111/j.1095-8649.2010.02762.x>.
- J. M. Elliott and M. A. Hurley. An individual-based model for predicting the emergence period of sea trout fry in a Lake District stream. *Journal of Fish Biology*, 53(2):414–433, 1998. ISSN 1095-8649. doi: 10.1111/j.1095-8649.1998.tb00990.x. URL <http://dx.doi.org/10.1111/j.1095-8649.1998.tb00990.x>.
- J. M. Elliott, M. A. Hurley, and R. J. Fryer. A new, improved growth model for Brown Trout, *Salmo trutta*. *Functional Ecology*, 9(2):290–298, 1995. URL <http://www.jstor.org/stable/2390576>.
- S. Fatichi, S. Rimkus, P. Burlando, R. Bordoy, and P. Molnar. High-resolution distributed analysis of climate and anthropogenic changes on the hydrology of an Alpine catchment. *Journal of Hydrology*, 525:362–382, 2015. ISSN 0022-1694. doi: <http://dx.doi.org/10.1016/j.jhydrol.2015.03.036>. URL <http://www.sciencedirect.com/science/article/pii/S0022169415002073>.
- M. R. Ferrari, J. R. Miller, and G. L. Russell. Modeling changes in summer temperature of the Fraser River during the next century. *Journal of Hydrology*, 342(3–4):336–346, 2007. ISSN 0022-1694. doi: <http://dx.doi.org/10.1016/j.jhydrol.2007.06.002>. URL <http://www.sciencedirect.com/science/article/pii/S0022169407003289>.
- D. L. Ficklin, Y. Luo, I. T. Stewart, and E. P. Maurer. Development and application of a hydroclimatological stream temperature model within the Soil and Water Assessment Tool. *Water Resources Research*, 48(W01511), 2012. ISSN 1944-7973. doi: 10.1029/2011WR011256. URL <http://dx.doi.org/10.1029/2011WR011256>.
- D. L. Ficklin, B. L. Barnhart, J. H. Knauft, I. T. Stewart, E. P. Maurer, S. L. Letsinger, and G. W. Whittaker. Climate change and stream temperature projections in the Columbia

## Bibliography

---

- River basin: habitat implications of spatial variation in hydrologic drivers. *Hydrology and Earth System Sciences*, 18(12):4897–4912, 2014. doi: 10.5194/hess-18-4897-2014. URL <http://www.hydrol-earth-syst-sci.net/18/4897/2014/>.
- D. Finger, G. Heinrich, A. Gobiet, and A. Bauder. Projections of future water resources and their uncertainty in a glacierized catchment in the Swiss Alps and the subsequent effects on hydropower production during the 21st century. *Water Resources Research*, 48(W02521), 2012. ISSN 1944-7973. doi: 10.1029/2011WR010733. URL <http://dx.doi.org/10.1029/2011WR010733>.
- A. Gallice, B. Schaeffli, M. Lehning, M. B. Parlange, and H. Huwald. Stream temperature prediction in ungauged basins: review of recent approaches and description of a new physics-derived statistical model. *Hydrology and Earth System Sciences*, 19(9):3727–3753, 2015. doi: 10.5194/hess-19-3727-2015. URL <http://www.hydrol-earth-syst-sci.net/19/3727/2015/>.
- E. Gamma, R. Helm, R. Johnson, and J. Vlissides. *Design patterns: elements of reusable object-oriented software*. Addison-Wesley, 1994. ISBN 0201633612.
- B. Gardner and P. J. Sullivan. Spatial and temporal stream temperature prediction: Modeling nonstationary temporal covariance structures. *Water Resources Research*, 40(1), 2004. ISSN 1944-7973. doi: 10.1029/2003WR002511. URL <http://dx.doi.org/10.1029/2003WR002511>.
- G. Garner, D. M. Hannah, J. P. Sadler, and H. G. Orr. River temperature regimes of England and Wales: spatial patterns, inter-annual variability and climatic sensitivity. *Hydrological Processes*, 28(22):5583–5598, 2014. ISSN 1099-1085. doi: 10.1002/hyp.9992. URL <http://dx.doi.org/10.1002/hyp.9992>.
- B. Goodison, P. Louie, and D. Yang. WMO solid precipitation measurement intercomparison. Technical Report WMO/TD-No. 872, IOM No. 67, World Meteorological Organization, 1998.
- J. P. Gosink. Synopsis of analytic solutions for the temperature distribution in a river downstream from a dam or reservoir. *Water Resources Research*, 22(6):979–983, 1986. ISSN 1944-7973. doi: 10.1029/WR022i006p00979. URL <http://dx.doi.org/10.1029/WR022i006p00979>.
- I. Gouttevin, M. Lehning, T. Jonas, D. Gustafsson, and M. Mölder. A two-layer canopy model with thermal inertia for an improved snowpack energy balance below needleleaf forest (model SNOWPACK, version 3.2.1, revision 741). *Geoscientific Model Development*, 8(8): 2379–2398, 2015. doi: 10.5194/gmd-8-2379-2015. URL <http://www.geosci-model-dev.net/8/2379/2015/>.
- C. T. Graham and C. Harrod. Implications of climate change for the fishes of the British Isles. *Journal of Fish Biology*, 74(6):1143–1205, 2009. ISSN 1095-8649. doi: 10.1111/j.1095-8649.2009.02180.x.

- R. Grbić, D. Kurtagić, and D. Slišković. Stream water temperature prediction based on Gaussian process regression. *Expert Systems with Applications*, 40(18):7407–7414, 2013. ISSN 0957-4174. doi: 10.1016/j.eswa.2013.06.077. URL <http://www.sciencedirect.com/science/article/pii/S0957417413004764>.
- M. G. Grillakis, I. K. Tsanis, and A. G. Koutroulis. Application of the HBV hydrological model in a flash flood case in Slovenia. *Natural Hazards and Earth System Sciences*, 10(12):2713–2725, 2010. doi: 10.5194/nhess-10-2713-2010. URL <http://www.nat-hazards-earth-syst-sci.net/10/2713/2010/>.
- C. D. Groot Zwaafink, R. Mott, and M. Lehning. Seasonal simulation of drifting snow sublimation in Alpine terrain. *Water Resources Research*, 49(3):1581–1590, 2013. ISSN 1944-7973. doi: 10.1002/wrcr.20137. URL <http://dx.doi.org/10.1002/wrcr.20137>.
- I. Haag and A. Luce. The integrated water balance and water temperature model LARSIM-WT. *Hydrological Processes*, 22(7):1046–1056, 2008. ISSN 1099-1085. doi: 10.1002/hyp.6983. URL <http://dx.doi.org/10.1002/hyp.6983>.
- D. M. Hannah, I. A. Malcolm, C. Soulsby, and A. F. Youngson. Heat exchanges and temperatures within a salmon spawning stream in the Cairngorms, Scotland: seasonal and sub-seasonal dynamics. *River Research and Applications*, 20(6):635–652, 2004. ISSN 1535-1467. doi: 10.1002/rra.771. URL <http://dx.doi.org/10.1002/rra.771>.
- R. E. Hari, D. M. Livingstone, R. Siber, P. Burkhardt-Holm, and H. Güttinger. Consequences of climatic change for water temperature and brown trout populations in Alpine rivers and streams. *Global Change Biology*, 12(1):10–26, 2006. ISSN 1365-2486. doi: 10.1111/j.1365-2486.2005.001051.x. URL <http://dx.doi.org/10.1111/j.1365-2486.2005.001051.x>.
- F. R. Hauer, J. S. Baron, D. H. Campbell, K. D. Fausch, S. W. Hostetler, G. H. Leavesley, P. R. Leavitt, D. M. McKnight, and J. A. Stanford. Assessment of climate change and freshwater ecosystems of the Rocky Mountains, USA and Canada. *Hydrological Processes*, 11(8):903–924, 1997. ISSN 1099-1085. doi: 10.1002/(SICI)1099-1085(19970630)11:8<903::AID-HYP511>3.0.CO;2-7. URL [http://dx.doi.org/10.1002/\(SICI\)1099-1085\(19970630\)11:8<903::AID-HYP511>3.0.CO;2-7](http://dx.doi.org/10.1002/(SICI)1099-1085(19970630)11:8<903::AID-HYP511>3.0.CO;2-7).
- C. P. Hawkins, J. N. Hogue, L. M. Decker, and J. W. Feminella. Channel morphology, water temperature, and assemblage structure of stream insects. *Journal of the North American Benthological Society*, 16(4):728–749, 1997. ISSN 08873593. URL <http://www.jstor.org/stable/1468167>.
- C. Hébert, D. Caissie, M. Satish, and N. El-Jabi. Predicting hourly stream temperatures using the equilibrium temperature model. *Journal of Water Resource and Protection*, 7(4):322–338, 2015. doi: 10.4236/jwarp.2015.74026.
- W. R. Herb and H. G. Stefan. Modified equilibrium temperature models for cold-water streams. *Water Resources Research*, 47(W06519), 2011. ISSN 1944-7973. doi: 10.1029/2010WR009586. URL <http://dx.doi.org/10.1029/2010WR009586>.

## Bibliography

---

- R. A. Hill, C. P. Hawkins, and D. M. Carlisle. Predicting thermal reference conditions for USA streams and rivers. *Freshwater Science*, 32(1):39–55, 2013. doi: 10.1899/12-009.1.
- B. Hoffmann, S. Häfele, and U. Karl. Analysis of performance losses of thermal power plants in Germany – A System Dynamics model approach using data from regional climate modelling. *Energy*, 49:193–203, 2013. ISSN 0360-5442. doi: <http://dx.doi.org/10.1016/j.energy.2012.10.034>. URL <http://www.sciencedirect.com/science/article/pii/S0360544212007967>.
- M. Hrachowitz, C. Soulsby, C. Imholt, I. A. Malcolm, and D. Tetzlaff. Thermal regimes in a large upland salmon river: a simple model to identify the influence of landscape controls and climate change on maximum temperatures. *Hydrological Processes*, 24(23):3374–3391, 2010. ISSN 1099-1085. doi: 10.1002/hyp.7756. URL <http://dx.doi.org/10.1002/hyp.7756>.
- M. Hrachowitz, H. Savenije, G. Blöschl, J. McDonnell, M. Sivapalan, J. Pomeroy, B. Arheimer, T. Blume, M. Clark, U. Ehret, F. Fenicia, J. Freer, A. Gelfan, H. Gupta, D. Hughes, R. Hut, A. Montanari, S. Pande, D. Tetzlaff, P. Troch, S. Uhlenbrook, T. Wagener, H. Winsemius, R. Woods, E. Zehe, and C. Cudennec. A decade of Predictions in Ungauged Basins (PUB)—a review. *Hydrological Sciences Journal*, 58(6):1198–1255, 2013. doi: 10.1080/02626667.2013.803183. URL <http://dx.doi.org/10.1080/02626667.2013.803183>.
- IAEA. Climate change and nuclear power 2015. Technical report, International Atomic Energy Agency (IAEA), Vienna, Austria, September 2015.
- C. Imholt, C. Soulsby, I. A. Malcolm, M. Hrachowitz, C. N. Gibbins, S. Langan, and D. Tetzlaff. Influence of scale on thermal characteristics in a large montane river basin. *River Research and Applications*, 29(4):403–419, 2013. ISSN 1535-1467. doi: 10.1002/rra.1608. URL <http://dx.doi.org/10.1002/rra.1608>.
- D. J. Isaak and W. A. Hubert. A hypothesis about factors that affect maximum summer stream temperatures across montane landscapes. *Journal of the American Water Resources Association*, 37(2):351–366, 2001. ISSN 1752-1688. doi: 10.1111/j.1752-1688.2001.tb00974.x. URL <http://dx.doi.org/10.1111/j.1752-1688.2001.tb00974.x>.
- D. J. Isaak, C. H. Luce, B. E. Rieman, D. E. Nagel, E. E. Peterson, D. L. Horan, S. Parkes, and G. L. Chandler. Effects of climate change and wildfire on stream temperatures and salmonid thermal habitat in a mountain river network. *Ecological Applications*, 20(5):1350–1371, 2010.
- A. Jakob. Temperaturen in Schweizer Fliessgewässern. *GWA*, 3:221–231, 2010.
- F. Johnson. Stream temperatures in an Alpine area. *Journal of Hydrology*, 14(3–4):322–336, 1971. ISSN 0022-1694. doi: 10.1016/0022-1694(71)90042-4. URL <http://www.sciencedirect.com/science/article/pii/0022169471900424>.
- M. F. Johnson, R. L. Wilby, and J. A. Toone. Inferring air–water temperature relationships from river and catchment properties. *Hydrological Processes*, 28(6):2912–2928, 2014. ISSN 1099-1085. doi: 10.1002/hyp.9842. URL <http://dx.doi.org/10.1002/hyp.9842>.

- K. L. Jones, G. C. Poole, J. L. Meyer, W. Bumback, and E. A. Kramer. Quantifying expected ecological response to natural resource legislation: a case study of riparian buffers, aquatic habitat, and trout populations. *Ecology and Society*, 11(15):15, 2006. URL <http://www.ecologyandsociety.org/vol11/iss2/art15/>.
- C. Kelleher, T. Wagener, M. Gooseff, B. McGlynn, K. McGuire, and L. Marshall. Investigating controls on the thermal sensitivity of Pennsylvania streams. *Hydrological Processes*, 26(5): 771–785, 2012. ISSN 1099-1085. doi: 10.1002/hyp.8186. URL <http://dx.doi.org/10.1002/hyp.8186>.
- B. Khakbaz, B. Imam, K. Hsu, and S. Sorooshian. From lumped to distributed via semi-distributed: Calibration strategies for semi-distributed hydrologic models. *Journal of Hydrology*, 418–419:61–77, 2012. ISSN 0022-1694. doi: <http://dx.doi.org/10.1016/j.jhydrol.2009.02.021>. URL <http://www.sciencedirect.com/science/article/pii/S0022169409000894>.
- D. Knighton. *Fluvial forms and processes: a new perspective*. Arnold, 1998. ISBN 0-340-66313-8.
- C. Kormann, T. Francke, and A. Bronstert. Detection of regional climate change effects on alpine hydrology by daily resolution trend analysis in Tyrol, Austria. *Journal of Water and Climate Change*, 6(1):124–143, 2015a. ISSN 2040-2244. doi: 10.2166/wcc.2014.099. URL <http://jwcc.iwaponline.com/content/6/1/124>.
- C. Kormann, T. Francke, M. Renner, and A. Bronstert. Attribution of high resolution streamflow trends in Western Austria – An approach based on climate and discharge station data. *Hydrology and Earth System Sciences*, 19(3):1225–1245, 2015b. doi: 10.5194/hess-19-1225-2015. URL <http://www.hydrol-earth-syst-sci.net/19/1225/2015/>.
- T. Langford. *Ecological Effects of Thermal Discharges*. Pollution Monitoring Series. Springer, 1990. ISBN 9781851664511. URL <http://books.google.ch/books?id=f1M6lkRZ7MUC>. Last access: 17 March 2015.
- J. A. Leach and R. D. Moore. Winter stream temperature in the rain-on-snow zone of the Pacific Northwest: influences of hillslope runoff and transient snow cover. *Hydrology and Earth System Sciences*, 18(2):819–838, 2014. doi: 10.5194/hess-18-819-2014. URL <http://www.hydrol-earth-syst-sci.net/18/819/2014/>.
- J. A. Leach and R. D. Moore. Observations and modeling of hillslope throughflow temperatures in a coastal forested catchment. *Water Resources Research*, 51(5):3770–3795, 2015. ISSN 1944-7973. doi: 10.1002/2014WR016763. URL <http://dx.doi.org/10.1002/2014WR016763>.
- M. Lehning, P. Bartelt, B. Brown, T. Russi, U. Stöckli, and M. Zimmerli. Snowpack model calculations for avalanche warning based upon a new network of weather and snow stations. *Cold Regions Science and Technology*, 30(1–3):145–157, 1999. ISSN 0165-232X. doi: [http://dx.doi.org/10.1016/S0165-232X\(99\)00022-1](http://dx.doi.org/10.1016/S0165-232X(99)00022-1). URL <http://www.sciencedirect.com/science/article/pii/S0165232X99000221>.

## Bibliography

---

- M. Lehning, P. Bartelt, B. Brown, and C. Fierz. A physical SNOWPACK model for the Swiss avalanche warning. Part III: Meteorological forcing, thin layer formation and evaluation. *Cold Regions Science and Technology*, 35(3):169–184, 2002a. ISSN 0165-232X. doi: [http://dx.doi.org/10.1016/S0165-232X\(02\)00072-1](http://dx.doi.org/10.1016/S0165-232X(02)00072-1). URL <http://www.sciencedirect.com/science/article/pii/S0165232X02000721>.
- M. Lehning, P. Bartelt, B. Brown, C. Fierz, and P. Satyawali. A physical SNOWPACK model for the Swiss avalanche warning. Part II: Snow microstructure. *Cold Regions Science and Technology*, 35(3):147–167, 2002b. ISSN 0165-232X. doi: [http://dx.doi.org/10.1016/S0165-232X\(02\)00073-3](http://dx.doi.org/10.1016/S0165-232X(02)00073-3). URL <http://www.sciencedirect.com/science/article/pii/S0165232X02000733>.
- M. Lehning, I. Völksch, D. Gustafsson, T. A. Nguyen, M. Stähli, and M. Zappa. ALPINE3D: a detailed model of mountain surface processes and its application to snow hydrology. *Hydrological Processes*, 20(10):2111–2128, 2006. ISSN 1099-1085. doi: 10.1002/hyp.6204. URL <http://dx.doi.org/10.1002/hyp.6204>.
- M. Lehning, H. Löwe, M. Ryser, and N. Raderschall. Inhomogeneous precipitation distribution and snow transport in steep terrain. *Water Resources Research*, 44(W07404), 2008. ISSN 1944-7973. doi: 10.1029/2007WR006545. URL <http://dx.doi.org/10.1029/2007WR006545>.
- R. J. LeVeque. *Finite volume methods for hyperbolic problems*. Cambridge University Press, 2002. ISBN 978-0-521-81087-6.
- K. Linnerud, T. K. Mideksa, and G. S. Eskeland. The impact of climate change on nuclear power supply. *The Energy Journal*, 32(1), 2011. doi: 10.5547/ISSN0195-6574-EJ-Vol32-No1-6.
- S. B. Lippman, J. Lajoie, and B. E. Moo. *C++ Primer (5th edition)*. Addison-Wesley, 2012. ISBN 0321714113.
- M. C. Loinaz, H. K. Davidsen, M. Butts, and P. Bauer-Gottwein. Integrated flow and temperature modeling at the catchment scale. *Journal of Hydrology*, 495:238–251, 2013. ISSN 0022-1694. doi: <http://dx.doi.org/10.1016/j.jhydrol.2013.04.039>. URL <http://www.sciencedirect.com/science/article/pii/S0022169413003338>.
- M. C. Loinaz, D. Gross, R. Unnasch, M. Butts, and P. Bauer-Gottwein. Modeling ecohydrological impacts of land management and water use in the Silver Creek basin, Idaho. *Journal of Geophysical Research: Biogeosciences*, 119(3):487–507, 2014. ISSN 2169-8961. doi: 10.1002/2012JG002133. URL <http://dx.doi.org/10.1002/2012JG002133>.
- C. L. Lowney. Stream temperature variation in regulated rivers: Evidence for a spatial pattern in daily minimum and maximum magnitudes. *Water Resources Research*, 36(10):2947–2955, 2000. ISSN 1944-7973. doi: 10.1029/2000WR900142. URL <http://dx.doi.org/10.1029/2000WR900142>.
- R. J. MacDonald, S. Boon, and J. M. Byrne. A process-based stream temperature modelling approach for mountain regions. *Journal of Hydrology*, 511:920–931, 2014. ISSN 0022-1694.

- doi: <http://dx.doi.org/10.1016/j.jhydrol.2014.02.009>. URL <http://www.sciencedirect.com/science/article/pii/S0022169414001061>.
- M. N. Macedo, M. T. Coe, R. DeFries, M. Uriarte, P. M. Brando, C. Neill, and W. S. Walker. Land-use-driven stream warming in southeastern Amazonia. *Philosophical Transactions of the Royal Society B: Biological Sciences*, 368(1619), 2013. doi: 10.1098/rstb.2012.0153. URL <http://rstb.royalsocietypublishing.org/content/368/1619/20120153.abstract>.
- J. Magnusson, T. Jonas, and J. W. Kirchner. Temperature dynamics of a proglacial stream: Identifying dominant energy balance components and inferring spatially integrated hydraulic geometry. *Water Resources Research*, 48(W06510), 2012. ISSN 1944-7973. doi: 10.1029/2011WR011378. URL <http://dx.doi.org/10.1029/2011WR011378>.
- B. Majone, F. Villa, R. Deidda, and A. Bellin. Impact of climate change and water use policies on hydropower potential in the south-eastern Alpine region. *Science of The Total Environment*, 543, Part B:965–980, 2016. ISSN 0048-9697. doi: <http://dx.doi.org/10.1016/j.scitotenv.2015.05.009>. URL <http://www.sciencedirect.com/science/article/pii/S004896971530067X>.
- T. D. Mayer. Controls of summer stream temperature in the Pacific Northwest. *Journal of Hydrology*, 475:323–335, 2012. ISSN 0022-1694. doi: 10.1016/j.jhydrol.2012.10.012. URL <http://www.sciencedirect.com/science/article/pii/S0022169412008864>.
- D. A. McCullough, J. M. Bartholow, H. I. Jager, R. L. Beschta, E. F. Cheslak, M. L. Deas, J. L. Ebersole, J. S. Foott, S. L. Johnson, K. R. Marine, M. G. Mesa, J. H. Petersen, Y. Souchon, K. F. Tiffan, and W. A. Wurtsbaugh. Research in thermal biology: Burning questions for coldwater stream fishes. *Reviews in Fisheries Science*, 17(1):90–115, 2009. doi: 10.1080/10641260802590152.
- W. Meier, C. Bonjour, A. Wüest, and P. Reichert. Modeling the effect of water diversion on the temperature of mountain streams. *Journal of Environmental Engineering*, 129(8):755–764, 2003. doi: 10.1061/(ASCE)0733-9372(2003)129:8(755). URL [http://dx.doi.org/10.1061/\(ASCE\)0733-9372\(2003\)129:8\(755\)](http://dx.doi.org/10.1061/(ASCE)0733-9372(2003)129:8(755)).
- Y. Miyake and U. Takeuchi. On the temperature of river waters of Japan. *Japanese Journal of Limnology*, 15:145–151, 1951.
- O. Mohseni, H. G. Stefan, and T. R. Erickson. A nonlinear regression model for weekly stream temperatures. *Water Resources Research*, 34(10):2685–2692, 1998. ISSN 1944-7973. doi: 10.1029/98WR01877. URL <http://dx.doi.org/10.1029/98WR01877>.
- Mollusc Specialist Group. *Margaritifera margaritifera*. The IUCN Red List of Threatened Species 1996: e.t12799a3382532, 1996. URL <http://dx.doi.org/10.2305/IUCN.UK.1996.RLTS.T12799A3382532.en>.
- R. Moore, M. Nelitz, and E. Parkinson. Empirical modelling of maximum weekly average stream temperature in British Columbia, Canada, to support assessment of fish habitat suitability.

## Bibliography

---

- Canadian Water Resources Journal*, 38(2):135–147, 2013. doi: 10.1080/07011784.2013.794992. URL <http://dx.doi.org/10.1080/07011784.2013.794992>.
- R. D. Moore, D. L. Spittlehouse, and A. Story. Riparian microclimate and stream temperature response to forest harvesting: a review. *Journal of the American Water Resources Association*, 41(4):813–834, 2005a. ISSN 1752-1688. doi: 10.1111/j.1752-1688.2005.tb03772.x. URL <http://dx.doi.org/10.1111/j.1752-1688.2005.tb03772.x>.
- R. D. Moore, P. Sutherland, T. Gomi, and A. Dhakal. Thermal regime of a headwater stream within a clear-cut, coastal british columbia, canada. *Hydrological Processes*, 19(13):2591–2608, 2005b. ISSN 1099-1085. doi: 10.1002/hyp.5733. URL <http://dx.doi.org/10.1002/hyp.5733>.
- R. D. Moore, J. A. Leach, and J. M. Knudson. Geometric calculation of view factors for stream surface radiation modelling in the presence of riparian forest. *Hydrological Processes*, 28(6): 2975–2986, 2014. ISSN 1099-1085. doi: 10.1002/hyp.9848. URL <http://dx.doi.org/10.1002/hyp.9848>.
- J. Morrison, M. C. Quick, and M. G. Foreman. Climate change in the Fraser River watershed: flow and temperature projections. *Journal of Hydrology*, 263(1–4):230–244, 2002. ISSN 0022-1694. doi: [http://dx.doi.org/10.1016/S0022-1694\(02\)00065-3](http://dx.doi.org/10.1016/S0022-1694(02)00065-3). URL <http://www.sciencedirect.com/science/article/pii/S0022169402000653>.
- R. Mott and M. Lehning. Meteorological modeling of very high-resolution wind fields and snow deposition for mountains. *Journal of Hydrometeorology*, 11(4):934–949, 2010. doi: 10.1175/2010JHM1216.1.
- R. Mott, D. Scipión, M. Schneebeli, N. Dawes, A. Berne, and M. Lehning. Orographic effects on snow deposition patterns in mountainous terrain. *Journal of Geophysical Research: Atmospheres*, 119(3):1419–1439, 2014. ISSN 2169-8996. doi: 10.1002/2013JD019880. URL <http://dx.doi.org/10.1002/2013JD019880>.
- J. Mouthon and M. Daufresne. Effects of the 2003 heatwave and climatic warming on mollusc communities of the Saône: a large lowland river and of its two main tributaries (France). *Global Change Biology*, 12(3):441–449, 2006. ISSN 1365-2486. doi: 10.1111/j.1365-2486.2006.01095.x. URL <http://dx.doi.org/10.1111/j.1365-2486.2006.01095.x>.
- V. Müller. Erarbeitung eines anthropogen unbeeinflussten, typischen Jahresgangs der Wassertemperatur nach biozönotischen Regionen. Master's thesis, Swiss Federal Institute of Technology Zurich, 2011.
- R. Mutzner, E. Bertuzzo, P. Tarolli, S. V. Weijs, L. Nicotina, S. Ceola, N. Tomasic, I. Rodriguez-Iturbe, M. B. Parlange, and A. Rinaldo. Geomorphic signatures on Brutsaert base flow recession analysis. *Water Resources Research*, 49(9):5462–5472, 2013. ISSN 1944-7973. doi: 10.1002/wrcr.20417. URL <http://dx.doi.org/10.1002/wrcr.20417>.



- J. Nash and J. Sutcliffe. River flow forecasting through conceptual models part I – A discussion of principles. *Journal of Hydrology*, 10(3):282–290, 1970. ISSN 0022-1694. doi: [http://dx.doi.org/10.1016/0022-1694\(70\)90255-6](http://dx.doi.org/10.1016/0022-1694(70)90255-6). URL <http://www.sciencedirect.com/science/article/pii/0022169470902556>.
- M. A. Nelitz, E. A. MacIsaac, and R. M. Peterman. A science-based approach for identifying temperature-sensitive streams for rainbow trout. *North American Journal of Fisheries Management*, 27(2):405–424, 2007. doi: 10.1577/M05-146.1. URL <http://dx.doi.org/10.1577/M05-146.1>.
- K. C. Nelson and M. A. Palmer. Stream temperature surges under urbanization and climate change: Data, models, and responses. *Journal of the American Water Resources Association*, 43(2):440–452, 2007. ISSN 1752-1688. doi: 10.1111/j.1752-1688.2007.00034.x. URL <http://dx.doi.org/10.1111/j.1752-1688.2007.00034.x>.
- S. E. Null, J. H. Viers, M. L. Deas, S. K. Tanaka, and J. F. Mount. Stream temperature sensitivity to climate warming in California’s Sierra Nevada: impacts to coldwater habitat. *Climatic Change*, 116(1):149–170, 2013. doi: 10.1007/s10584-012-0459-8.
- N. Ozaki, T. Fukushima, H. Harasawa, T. Kojiri, K. Kawashima, and M. Ono. Statistical analyses on the effects of air temperature fluctuations on river water qualities. *Hydrological Processes*, 17(14):2837–2853, 2003.
- A. Padilla, K. Rasouli, and S. J. Déry. Impacts of variability and trends in runoff and water temperature on salmon migration in the Fraser River Basin, Canada. *Hydrological Sciences Journal*, 60(3):523–533, 2015. doi: 10.1080/02626667.2014.892602. URL <http://dx.doi.org/10.1080/02626667.2014.892602>.
- J. Phillips and S. Tadayon. Selection of Manning’s roughness coefficient for natural and constructed vegetated and non-vegetated channels, and vegetation maintenance plan guidelines for vegetated channels in central Arizona. Technical Report Scientific Investigations Report 2006–5108, U.S. Geological Survey, Reston, Virginia, U.S.A., 2006.
- S. Piccolroaz, E. Calamita, B. Majone, A. Gallice, A. Siviglia, and M. Toffolon. Prediction of river water temperature: a comparison between a new family of hybrid models and statistical approaches. *Hydrological Processes*, 2016. ISSN 1099-1085. doi: 10.1002/hyp.10913. URL <http://dx.doi.org/10.1002/hyp.10913>.
- R. A. Polehn and W. C. Kinsel. Transient temperature solution for stream flow from a controlled temperature source. *Water Resources Research*, 33(1):261–265, 1997. ISSN 1944-7973. doi: 10.1029/96WR03016. URL <http://dx.doi.org/10.1029/96WR03016>.
- R. A. Polehn and W. C. Kinsel. Transient temperature solution for a river with distributed inflows. *Water Resources Research*, 36(3):787–791, 2000. ISSN 1944-7973. doi: 10.1029/1999WR900350. URL <http://dx.doi.org/10.1029/1999WR900350>.

## Bibliography

---

- V. Ponce and P. Changanti. Variable-parameter Muskingum-Cunge method revisited. *Journal of Hydrology*, 162(3–4):433–439, 1994. ISSN 0022-1694. doi: [http://dx.doi.org/10.1016/0022-1694\(94\)90241-0](http://dx.doi.org/10.1016/0022-1694(94)90241-0). URL <http://www.sciencedirect.com/science/article/pii/0022169494902410>.
- B. Pratt and H. Chang. Effects of land cover, topography, and built structure on seasonal water quality at multiple spatial scales. *Journal of Hazardous Materials*, 209–210:48–58, 2012. ISSN 0304-3894. doi: 10.1016/j.jhazmat.2011.12.068. URL <http://www.sciencedirect.com/science/article/pii/S0304389412000052>.
- S. Ragettli, G. Cortés, J. McPhee, and F. Pellicciotti. An evaluation of approaches for modelling hydrological processes in high-elevation, glacierized Andean watersheds. *Hydrological Processes*, 28(23):5674–5695, 2014. ISSN 1099-1085. doi: 10.1002/hyp.10055. URL <http://dx.doi.org/10.1002/hyp.10055>.
- P. Raymond, J. Hartmann, R. Lauerwald, S. Sobek, C. McDonald, M. Hoover, D. Butman, R. Striegl, E. Mayorga, C. Humborg, P. Kortelainen, H. Dürr, M. Meybeck, P. Ciais, and P. Guth. Global carbon dioxide emissions from inland waters. *Nature*, 503(7476):355–359, 2013. doi: 10.1038/nature12760.
- J. Richards and R. D. Moore. Discharge dependence of stream albedo in a steep proglacial channel. *Hydrological Processes*, 25(26):4154–4158, 2011. ISSN 1099-1085. doi: 10.1002/hyp.8343.
- J. C. Risley, E. A. Roehl, and P. A. Conrads. Estimating water temperatures in small streams in Western Oregon using neural network models. Water-Resources Investigations Report 02-4218, U.S. Geological Survey, Portland, Oregon, USA, 2003.
- N. Rivers-Moore, A. Mantel, and H. Dallas. Prediction of water temperature metrics using spatial modelling in the Eastern and Western Cape, South Africa. *Water SA*, 32(2):167–176, 2012. doi: 10.4314/wsa.v38i2.2.
- T. R. Roth, M. C. Westhoff, H. Huwald, J. A. Huff, J. F. Rubin, G. Barrenetxea, M. Vetterli, A. Parriaux, J. S. Selker, and M. B. Parlange. Stream temperature response to three riparian vegetation scenarios by use of a distributed temperature validated model. *Environmental Science & Technology*, 44(6):2072–2078, 2010. doi: 10.1021/es902654f. URL <http://pubs.acs.org/doi/abs/10.1021/es902654f>.
- J.-F. Rubin, A. Richard, P.-A. Chevalley, J. O'Rourke, S. Ingold, M. Rebetez, H. Huwald, G. Barrenetxea, P. Hass, R. Montavon, O. Travaglini, A. Guisan, P.-A. Frossard, P. Prunier, I. Zouaoui, C. Pusterla, M. Cid, G. Gavillet, N. Kummer, and V. Ciotti. Rapport Clim-arbres. Technical report, La Maison de la Rivière and Haute École du Paysage, d'Ingénierie et d'Architecture de Genève, 2012.
- A. S. Ruesch, C. E. Torgersen, J. J. Lawler, J. D. Olden, E. E. Peterson, C. J. Volk, and D. J. Lawrence. Projected climate-induced habitat loss for salmonids in the John Day River

- network, Oregon, U.S.A. *Conservation Biology*, 26(5):873–882, 2012. ISSN 1523-1739. doi: 10.1111/j.1523-1739.2012.01897.x. URL <http://dx.doi.org/10.1111/j.1523-1739.2012.01897.x>.
- M. Schädler. Die Temperatur schweizerischer Fließgewässer. Technical report, Swiss Federal Office for the Environment, Section Hydrology, Bern, Switzerland, 2008.
- B. Schaefli. Projecting hydropower production under future climates: a guide for decision-makers and modelers to interpret and design climate change impact assessments. *Wiley Interdisciplinary Reviews: Water*, 2(4):271–289, 2015. ISSN 2049-1948. doi: 10.1002/wat2.1083. URL <http://dx.doi.org/10.1002/wat2.1083>.
- B. Schaefli and H. V. Gupta. Do Nash values have value? *Hydrological Processes*, 21(15): 2075–2080, 2007. ISSN 1099-1085. doi: 10.1002/hyp.6825. URL <http://dx.doi.org/10.1002/hyp.6825>.
- B. Schaefli, B. Hingray, and A. Musy. Climate change and hydropower production in the Swiss Alps: quantification of potential impacts and related modelling uncertainties. *Hydrology and Earth System Sciences*, 11(3):1191–1205, 2007. doi: 10.5194/hess-11-1191-2007. URL <http://www.hydrol-earth-syst-sci.net/11/1191/2007/>.
- B. Schaefli, L. Nicótina, C. Imfeld, P. Da Ronco, E. Bertuzzo, and A. Rinaldo. SEHR-ECHO v1.0: a Spatially Explicit Hydrologic Response model for ecohydrologic applications. *Geoscientific Model Development*, 7(6):2733–2746, 2014. doi: 10.5194/gmd-7-2733-2014. URL <http://www.geosci-model-dev.net/7/2733/2014/>.
- M. C. Scott, G. S. Helfman, M. E. McTammany, E. F. Benfield, and P. V. Bolstad. Multiscale influences on physical and chemical stream conditions across blue ridge landscapes. *Journal of the American Water Resources Association*, 38(5):1379–1392, 2002. ISSN 1752-1688. doi: 10.1111/j.1752-1688.2002.tb04353.x. URL <http://dx.doi.org/10.1111/j.1752-1688.2002.tb04353.x>.
- C. Segura, P. Caldwell, G. Sun, S. McNulty, and Y. Zhang. A model to predict stream water temperature across the conterminous USA. *Hydrological Processes*, 2014. ISSN 1099-1085. doi: 10.1002/hyp.10357. URL <http://dx.doi.org/10.1002/hyp.10357>.
- R. A. Short and J. V. Ward. Macroinvertebrates of a Colorado high mountain stream. *The Southwestern Naturalist*, 25(1):23–32, 1980. ISSN 00384909.
- B. A. Sinokrot and H. G. Stefan. Stream temperature dynamics: Measurements and modeling. *Water Resources Research*, 29(7):2299–2312, 1993. ISSN 1944-7973. doi: 10.1029/93WR00540. URL <http://dx.doi.org/10.1029/93WR00540>.
- M. Sivapalan, K. Takeuchi, S. W. Franks, V. K. Gupta, H. Karambiri, V. Lakshmi, X. Liang, J. J. McDonnell, E. M. Mendiola, P. E. O’Connell, T. Oki, J. W. Pomeroy, D. Schertzer, S. Uhlenbrook, and E. Zehe. IAHS decade on Predictions in Ungauged Basins (PUB), 2003–2012: Shaping an exciting future for the hydrological sciences. *Hydrological Sciences Journal*,

## Bibliography

---

- 48(6):857–880, 2003. doi: 10.1623/hysj.48.6.857.51421. URL <http://dx.doi.org/10.1623/hysj.48.6.857.51421>.
- R. A. Sponseller, E. F. Benfield, and H. M. Valett. Relationships between land use, spatial scale and stream macroinvertebrate communities. *Freshwater Biology*, 46(10):1409–1424, 2001. ISSN 1365-2427. doi: 10.1046/j.1365-2427.2001.00758.x. URL <http://dx.doi.org/10.1046/j.1365-2427.2001.00758.x>.
- A. St-Hilaire, G. Morin, N. El-Jabi, and D. Caissie. Water temperature modelling in a small forested stream: implication of forest canopy and soil temperature. *Canadian Journal of Civil Engineering*, 27(6):1095–1108, 2000. doi: 10.1139/100-021. URL <http://www.nrcresearchpress.com/doi/abs/10.1139/100-021>.
- S. A. Stage. Comments on an improvement to the Brent’s method. *International Journal of Experimental Algorithms*, 4(1):1–16, 2013.
- H. G. Stefan and E. B. Preud’homme. Stream temperature estimation from air temperature. *Journal of the American Water Resources Association*, 29(1):27–45, 1993. ISSN 1752-1688. doi: 10.1111/j.1752-1688.1993.tb01502.x. URL <http://dx.doi.org/10.1111/j.1752-1688.1993.tb01502.x>.
- I. T. Stewart, D. R. Cayan, and M. D. Dettinger. Changes toward earlier streamflow timing across western North America. *Journal of Climate*, 18(8):1136–1155, 2005. doi: 10.1175/JCLI3321.1. URL <http://dx.doi.org/10.1175/JCLI3321.1>.
- I. T. Stewart, D. L. Ficklin, C. A. Carrillo, and R. McIntosh. 21st century increases in the likelihood of extreme hydrologic conditions for the mountainous basins of the Southwestern United States. *Journal of Hydrology*, 529, Part 1:340–353, 2015. ISSN 0022-1694. doi: <http://dx.doi.org/10.1016/j.jhydrol.2015.07.043>. URL <http://www.sciencedirect.com/science/article/pii/S0022169415005491>.
- A. Strässle, F. Kupferschmid-Enderlin, and M. Spinelli. Pro Natura magazine spécial 2016. *Hydrology and Earth System Sciences*, 2016. ISSN 1422-6235.
- K. Sullivan, J. Tooley, K. Doughty, J. Caldwell, and P. Knudsen. Evaluation of prediction models and characterization of stream temperature regimes in Washington. Technical Report Timber/Fish/Wildlife Rep. No. TFW-WQ3-90-006, Washington Dept. Nat. Resources, Olympia, Washington, 1990.
- K. Sullivan, D. Martin, R. Cardwell, J. E. Toll, and S. Duke. An analysis of the effects of temperature on salmonids of the Pacific Northwest with implications for selecting temperature criteria. Technical report, Sustainable Ecosystems Institute, Portland Oregon (USA), 2000.
- N. Sun, J. Yearsley, N. Voisin, and D. P. Lettenmaier. A spatially distributed model for the assessment of land use impacts on stream temperature in small urban watersheds. *Hydrological Processes*, 29(10):2331–2345, 2015. ISSN 1099-1085. doi: 10.1002/hyp.10363. URL <http://dx.doi.org/10.1002/hyp.10363>.

- C. Tague, M. Farrell, G. Grant, S. Lewis, and S. Rey. Hydrogeologic controls on summer stream temperatures in the McKenzie River basin, Oregon. *Hydrological Processes*, 21(24):3288–3300, 2007. ISSN 1099-1085. doi: 10.1002/hyp.6538. URL <http://dx.doi.org/10.1002/hyp.6538>.
- X. Tang, D. W. Knight, and P. G. Samuels. Variable parameter Muskingum-Cunge method for flood routing in a compound channel. *Journal of Hydraulic Research*, 37(5):591–614, 1999. doi: 10.1080/00221689909498519. URL <http://dx.doi.org/10.1080/00221689909498519>.
- D. G. Tarboton. A new method for the determination of flow directions and upslope areas in grid digital elevation models. *Water Resources Research*, 33(2):309–319, 1997. ISSN 1944-7973. doi: 10.1029/96WR03137. URL <http://dx.doi.org/10.1029/96WR03137>.
- F. D. Theurer, K. A. Voos, and W. J. Miller. Instream water temperature model. Instream flow information paper 16. Federal Government Series 16, FWS/OBS-84/15, Fort Collins, Colorado, USA, 1984.
- M. Toffolon and S. Piccolroaz. A hybrid model for river water temperature as a function of air temperature and discharge. *Environmental Research Letters*, 10(11):114011, 2015. URL <http://stacks.iop.org/1748-9326/10/i=11/a=114011>.
- M. Toffolon, A. Siviglia, and G. Zolezzi. Thermal wave dynamics in rivers affected by hydropeaking. *Water Resources Research*, 46(8), 2010. ISSN 1944-7973. doi: 10.1029/2009WR008234. URL <http://dx.doi.org/10.1029/2009WR008234>.
- C.-P. Tung, T.-Y. Lee, J.-C. Huang, P.-W. Perng, S.-J. Kao, and L.-Y. Liao. The development of stream temperature model in a mountainous river of Taiwan. *Environmental Monitoring and Assessment*, 186(11):7489–7503, 2014. ISSN 1573-2959. doi: 10.1007/s10661-014-3942-z. URL <http://dx.doi.org/10.1007/s10661-014-3942-z>.
- L. P. H. van Beek, T. Eikelboom, M. T. H. van Vliet, and M. F. P. Bierkens. A physically based model of global freshwater surface temperature. *Water Resources Research*, 48(W09530), 2012. ISSN 1944-7973. doi: 10.1029/2012WR011819. URL <http://dx.doi.org/10.1029/2012WR011819>.
- A. I. J. M. van Dijk. Climate and terrain factors explaining streamflow response and recession in Australian catchments. *Hydrology and Earth System Sciences*, 14(1):159–169, 2010. doi: 10.5194/hess-14-159-2010. URL <http://www.hydrol-earth-syst-sci.net/14/159/2010/>.
- D. van Heesch. Doxygen: Source code documentation generator tool. available at: <http://www.doxygen.org/> (last access: 30 May 2016), 2008.
- M. T. H. van Vliet, J. R. Yearsley, W. H. P. Franssen, F. Ludwig, I. Haddeland, D. P. Lettenmaier, and P. Kabat. Coupled daily streamflow and water temperature modelling in large river basins. *Hydrology and Earth System Sciences*, 16(11):4303–4321, 2012a. doi: 10.5194/hess-16-4303-2012. URL <http://www.hydrol-earth-syst-sci.net/16/4303/2012/>.

## Bibliography

---

- M. T. H. van Vliet, J. R. Yearsley, F. Ludwig, S. Voge, D. P. Lettenmaier, and P. Kabat. Vulnerability of US and European electricity supply to climate change. *Nature Clim. Change*, 2(9):676–681, 2012b. doi: 10.1038/nclimate1546. URL <http://www.nature.com/nclimate/journal/v2/n9/full/nclimate1546.html>.
- D. Viviroli, D. R. Archer, W. Buytaert, H. J. Fowler, G. B. Greenwood, A. F. Hamlet, Y. Huang, G. Koboltschnig, M. I. Litaor, J. I. López-Moreno, S. Lorentz, B. Schädler, H. Schreier, K. Schwaiger, M. Vuille, and R. Woods. Climate change and mountain water resources: overview and recommendations for research, management and policy. *Hydrology and Earth System Sciences*, 15(2):471–504, 2011. doi: 10.5194/hess-15-471-2011. URL <http://www.hydrol-earth-syst-sci.net/15/471/2011/>.
- C. Voegeli, M. Lehning, N. Wever, and M. Bavay. Scaling precipitation input to distributed hydrological models by measured snow distribution. prepared for submission to *Frontiers in Earth Science*, 2016.
- J. A. Vrugt and C. J. F. Ter Braak. DREAM<sub>(D)</sub>: an adaptive Markov Chain Monte Carlo simulation algorithm to solve discrete, noncontinuous, and combinatorial posterior parameter estimation problems. *Hydrology and Earth System Sciences*, 15(12):3701–3713, 2011. doi: 10.5194/hess-15-3701-2011. URL <http://www.hydrol-earth-syst-sci.net/15/3701/2011/>.
- E.-J. Wagenmakers and S. Farrell. Aic model selection using Akaike weights. *Psychonomic Bulletin & Review*, 11(1):192–196, 2004. ISSN 1069-9384. doi: 10.3758/BF03206482. URL <http://dx.doi.org/10.3758/BF03206482>.
- B. W. Webb and Y. Zhang. Spatial and seasonal variability in the components of the river heat budget. *Hydrological Processes*, 11(1):79–101, 1997. ISSN 1099-1085. doi: 10.1002/(SICI)1099-1085(199701)11:1<79::AID-HYP404>3.0.CO;2-N. URL [http://dx.doi.org/10.1002/\(SICI\)1099-1085\(199701\)11:1<79::AID-HYP404>3.0.CO;2-N](http://dx.doi.org/10.1002/(SICI)1099-1085(199701)11:1<79::AID-HYP404>3.0.CO;2-N).
- B. W. Webb, D. M. Hannah, R. D. Moore, L. E. Brown, and F. Nobilis. Recent advances in stream and river temperature research. *Hydrological Processes*, 22(7):902–918, 2008. ISSN 1099-1085. doi: 10.1002/hyp.6994. URL <http://dx.doi.org/10.1002/hyp.6994>.
- K. E. Wehrly, L. Wang, and M. Mitro. Field-based estimates of thermal tolerance limits for trout: Incorporating exposure time and temperature fluctuation. *Transactions of the American Fisheries Society*, 136(2):365–374, 2007. doi: 10.1577/T06-163.1. URL <http://dx.doi.org/10.1577/T06-163.1>.
- K. E. Wehrly, T. O. Brenden, and L. Wang. A comparison of statistical approaches for predicting stream temperatures across heterogeneous landscapes. *Journal of the American Water Resources Association*, 45(4):986–997, 2009. ISSN 1752-1688. doi: 10.1111/j.1752-1688.2009.00341.x. URL <http://dx.doi.org/10.1111/j.1752-1688.2009.00341.x>.
- S. V. Weijers, R. Mutzner, and M. B. Parlange. Could electrical conductivity replace water level in rating curves for alpine streams? *Water Resources Research*, 49(1):343–351, 2013. ISSN 1944-7973. doi: 10.1029/2012WR012181. URL <http://dx.doi.org/10.1029/2012WR012181>.

- S. Westenbroek, J. Stewart, C. Buchwald, M. Mitro, J. Lyons, and S. Greb. A model for evaluating stream temperature response to climate change scenarios in Wisconsin. In *Watershed Management Conference 2010*, pages 1–12, Madison, Wisconsin, United States, August 2010. American Society of Civil Engineers. ISBN 978-0-7844-1143-8. doi: 10.1061/41143(394)1.
- M. C. Westhoff, H. H. G. Savenije, W. M. J. . Luxemburg, G. S. Stelling, N. C. van de Giesen, J. S. Selker, L. Pfister, and S. Uhlenbrook. A distributed stream temperature model using high resolution temperature observations. *Hydrology and Earth System Sciences*, 11(4): 1469–1480, 2007. doi: 10.5194/hess-11-1469-2007. URL <http://www.hydrol-earth-syst-sci.net/11/1469/2007/>.
- N. Wever, C. Fierz, C. Mitterer, H. Hirashima, and M. Lehning. Solving Richards Equation for snow improves snowpack meltwater runoff estimations in detailed multi-layer snowpack model. *The Cryosphere*, 8(1):257–274, 2014. doi: 10.5194/tc-8-257-2014. URL <http://www.the-cryosphere.net/8/257/2014/>.
- N. Wever, L. Schmid, A. Heilig, O. Eisen, C. Fierz, and M. Lehning. Verification of the multi-layer SNOWPACK model with different water transport schemes. *The Cryosphere*, 9(6):2271–2293, 2015. doi: 10.5194/tc-9-2271-2015. URL <http://www.the-cryosphere.net/9/2271/2015/>.
- L. Wilhelm, K. Besemer, L. Fragner, H. Peter, W. Weckwerth, and T. Battin. Altitudinal patterns of diversity and functional traits of metabolically active microorganisms in stream biofilms. *ISME Journal*, 9(11):2454–2464, 2015. doi: 10.1038/ismej.2015.56.
- R. G. Young, A. J. Quarterman, R. F. Eyles, R. A. Smith, and W. B. Bowden. Water quality and thermal regime of the Motueka river: Influences of land cover, geology and position in the catchment. *New Zealand Journal of Marine and Freshwater Research*, 39(4):803–825, 2005. doi: 10.1080/00288330.2005.9517354. URL <http://dx.doi.org/10.1080/00288330.2005.9517354>.
- M. Zappa, F. Pos, U. Strasser, P. Warmerdam, and J. Gurtz. Seasonal water balance of an alpine catchment as evaluated by different methods for spatially distributed snowmelt modelling. *Hydrology Research*, 34(3):179–202, 2003. ISSN 0029-1277. URL <http://hr.iwaponline.com/content/34/3/179>.
- X. Zeng. A general approach to enhance slope limiters on non-uniform rectilinear grids. Available at: <http://arxiv.org/abs/1301.0967>, 2013.





## Aurélien GALLICE

Avenue de Morges 101  
1004 Lausanne (Switzerland)  
Phone : +41 78 807 93 18  
Email : aurelien.gallice@epfl.ch

### EXPERIENCE

- 2013–2016 **PhD student in Environmental Sciences at the Swiss Federal Institute of Technology Lausanne (EPFL), Switzerland**  
3.5 years  
I developed a **statistical model** based on data that I extracted from geographic maps using a dedicated software. I also conceived, developed and fully documented a **computer program** used to forecast the temperature of streams. In addition, I took part in the preparation and supervision of **exercise sessions** for first-year students.
- 2011–2012 **Computational engineer at TWT GmbH (engineering department), Germany**  
13 months  
*Company specialized in technology consulting*  
I was responsible for the development of a **numerical model** aimed at computing the energy consumption of trucks. I used it to perform **simulations**, whose results I **presented** to the company's main client (Daimler AG, Germany).
- 2011 **Internship in numerical simulation at Sensirion AG (R&D department), Switzerland**  
6 months  
*Company developing, producing and selling flow and temperature sensors worldwide*  
I performed temperature and flow **simulations** using a commercial software to optimize the sensors sold by the company. I also developed a **computational tool** with graphical interface to estimate the sensor measurement errors.
- 2010 **Scientific assistant at the Swiss Federal Institute of Technology Zurich (ETHZ), Switzerland**  
4 months  
I worked in complete **autonomy** on the further development of the study conducted during my Master's thesis. I wrote a scientific article to present my final results.

### EDUCATION

- 2010 **Master of Science MCs in Physics** with a **minor** (additional course semester) in **biomedical technologies** from the Swiss Federal Institute of Technology Lausanne (EPFL)  
Master project (4 months) done at the Swiss Federal of Institute Zurich (ETHZ)
- 2007–2008 **Academic exchange of 9 months** in McGill University, Montreal (Canada)
- 2005 Baccalauréat (French high school diploma)

## PUBLICATIONS

- Gallice, A.**, Comola, F., Bavay, M., Lehning, M. and Huwald, H.: Add-on to the spatially distributed snow model Alpine3D for hydrological modeling and deterministic stream temperature prediction. *Geophysical Model Development* (to be submitted)
- Piccolroaz, S., Calamita, E., Majone, B., **Gallice, A.**, Siviglia, A. and Toffolon, M.: Prediction of river water temperature: a comparison between a new family of hybrid models and statistical approaches. *Hydrological Processes*, 2016 (in press).
- Gallice, A.**, Schaefli, B., Lehning, M., Parlange, M. B. and Huwald, H.: Stream temperature prediction in ungauged basins: review of recent approaches and description of a new physics-derived statistical model. *Hydrology and Earth System Sciences*, 19(9):3727–3753, 2015.
- Gallice, A.**, Wienhold, F. G., Hoyle, C. R., Immler, F., and Peter, T.: Modeling the ascent of sounding balloons: derivation of the vertical air motion, *Atmos. Meas. Tech.*, 4, 2235–2253, 2011.

## TECHNICAL SKILLS

**Areas of expertise:** scientific programming, numerical modeling (fluid and heat transport, hydrology), statistical data analysis

**Programming languages:** C++, Python (incl. library PyQt4), Matlab/Simulink, Fortran 77/99, MySQL

**Numerical simulation softwares:** COMSOL, Fluent, Abaqus, Star-CCM+

## LANGUAGES

<b>French</b>	mother tongue
<b>English</b>	C1 (fluent)
<b>German</b>	B2 (very good knowledge)
<b>Italian</b>	A1 (basic)

## PERSONAL INFORMATION

Born on 28.12.1987 in Saint-Julien-en-Genevois (France)

Nationality: French

Marital status: single